Turbulent Flow in Rooms Ventilated by Mixing Principle

Comparision Between Computational Fluid Dynamics and Full-Scale Experiments

Skovgaard, Michael

Publication date:
1991

Document Version
Publisher's PDF, also known as Version of record

THE UNIVERSITY OF AALBORG
DEPARTMENT OF BUILDING TECHNOLOGY
AND STRUCTURAL ENGINEERING
9000 AALBORG, DENMARK

TURBULENT FLOW IN ROOMS VENTILATED BY THE MIXING PRINCIPLE -

Comparisons between Computational Fluid Dynamics and Full-Scale Experiments

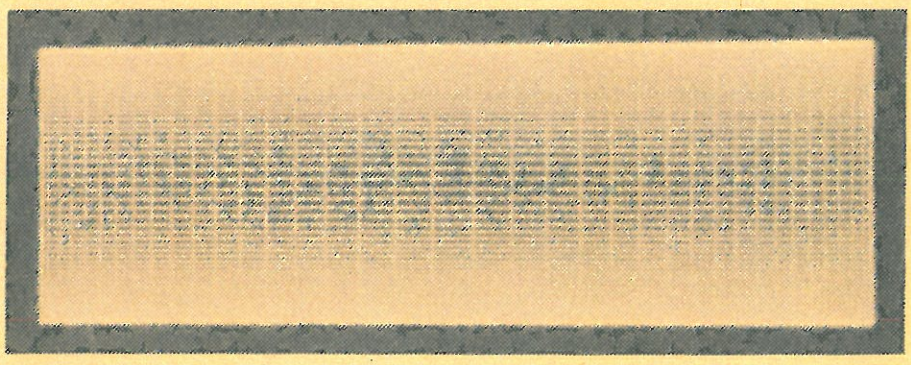

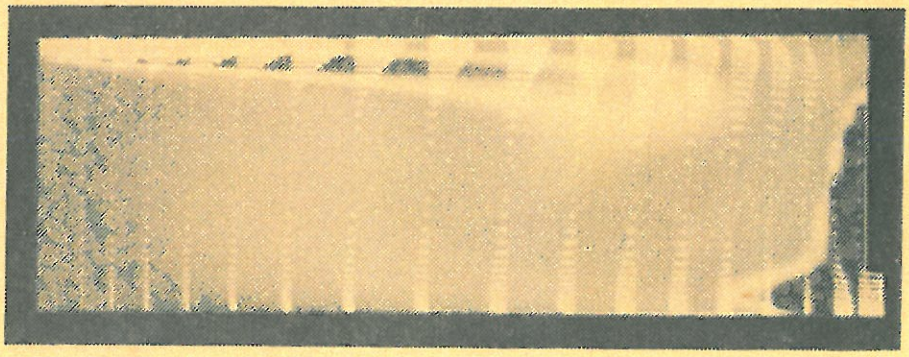

MICHAEL SKOVGAARD

TURBULENT FLOW IN ROOMS VENTILATED BY THE MIXING PRINCIPLE -
Comparisons between Computational Fluid Dynamics and Full-Scale Experiments

PH.D THESIS DECEMBER 1991
ISSN 0902-7513 R9145

THE UNIVERSITY OF AALBORG
DEPARTMENT OF BUILDING TECHNOLOGY
AND STRUCTURAL ENGINEERING
9000 AALBORG, DENMARK

TURBULENT FLOW IN ROOMS VENTILATED BY THE MIXING PRINCIPLE -

Comparisons between Computational Fluid Dynamics and Full-Scale Experiments

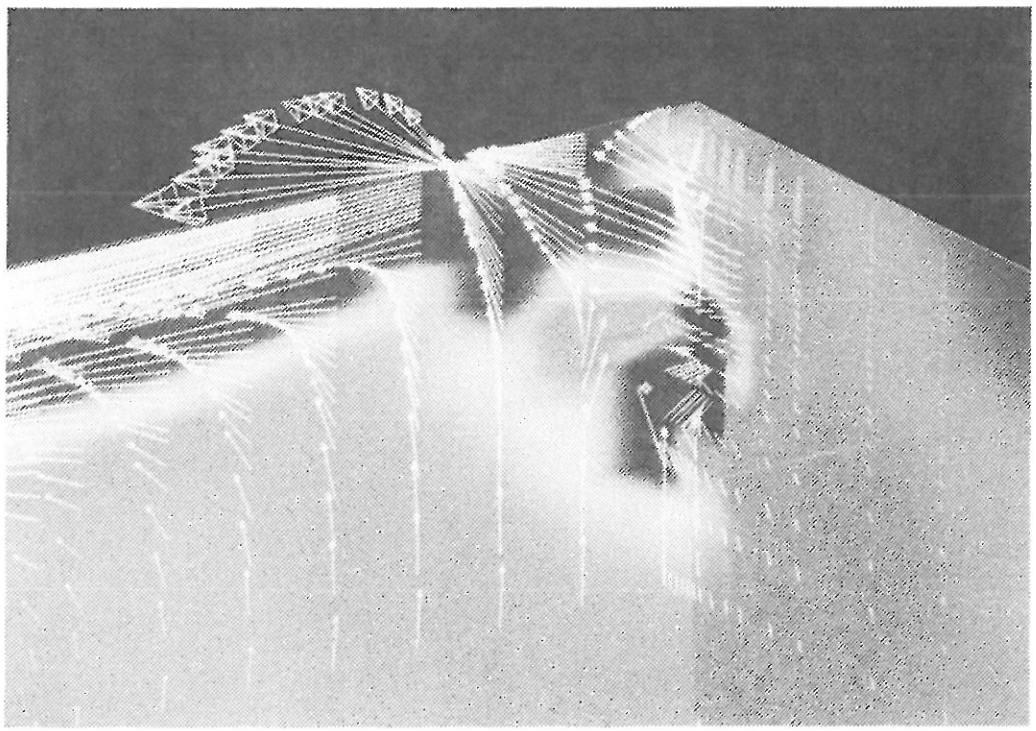

MICHAEL SKOVGAARD

TURBULENT FLOW IN ROOMS VENTILATED BY THE MIXING PRINCIPLE -
Comparisons between Computational Fluid Dynamics and Full-Scale Experiments

PH.D THESIS DECEMBER 1991 ISSN 0902-7513 R9145

PREFACE

This thesis represents the end of my Ph.D. study at the University of Aalborg, Institute of Building Technology and Structural Engineering with Professor, Dr. P.V. Nielsen as supervisor.

In the thesis the following system of symbols is used:

Section:	1.2	
		The number of the chapter.
		The number of the section.
Figure:	1.2	
		The number of the chapter.
		The consecutive number of the figure in the chapter.
Formula:	(1.2)	
		The number of the chapter.
		The consecutive number of the formula in the chapter.

In appendix the same system of symbols is used but with a preceding capital A.

References made in the text are written in *italic* and may be found in the table of references in the end of the thesis. A list of technical symbols and abbreviations is found in the beginning of the thesis.

Acknowledgements

The work presented in this thesis is founded by the Danish Technical Research Council (STVF) and the Danish Agency of Energy via the Danish Building Research Institute (SBI). I would hereby like to express my thanks for this support.

I would also like to thank Professor, Dr. P.V. Nielsen at the University of Aalborg for being a splendid source of inspiration, guidance and advice during the Ph.D. period. Also many thanks to the staff at the University of Manchester Institute of Science and Technology (UMIST) especially Professor, Dr. B.E. Launder, Dr. N. Ince and Julie for their openness and helpful assistance.

I want to thank C.E. Hyldgaard for guidance and genuine interest during the ex-

perimental work and T. Christensen whose practical assistance made the experiments possible. Also thanks to Ingrid Christensen for making a fair copy of the sketches in the thesis and to Torsten Jacobsen for many inspiring discussions.

Finally my thanks go to Inge for many months of patience.

M. Skovgaard december 1991.

TABLE OF CONTENT

LIST OF SYMBOLS

All units in the thesis are represented in SI-units (metric-units).

A	Area, area of cell face (e.g. $\Delta x\Delta y$ or $\Delta y\Delta z$)	[m^2]
ADI	Altenating direction implicit	
a	Coefficient in difference equation, area	[m^2]
C_1	Constant in the ϵ-equation in the turbulence model, constant for determination of velocity in the occupied zone	
C_2	Constant in the ϵ-equation in the turbulence model, constant for determination of velocity in the occupied zone	
C_3	Constant in the ϵ-equation in the LRN turbulence model	
C_D	Constant in the k-equation in the turbulence model	
C_μ	Proportionality factor in the equation for the turbulent viscosity	
D_a	Constant in growth of jet width	
∂	Partial differential operator	
E	Wall roughness function in the logarithmic law (for smooth walls E=9.793)	
F	Body force	[N]
FD	Finite difference	
FEM	Finite element method	
FV	Finite volume	
f_1	Function for determination of the velocity in occupied zone ($f_1 = U_{rm}/U_L$)	
f_1	Function to increase the dissipation near the wall in the LRN turbulence model	
f_2	Function to incorporate low Reynolds number effects in the destruction term of the ϵ-equation in the LRN turbulence model	
f_μ	Function which mimics the direct effect of the molecular viscosity on the shear stress in the LRN turbulence model	
H	Height of geometry	[m]
HYB	Hybrid	
h	Inlet height	[m]
I	Turbulence intensity	[- or %]
I_0	Inlet momentum flow ($I_0=\rho a_0 U_{inlet}^2$)	[kg m/s^2]
K	Function i the radial wall-jet decay	
K_a	Constant in the decay of a wall-jet	
K_1	Function in the decay of a radial impinging jet	
K_{3D}	Constant in the decay of a three-dimensional wall-jet	

K_{2D}	Constant in the decay of a two-dimensional wall-jet	
k	Turbulent kinetic energy	[J/kg]
L	Length of geometry	[m]
LRN	Low Reynolds number	
l	Length scale, mixing lenght	[m]
n	Air change rate, normal to surface	[h^{-1}]
P	Pressure, production term	[Pa]
PD	Percentage Dissatisfied people due to draught	[%]
PDE	Partial differential equation	
Pe	Peclet number	
PLDS	Power law differencing scheme	
PISO	Pressure implicit solution by split operator	
p	Pressure fluctuations	[Pa]
Q	Volume flow	[m^3/s]
R	Turbulent Reynolds number ($R=(\rho k^2)/(\mu\epsilon)$)	
Re	Reynolds number ($\rho l U/\mu$)	
RMS	Root-mean-square	
RSM	Reynolds stress model	
r	Radius	[m]
S	Source term	
SIMPLE	Semi implicit method for pressure linked equations	
SIMPLER	Semi implicit method for pressure linked equations - revised	
T	Temperature	[C^o or K]
TDMA	Tri-diagonal matrix algorithm	
Tu	Turbulence intensity	[- or %]
U,V,W	Time averaged velocities, U with index i, j or k used as generalized velocity variable	[m/s]
U^+	Dimensionless velocity parallel to the surface (U_p/U_τ)	
u,v,w	Velocity fluctuations	[m/s]
x	Distance from origin in the x direction	[m]
x_0	Distance to virtual origin	[m]
x,y,z	Directions in a carthesian system of coordinates	
y	Normal distance from surface	[m]
y^+	Dimensionless wall distance ($U_\tau y_p \rho/\mu$)	

Greek

Γ	Generalized diffusivity parameter	[m^2/s]

δ	Wall jet width, area, boundary layer thickness, distance	[m or m^2]
δ_{ij}	Kronecker delta (if i=j then $\delta_{ij}=1$, if i≠j then $\delta_{ij}=0$)	
ϵ	Energy dissipation	[J/kg s]
$\tilde{\epsilon}$	Energy dissipation in the Launder-Sharma k,$\tilde{\epsilon}$-model	[J/kg s]
κ	Von Karman constant ($\kappa=0.4187$)	
μ	Dynamic viscosity (for dry air at 20°C: $\mu=1.817\text{x}10^{-5}$)	[kg/m s]
ρ	Density (for dry air at 20°C: $\rho=1.204$)	[kg/m^3]
τ	Shear stress	[Pa or N/m^2]
σ_{ij}	Stress tensor	[Pa or N/m^2]
σ	Molecular Prandtl' number - ratio of viscosity/thermal diffusivity (ν/α, for air at 20°C: $\sigma=0.713$)	
σ_t	Turbulent Prandtl' number - ratio of viscosity/turbulent diffusivity (ν_t/Γ_t, for turbulent flow: $\sigma_t=1.0$)	
σ_k	Turbulent Prandtl' number - ratio of viscosity/diffusivity of turbulent kinetic energy (ν_t/Γ_k, for turbulent flow: $\sigma_k=1.0$)	
σ_k	Turbulent Prandtl' number - ratio of viscosity/diffusivity of energy dissipation (ν_t/Γ_ϵ, for turbulent flow: $\sigma_\epsilon=1.3$)	
Φ	Generalized variable	
ϕ	Generalized variable for turbulent fluctuation, angle in the (x,y)-plane	[radians]
θ	Angle in the radial direction	[radians]
ν	Kinematic viscosity (μ/ρ, for dry air at 20°C: $\nu=1.509\text{x}10^{-5}$)	[m^2/s]

Subscripts

D	Downstream point
d	Diameter of nozzle in the inlet device, downstream cell face
E	East point
e	East cell face
i,j,k	Carthesian indicators of direction. Any three may take the value of 1,2 and 3 in the tensor notation
l	Laminar
N	North point
n	North cell face
o	Inlet, effective
P	Centre point
RE	Recirculation

r	Radial
rm	Recirculation maximum
S	Shear, south point
s	South cell face
t	Turbulent
U	Upstream point
u	Upstream cell face
W	West point
w	West cell face
x	Maximum in x - direction.

LIST OF FIGURES

Figure 6.3. The effective inlet area as a function of the inlet velocity

Figure 6.4. The location of the imaginary box in front of the inlet device.

Figure 6.5. The flow field in front of the diffuser visualized by smoke (Nielsen 1991).

Figure 6.6. K(θ) interpolated from the velocity experiments in A.6 and the smoke experiments in fig. 6.5.

Figure 6.7. Air flow patterns from the basic model (b3). a) Velocity vectors in the centre line. b) Velocity vector in a plane 0.04m below the ceiling. c)-e) Speed contours in the planes z = 0.02, 1.0 and 1.7m. f) Iso-kinetic energy in plane z = 0.02. g)-h) Speed contours in y = 2.36 and y = 0.05.

Figure 6.8. Air flow patterns from the "actual area" model (a3). a) Velocity vectors in the centre line. b) Velocity vector in a plane 0.04m below the ceiling. c)-e) Speed contours in the planes z = 0.02, 1.0 and 1.7m. f) Iso-kinetic energy in plane z = 0.02. g)-h) Speed contours in y = 2.36 and y = 0.05.

Figure 6.9. Air flow patterns from the "momentum" model (m3). a) Velocity vectors in the centre line. b) Velocity vector in a plane 0.04m below the ceiling. c)-e) Speed contours in the planes z = 0.02, 1.0 and 1.7m. f) Iso-kinetic energy in plane z = 0.02. g)-h) Speed contours in y = 2.36 and y = 0.05.

Figure 6.10. Air flow patterns from the "prescribed velocity" model (p3). a) Velocity vectors in the centre line. b) Velocity vector in a plane 0.04m below the ceiling. c)-e) Speed contours in the planes z = 0.02, 1.0 and 1.7m. f) Iso-kinetic energy in plane z = 0.02. g)-h) Speed contours in y = 2.36 and y = 0.05.

Figure 6.11. Measured and simulated decay of peak centre line velocity.

Figure 6.12. Spread of the wall-jet in the centre plane.

Figure 6.13. Simulated U-velocity profiles in the plane z=0.02. a) x/H=0.33 and b) x/H=0.67.

Figure 6.14. U_{rm} as a function of air change rate.

Figure A.6.2. Measured decay of the centre line velocity for. The K-value is found to 5.2 for n = 1 and 4.2 - 4.5 for n = 2, 3, 4, 6, 8.

Figure A.6.3. The centre line maximum velocity for different air-change-rates at different xy - planes located at ref. 1, 2, 3, 4, 5 in table 5.1.

Figure A.6.4. The maximum velocity at y = 0 and $\pm\pi/4$ as functions of the air-change-rate.

Figure A.6.5. The decay of the maximum velocity for different air-change-rates. The K(40,0) is found to 4.2 (fig. A.6.2) and the K(40, $\pm\pi/4$) is found to 1.1-1.5.

Figure A.6.6. Comparison of the two K-values found in a circular impinging jet and in the inlet flow from a HESCO diffuser.

Figure A.6.7. Velocity profiles in the occupied zone at different x distances from the inlet.

Figure A.6.8. The velocity in the occupied zone as a function of the air-change-rate for different distances from inlet. All measurements is in the mean plane.

Figure A.6.9. Estimation of the function f_1. Calculated from the maximum velocity in the occupied zone.

CHAPTER 1 - INTRODUCTION

1.1 Preamble

Mechanical ventilation of enclosures has been used widely for the last century and much effort has been done to develop new and better ways to ensure the indoor environment for the occupants in the room with a minimum of energy consumption.

The trend in office building development is going towards a higher air-tightness with controlled air change and fresh air supply, resulting in higher demands to the ventilation system. Also in the field of process ventilation the demand for better performing ventilation systems is outspoken because our knowledge about pollutants has increased in the last couple of decades. So the demand for effective ventilation systems are found in many different environments and the demand for its effectiveness is increasing.

In order to fulfill these goals in the design of an effective air conditioning system one must be able to predict the thermal comfort of the occupants in the room. Thermal comfort is governed by several parameters, e.g. heat productions and - losses, room dimensions, velocity distribution, turbulence level, temperature distribution etc.

The work reported in this thesis deals with measurements and predictions of isothermal velocity patterns and turbulence levels in enclosures ventilated by the mixing principle.

In the next section is a more detailed description of the content and the outline of the thesis made, but first a brief discussion of ventilation by the mixing principle.

1.2 Flow characteristics in a room ventilated by the mixing principle

One of the main purposes for a ventilation system is, as mentioned before, to ensure uniform and acceptable conditions in the occupied zone. To design such a system is often a difficult task because calculation of the flow pattern is complicated, with many involved parameters.

In a ventilation system of the mixing type the fresh air is lead into the enclosure by

one or several jets located outside the occupied zone (fig. 1.1). These jets has significant impact on the flow field in the entire room and therefore also in the occupied zone (*McRee et al. 1967*). The jets are created by an inlet diffuser, which often has a very complex geometry. A factor which also affects the flow in the room is the presence of boundary layers of different kinds (in isothermal flow especially near the walls). These factors are discussed in the following sections.

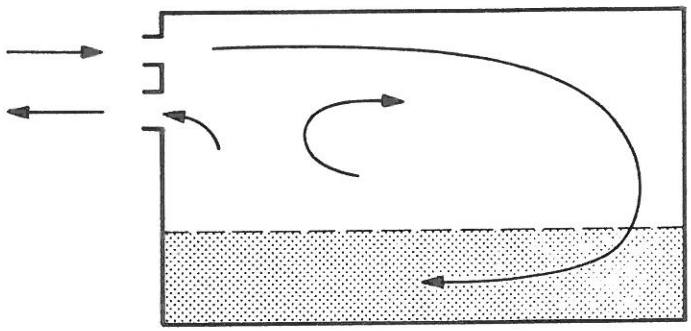

Figure 1.1. Schematic flow pattern in a room ventilated by the mixing principle.

1.2.1 Turbulent wall-jet flow

In most cases the resulting flow from a specific inlet device, in a certain distance from the inlet, may be described as a jet or have a "jet-like" character. This jet is in most practical situations either a three-dimensional free jet or a wall-jet.

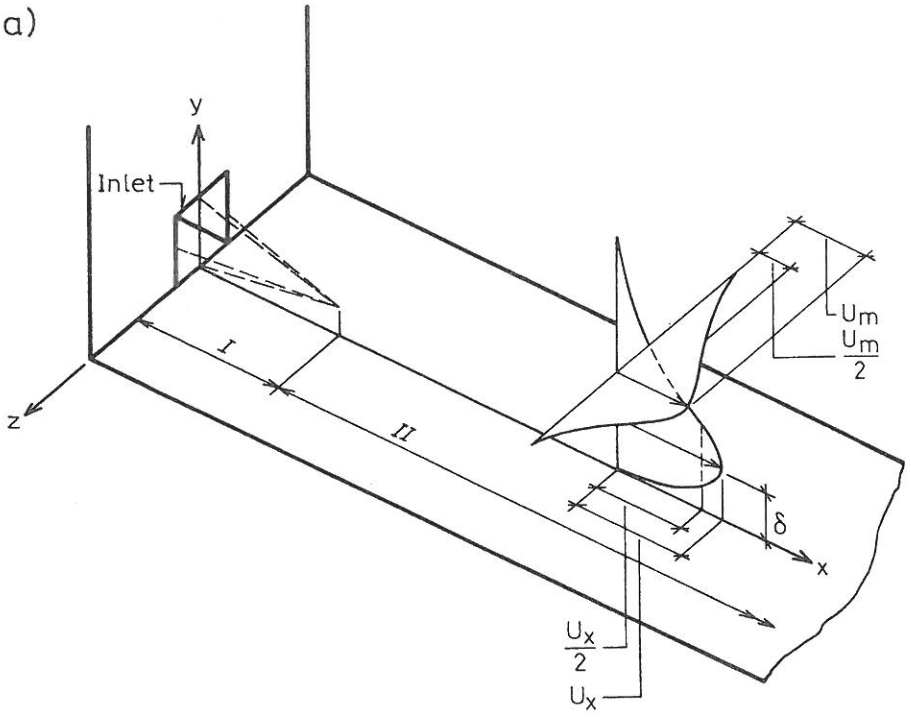

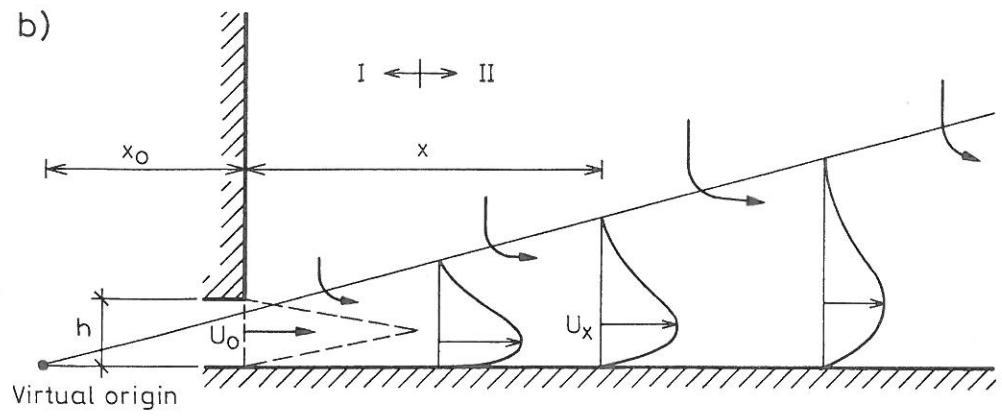

Figure 1.2. Three-dimensional wall-jet. a) Schematic representation of a three-dimensional wall-jet. b) Definition sketch.

Fig. 1.2. shows the development of a three-dimensional wall-jet along a plane surface. Region I is the potential core of the jet. This core is affected by the boundary layer (see next sub-section) and the shear layer. When these two layers meet the core is "consumed" and the next region (II), known as the fully developed region, begins. As the jet develops it will entrain fluid from the surroundings and the width of the jet will grow linearly from a virtual origin. Experiments have shown that region II subdivides into two regions. *Viets and Sforsa 1966* showed that from the end of region I there is a region where U_x decays roughly with $(x/h)^{-1/2}$ (as in a two-dimensional wall-jet). This region is termed the characteristic decay region and reaches up to where the shear layers from the two sides meet (*Rajaratnam 1976*). After this region the velocity U_x decays approximately as $(x/h)^{-1}$ (*Sforza and Herbst 1967* found a decay rate proportional to $(x/h)^{-1.14}$).

From the things mentioned above we can derive following relations for the decay of the maximum velocity

$$\begin{aligned} \frac{U_x}{U_0} &= K_{2D}\left[\frac{h}{x+x_0}\right]^{-1/2} \quad \textit{two-dimensional} \\ \frac{U_x}{U_0} &= K_{3D}\left[\frac{h}{x+x_0}\right]^{-1} \quad \textit{three-dimensional} \end{aligned} \tag{1.1}$$

The factors K_{2D} and K_{3D} are depending on the inlet geometry.

Relation (1.1) is valid for isothermal conditions.

1.2.2 Isothermal turbulent boundary-layer flow

Boundary-layer flow has a pronounced influence on the flow pattern in a room. When a surface or an obstacle is present (e.g. a piece of furniture) the velocity is forced to zero through a boundary layer. The boundary-layer near walls plays also an important role when one wants to predict the flow pattern numerically, as we shall discuss in chapter 3.

The types of boundary-layers, which are dealt with in this section, are boundary layers near walls, but another type of boundary flows exist where fluid (air) is introduced into another fluid (which may have the same physical properties) with a different velocity - this is termed a shear layer. This layer has also an influence on the flow in a room (it is e.g. a source of creating turbulence (this is discussed to some extent in chapter 4 and 7)).

The emergence of turbulence is one of the big issues in fluid dynamics. Researches like Von Karman, Reynolds, Orr, Sommerfeld, Tolmien, Schlichting and others have made great efforts in this area and it is now almost agreed upon seeing the problem as an instability phenomenon where the transition from laminar conditions to turbulent conditions in the boundary layer is caused by an overproduction of vorticity. The transition is possible if the Reynolds number is sufficiently high (above a certain $Re_{critical}$ based on the boundary-layer thickness).

In real flow conditions in ventilated rooms the conditions are nearly always such that the boundary layers are of turbulent nature.

The turbulent flow can under certain presumptions (see chapter 2) be described

$$\rho\frac{DU_i}{Dt} = -\frac{\partial P}{\partial x_i} + \mu\left[\frac{\partial^2 U_i}{\partial x_j^2}+\frac{\partial^2 U_j}{\partial x_i^2}\right] + \frac{\partial}{\partial x_j}\left(-\rho\overline{u_i u_j}\right) \qquad (1.2)$$

If we assume plane steady flow conditions and that V is small compared to U, that changes in the x-directions are small compared to changes in the y-direction, that the Reynolds stresses (see chapter 2) are large compared to viscous stresses and

that the pressure gradient is small, we can after some manipulations (*Engelund 1968*) obtain following relation

$$\rho\left[U\frac{\partial U}{\partial x}+V\frac{\partial U}{\partial y}\right] = \frac{\partial}{\partial y}\left(-\rho\overline{uv}\right) = \frac{\partial \tau}{\partial y} \tag{1.3}$$

We can under the presumptions made above which are the classic boundary layer approximations see that the forces of inertia are in equilibrium with the turbulent forces.

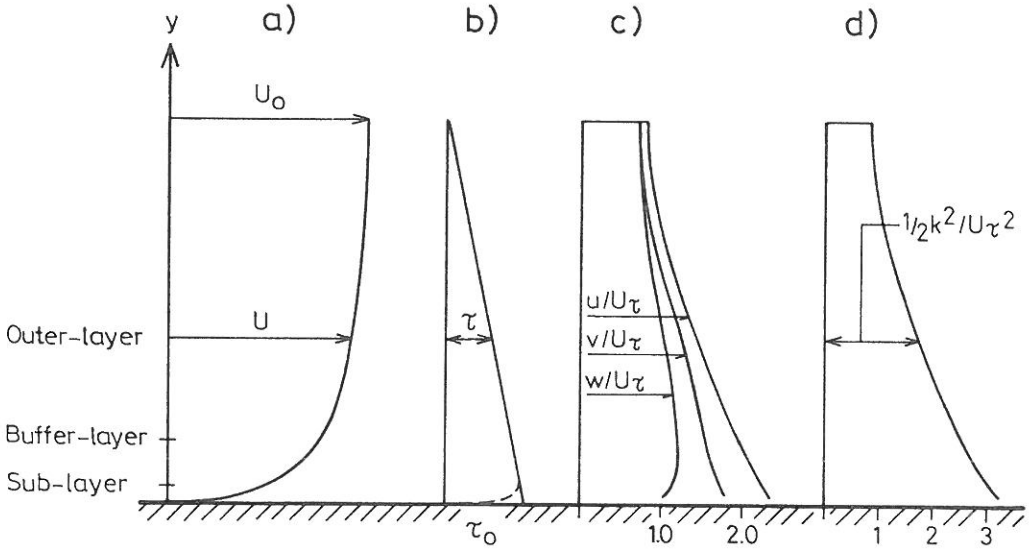

Figure 1.3. Schematic depiction of turbulent flow parameters based on measurement by Laufer 1949. a) Mean velocity profile. b) Shear stress. c) Velocity fluctuations. d) Turbulent kinetic energy. All measurements are made in air.

In order to be able to proceed with the investigations we have to assume that the velocity profiles and the turbulence are self-preserving

$$\begin{aligned} U_0-U &= U_\tau f\left[\frac{y}{\delta}\right] \\ -\overline{uv} &= U_\tau^2 g\left[\frac{y}{\delta}\right] \end{aligned} \tag{1.4}$$

This corresponds very well with measurements made by *Laufer 1949* in plane channel flow and flow in pipes (fig. 1.3) at high Reynolds numbers.

7

Fig 1.3a shows that the turbulent boundary layer can be sub-divided into three characteristic layers: The sub-layer, the buffer-layer and the outer-layer.

The sub-layer

In the sub-layer the dominant forces are arising from the molecular viscosity resulting in an almost constant level of shear stress. From (1.2) is obtained

$$\mu\frac{\partial^2 U}{\partial y^2} = \frac{\partial \tau}{\partial y} = 0 \Rightarrow$$
$$\mu\frac{\partial U}{\partial y} = \tau_0$$

and from (1.4) in connection with fig. 1.3b

$$\frac{\mu}{\rho}\frac{\partial U}{\partial y} = U_\tau^2 \Rightarrow$$
$$\frac{\rho U_\tau y}{\mu} = \frac{U}{U_\tau} \Rightarrow U^+ = y^+ \qquad (1.5)$$

The Outer-layer

In the outer-layer is the solution to (1.4) (*Engelund 1968*) equal to

$$\frac{U_0 - U}{U_\tau} = A \ln\left[\frac{\delta}{y}\right] + B$$

This equation can be written in the following form

$$\frac{U}{U\tau} = \frac{1}{\kappa}\ln\left[\frac{\rho U_\tau y}{\mu}\right] + 5.5 = \frac{1}{\kappa}\ln\left[E\frac{\rho U_\tau y}{\mu}\right]$$

or

$$U^+ = \frac{1}{\kappa}\ln y^+ + 5.5 \qquad (1.6)$$

The exact location of the sub- and the outer-layer is difficult to establish. *Laufer 1949* establishes the range of the sub- and buffer-layer to $0 < y^+ < 30$ and the outer layer from $y^+ > 30$. *Engelund 1968* on the other hand fixes the validity range of (1.5) to $0 < y^+ < 11.7$ and (1.6) from $y^+ > 11.7$ based on fully turbulent flow in pipes. Von Karman has proposed a three-layer model where (1.5) is valid in $0 < y^+ < 7$ and (1.6) in $y^+ > 30$ and a third relation in the buffer-layer.

1.2.3 Inlet devices and simplified models

It is previously mentioned that the momentum flow in the resulting jet influences the flow in the hole room and the jet is created by the inlet. Which kind of jet is determined by the geometrical design of the inlet diffuser and its location. It is

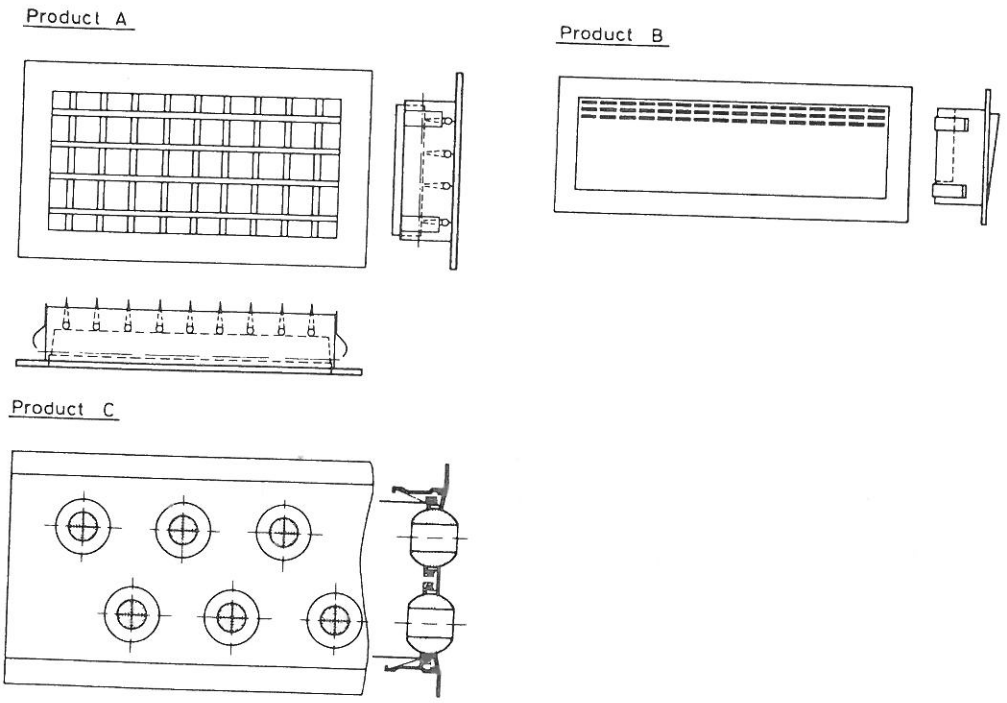

Figure 1.4. Different designs of inlet devices.

therefore very important that the inlet device is located according to it's specifications and the design of the room.

Fig 1.4 shows different designs of inlet devices investigated by *Heiselberg 1990* and *Nielsen et al. 1985*. Product A is a traditional wall mounted diffuser. This device is mounted on the wall at a distance from the ceiling. The resulting flow close to the diffuser has a circular jet structure. Product B and C is typical modern inlet diffusers. These are mounted on the wall in a distance of 0.2-0.3m from the ceiling with an upward directed air stream. The resulting flow has wall-jet character.

The design criterion for an air conditioning system is often based upon comfort parameters in the occupied zone, that is, in the isothermal case, draft (velocity and turbulence). For a long period of time the impact from turbulence on human comfort has been neglected, because our knowledge in this area has been limited and the accessibility of such data have been and still are difficult. This has lead to a comfort criterion based on the maximum mean velocity in the occupied zone of 0.15 m/s at 20°C (*Christensen 1983*).

The dimensioning of a ventilation system is done by a set of simplified models based on equation (1.1) and experimental data. The outline of the model is listed below (for a more comprehensive analysis is referred to *Nielsen 1988b*).

The decay of the maximum velocity in the centre line of the jet is described by

$$\frac{U_x}{U_0} = K_a \frac{\sqrt{a_0}}{x+x_0} \tag{1.7}$$

K_a is for fully turbulent jet flow a constant depending on the inlet geometry. For the inlet diffusers shown in fig. 1.4 the K_a-factor was found to be in the interval 2-5.5 (*Heiselberg 1990*). a_o is the effective inlet area defined as Q_o/U_o. For fully developed turbulent flow in the diffuser a_o is constant.

Assuming fully turbulent flow (that is, to assume self preserving flow patterns at different Reynolds numbers) in the diffuser and in the room the following relations are valid

$$U_{rm} = C_1 n \tag{1.8}$$

$$U_{rm} = C_2\sqrt{I_0} \tag{1.9}$$

By substituting (1.7) in (1.9) an expression for the velocity at the wall opposite the inlet wall can be derived

$$U_{rm} = U_0 f_1 K_a \frac{\sqrt{a_0}}{L} \quad , \quad where\ f_1 = \frac{U_{rm}}{U_L} \tag{1.10}$$

This relation is more universal than (1.8) and (1.9) and because of this it has been a subject of investigation by different authors (see e.g. *Hestad 1974*).

Recent research has shown that the turbulence level has a not neglible impact on the sensation of draft which has lead *Fanger and co-workers 1989* to propose a model of draft risk which is to be considered in the design process. The empirical model takes the local room temperature into account and predicts the percentage of dissatisfied people to be found in a room due to draft. For a room with a constant temperature of 20^{0}C the following empirical relation for sedentary persons is proposed

$$PD = 14(U-0.05)^{0.62}(0.37Tu+3.14) \tag{1.11}$$

1.3 Closure

The previous section has been a brief discussion of ventilation by the mixing principle. The complexities of the involving flow phenomena combined with often complex building designs turns the design of a ventilation system into a difficult task which is impossible to carry out without extensive full-scale experimental work.

Besides this the demand of higher efficiency of the air conditioning systems and lower inlet velocities have made the presumptions of fully turbulent flow inade-

quate. Recent studies have shown that so-called low Reynolds number (LRN) effects are present at lower velocities[1] (see e.g. *Restivo 1979*, *Murakami 1983*, *Heiselberg et al. 1987*, *Nielsen et al. 1988a* or *Chen 1990*). *Heiselberg 1987* showed experimentally that LRN effects are present, are dependent of the inlet device and are becoming more significant and important because modern inlet devices provides lower velocities in the occupied zone compared to traditional inlets.

The LRN effects are to a certain extent possible to include in the simplified models because a_o, K_a, x_o and f_1 all may be functions of the inlet velocity. The main disadvantages about the simplified models are that they require diffuser specific experiments and the velocity prediction is limited to the maximum velocity in the occupied zone. If e.g. the K_a factor is dependent of more than the inlet velocity (e.g. the flow-direction in front of the diffuser) it will only be possible in few cases to produce reliable results by the simplified models (*Heiselberg 1990*).

Comfort for the occupants does also include uniform conditions which are impossible to ensure by the simplified models and if calculation of the PD-index is required the only way of doing this will be through an extensive and expensive experimental effort.

Therefore the field of ventilation engineering has in recent years started to look upon computational fluid dynamics (CFD) as a design and analyzing tool because CFD offers a radical change in analytical design tools.

Up though the 1970 and -80 CFD showed that it was possible to predict the flow field in large domains with small openings (see e.g *Nielsen 1976*, *Nielsen 1978* or *Gosman et al. 1980*). In recent years further research by e.g *Davidson 1989* or *Chen 1988* has given more information in this area.

The work reported in this thesis is looking upon three-dimensional CFD as a modern analyzing tool in the scope of the new trends in the field of ventilation engineering.

1.3.1 Content of the Ph.D. work

This work is delimited to isothermal three-dimensional flow patterns in enclosures

[1] The flow patterns at lower air speed deviates from what one may expect under fully turbulent conditions

ventilated by the mixing principle. However, many of the ideas may be applied in other field of ventilation engineering or in other areas where CFD is used.

The scope of this work is:

- Through literature, numerical study and full-scale measurements to investigate three-dimensional flow patterns in rooms.

- To study and deepen existing three-dimensional methods for predicting incompressible turbulent flow.

- To investigate methods to model complicated inlet devices, which can be handled with the available computer resources (work-station level).

- To study low Reynolds number (LRN) phenomena experimentally and numerically.

- To verify the numerical results through experiments or literature.

The practical outcome of these studies is to produce some guidelines for use of CFD as a design tool.

1.3.2 Thesis outline

The following chapter of this thesis gives a description of the air movement in enclosures ventilated by the mixing principle and proposes a mathematical model for turbulent fluid flow.

Chapter 3 describes the solution techniques applied and discusses the particular problems related to prediction of flow fields in ventilated rooms.

In chapter 4 a rather simple application of CFD is presented in order to discuss the general performance of the mathematical model and relate this to the traditional simplified model approach.

5th chapter is a discussion of the experimental setup which is used to obtain mean-flow parameters in a room ventilated by a modern inlet diffuser. The apparatus and the measurering technique is presented and the specific experimental problems occurring are discussed.

Chapter 6 is a comparative study between the experimental results and the numerical predictions. Several approaches to model the inlet are presented.

Chapter 7 is a numerical investigation of the LRN phenomena in a two-dimensional geometry.

The final chapter draws together conclusions of this work and suggest areas of future research.

CHAPTER 2 - DESCRIPTION OF AIR MOVEMENT

2.1 Preamble

Turbulent flow is characterized by the appearance of random almost chaotic fluctuations in the flow. Contrary to laminar flow, which is believed to be described exactly, turbulent flow is to complex to describe exactly.

The emergence of turbulence is still a big issue in fluid dynamics and is not yet fully understood. But it is believed (as mentioned in the previous section) that turbulence is generated mainly by shear (e.g. in boundary or in shear layers) which is causing an overproduction of vorticity if the Reynolds number is sufficiently high. It is also believed that the transition from laminar to turbulent flow is an instability phenomenon and that turbulent flow is generally unstable. This can be illustrated in the following way. If a turbulent flow is perturbated, the perturbation will normally amplify while under laminar conditions the perturbation dies out (*Lesiur 1987*).

If one want to be able to predict the turbulence one have to accept the fact that even if the phenomenon isn't fully understood it is at least deterministic and governed by the basic equations of fluid dynamics.

Due to the extraordinary development in available computer capacity CFD has in the last 2-3 decades become a large field of research. The different approaches to prediction of turbulent flows can roughly be divided in two categories.

Direct numerical simulation (DNS) compute the time-dependent solutions of (2.3) and (2.4) with a very fine grid resolution in order to capture all scales of the turbulent eddies. In order to resolve e.g. isotropic turbulence *Page 1990* states that a three-dimensional grid of 128*128*128 will be limited to a Reynolds number of 500. This means that computer resources have to be developed immensely before the method is applicable in engineering problems. A similar approach is taken by the large eddy simulation (LES) approach. This method resolves only the largest and most important scales of the turbulent spectrum and uses a simple relation to compute the smaller scales. This method is much less demanding in terms of necessary computer resources, but is still too demanding for use in engineering types of flow calculations on work-station level. Attempt to use this method in prediction of air flow patterns in rooms has been done e.g. by *Murakami et al. 1986*.

The other category of turbulence modeling, which is used in present work, is a statistical approach. The approach looks upon an ensemble of investigations taken over a period of time. If this ensemble of investigations is averaged then Reynolds proposed that the instantaneous value may be regarded as a mean and a fluctuating part (*Schlicthing 1960*)

$$\Phi = \overline{\Phi} + \Phi' \quad or \qquad \Phi = \Phi + \phi \tag{2.1}$$

The latter notation of (2.1) is used throughout this thesis.

2.2 The mathematical model

The mathematical model, which will be set up in this chapter is based upon the governing equations for fluid dynamics and the latter of the two approaches of turbulence modelling - the statistical approach - mentioned in the preamble.

2.2.1 The flow equations

The governing equations for fluid motion are described by the Navier-Stokes equations, which essentially are Newtons 2. law of motion, and conservation of mass. The equations are here written in conservation form which is the most suitable form for the solution scheme applied in chapter 3.

$$\frac{\partial}{\partial t}(\rho U_i) + \frac{\partial}{\partial x_i}(\rho U_i U_j) = \frac{\partial \sigma_{ij}}{\partial x_j} + \rho F_i \tag{2.2}$$

$$\frac{\partial \rho}{\partial t} + \frac{\partial}{\partial x_i}(\rho U_i) = 0 \tag{2.3}$$

By applying Stokes hypothesis to the stress-tensor in (2.2) following equation occur

$$\frac{\partial}{\partial t}(\rho U_i) + \frac{\partial}{\partial x_i}(\rho U_i U_j) = -\frac{\partial P}{\partial x_i} + \frac{\partial}{\partial x_i}\left[\mu\left[\frac{\partial U_i}{\partial x_j} + \frac{\partial U_j}{\partial x_i} - \frac{2}{3}\delta_{ij}\frac{\partial U_k}{\partial x_k}\right]\right] + \rho F_i \tag{2.4}$$

Stokes hypothesis is still a matter of dispute, but quite a large number of experimental verifications have been made and it has proven to be at least an excellent approximation for most kind of flows (*Schlichting 1960*).

As present work only deals with stationary incompressible isothermal airflow the equations can be simplified.

Conservation of mass

$$\frac{\partial}{\partial x_i}(\rho U_i) = 0 \tag{2.5}$$

Conservation of momentum

$$\frac{\partial}{\partial x_i}(\rho U_i U_j) = -\frac{\partial P}{\partial x_i} + \frac{\partial}{\partial x_i}\left[\mu\left[\frac{\partial U_i}{\partial x_j} + \frac{\partial U_j}{\partial x_i}\right]\right] + \rho F_i \tag{2.6}$$

This relation is the description of laminar as well as turbulent flow. The problem is that the inhomogeneity and the unlinearity of the equations makes it impossible to solve the equations theoretically (solutions exist only in very few simple flows). For high Re-numbers the ulinearities become very difficult to resolve because the length scales for the important eddies decreases. By looking at the time-averaged flow field from a statistical point of view it is possible to develop a model which describes the macroscopic behavior of the turbulent motion.

A typical responds for a turbulent velocity field recorded in a full scale measurement of air flow in a ventilated room is shown in fig. 2.1.

The velocities are represented by a mean and a fluctuating part as in (2.1). The velocity variable is treated as statistical variables and regarded as normal-distributed.

$\Phi_i = \Phi_i + \phi_i$ *instantaniously value (Reynolds decomposition)*
$\overline{\Phi_i} = \Phi_i + \overline{\phi_i}$, $\overline{\phi_i} = 0$, *time-averaged value*

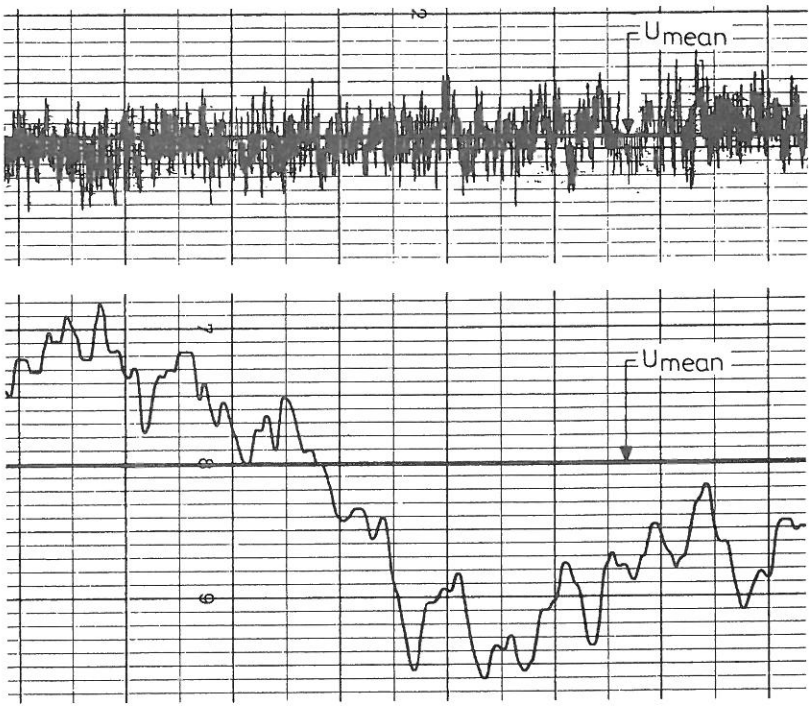

Figure 2.1. Typical recording of a turbulent velocity measurement in a ventilated room (hotwire measurements in air). The figure shows two different recordings of a turbulent velocity. It shows that the length of time in which the turbulent velocity signal (or any turbulent signal) is recorded is important in order to record all turbulent scales. In order to use Reynolds decomposition one must at least have a turbulent signal like the first of the two recordings. ($U_{mean} = U$).

This velocity field is imposed in (2.5) and (2.6) resulting in following relations

Time-averaged conservation of mass

$$\frac{\partial}{\partial x_i}\left(\rho\left(\overline{U_i+u_i}\right)\right) = 0 \quad \Rightarrow$$

$$\frac{\partial}{\partial x_i}\left(\rho U_i\right) = 0 \tag{2.7}$$

Time-averaged conservation of momentum

$$\frac{\partial}{\partial x_i}\left(\rho\left(\overline{U_i+u_i}\right)\left(\overline{U_j+u_j}\right)\right) = -\frac{\partial(\overline{P+p})}{\partial x_i} + \frac{\partial}{\partial x_i}\left[\mu\left[\frac{\partial(\overline{U_i+u_i})}{\partial x_j} + \frac{\partial(\overline{U_j+u_j})}{\partial x_i}\right]\right] + \rho F_i \Rightarrow$$

$$\frac{\partial}{\partial x_i}\left(\rho U_i U_j\right) = -\frac{\partial P}{\partial x_i} + \frac{\partial}{\partial x_i}\left[\mu\left[\frac{\partial U_i}{\partial x_j} + \frac{\partial U_j}{\partial x_i}\right] - \rho\overline{u_i u_j}\right] + \rho F_i \qquad (2.8)$$

Equation (2.7) and (2.8) describes the time-averaged behavior of the turbulent fluid motion. As seen these equations are similar to (2.5) and (2.6). The equation for conservation of mass is exactly the same while the equation for conservation of momentum has an additional second order tensor term. The term $\rho\overline{u_i u_j}$ is called Reynolds stress and the calculation of this tensor is the essence of statistical turbulence modeling.

2.2.2 Reynolds stresses and turbulent viscosity

Reynolds stresses or apparent turbulent stresses has following definition

$$\sigma_{Re} = \rho\overline{u_i u_j} \qquad (2.9)$$

and may interpreted in the following way. In calculation of the mean velocity field the exchange of momentum coming from the turbulent fluctuations is neglected. This may be done if additional apparent stresses (Reynolds stresses) are calculated.

Equation (2.7) and (2.8) constitutes a set of equations which describes turbulent motion, but it isn't possible to solve the set of equations because the appearance of the velocity fluctuations make the set incomplete. In order to be able to solve the set of equations it must be made complete by a model of the stresses. This type of turbulence model is described as closure modeling. The closure modeling can at present be divided in two groups : x-equations models and Reynolds stress models. The former group uses the Boussinesq eddy-viscosity approximation (see later) which the latter do not.

In the work presented in this report the eddy-viscosity concept is used in the high Reynolds number model as well as in the low Reynolds version. The models will be discussed in the subsequent, but first a couple of remarks about the stress modelling

approach.

In complex turbulent flows (e.g. recirculating or swirling flows) the Boussinesq approximation and the x-equation models are considered inadequate to represent the turbulence. Therefore the Reynolds stresses are calculated explicitly by differential transport equations. Much work has been done in this area (e.g. Chou, Rotta, Rodi or Launder and the group at UMIST, UK) (see e.g. *Rodi 1980* or *Nallasamy 1987*) but mostly in the area of turbulence research. Although promising results have been achieved (e.g. *Ince et al. 1986*) the use of Reynolds stress closures are still too complicated and too cpu-demanding for use in engineering problems.

Boussinesq eddy viscosity concept relates the Reynolds stresses to a turbulent viscosity which, in contrast to the molecular viscosity, is not a fluid property but depends on the nature of the turbulence. Boussinesq 1877 assumed that the turbulent stresses are proportional to the mean velocity gradients (*Rodi 1980*)

$$-\rho\overline{u_i u_j} = \mu_t \left(\frac{\partial U_i}{\partial x_j} + \frac{\partial U_j}{\partial x_i} \right) - \frac{2}{3}\rho k \delta_{ij} \tag{2.10}$$

The analogy with the stress tensor (- and Stokes hypothesis) is seen clearly. The last term including the Kronecker delta is necessary to fulfill the standard definition of turbulent kinetic energy (the sum of the normal stresses must be equal to the trace of the Reynolds stress tensor)

$$-\rho \left(\overline{u^2} + \overline{v^2} + \overline{w^2} \right) = \mu_t 2 \left(\frac{\partial U}{\partial x} + \frac{\partial V}{\partial y} + \frac{\partial W}{\partial z} \right) - \frac{2}{3}\rho 3k = -2k$$

The basic idea behind the Boussinesq approximation is, as stated above, the analogy between molecular motion and motion of the eddies. This idea cannot be fully correct simply because there is a conceptional difference between turbulence and small "lumps" of fluid exchanging momentum. Nevertheless eq. (2.10) has proven to work well in many flow situations.

By introducing (2.10) in (2.8) the task is reformulated to, instead of finding the Reynolds stresses, to finding the turbulent viscosity. A number of such models has been developed by different authors and in the following paragraph some of them

are discussed.

Prandtls mixing length hypothesis was one of the first models of turbulent viscosity (*Nallasamy 1987*). The mixing length hypothesis calculates the turbulent viscosity from the mean velocity field

$$\mu_t = \rho C_\mu l^2 \left| \frac{\partial U}{\partial y} \right| \tag{2.11}$$

As seen is the turbulent viscosity calculated directly from the velocity field aided by a "mixing length" parameter, l. This "mixing length" parameter is the main drawback of the model, because it has to be modified for different kinds of flows and it is very difficult to evaluate for more complex types of flow. The "mixing length" parameter has also to account for transport of turbulence and other history effects. The model has, however, been used with success in shear- and boundary-layer flows where l can be determined (e.g. by Nikuradses experiments in tubes or by von Karmans similarity hypothesis (*Schlichting 1960*)).

In order to overcome the problem of transport of turbulence, one-equation models based on the turbulent kinetic energy, instead of the mean velocity gradients only, has been developed. These models have never become very popular because the length scale parameter still has to be specified throughout the flow domain (or calculated) according to the flow type and structure.

In attempt to eliminate the need for specification of the length scale parameter throughout the flow regime Harlow and Spalding indepently made proposals for a two-equation model. The k-equation was, as in the one-equation models, used as variable in the first equation. For determination of the length scale different proposals has been made, but the choice of the dissipation of turbulent kinetic energy, ϵ has now become the most widely used and the k,ϵ-model is possibly, at this time, the best choice for a turbulence model for engineering proposals.

The k,ϵ-model is used in all calculations made is this thesis, both in a high Reynolds number form and a low Reynolds number form and is therefore discussed in greater detail in the following section.

2.2.3 The effective viscosity concept and the k,ϵ-model

It is possible to derive an exact transport equation for the turbulent kinetic energy and its dissipation from the Navier-Stokes equations (2.8), but this only leads to more unknown correlations of the velocity fluctuations. So what we are looking for is a modelled form of the k and ϵ equations which are dependent of the mean velocity field only.

The use of Boussinesq approximation lead to Navier-Stokes equation on the following form

$$\frac{\partial}{\partial x_i}(\rho U_i U_j) = -\frac{\partial P}{\partial x_i} + \frac{\partial}{\partial x_j}\left[\mu+\mu_t\left[\frac{\partial U_i}{\partial x_j} + \frac{\partial U_j}{\partial x_i}\right]\right] - \frac{2}{3}\rho\delta_{ij}\frac{\partial k}{\partial x_i} + \rho F_i \qquad (2.12)$$

where the effective viscosity is defined as the sum of the molecular viscosity and the turbulent viscosity

$$\mu_{eff} = \mu + \mu_t \qquad (2.13)$$

In the k,ϵ-model the turbulent viscosity is approximated in the following way (*Rodi 1980*)

$$\mu_t = \rho C_\mu \frac{k^2}{\varepsilon} \qquad (2.14)$$

k and ϵ are defined

$$k = \frac{1}{2}\left(\overline{u^2} + \overline{v^2} + \overline{w^2}\right)$$
$$\varepsilon = \frac{\mu}{\rho}\left[\overline{\frac{\partial u_i}{\partial x_j}\frac{\partial u_i}{\partial x_j}}\right] \qquad (2.15)$$

It is seen that the turbulent kinetic energy is a direct measure for the intensity of the velocity fluctuations in the three directions and the dissipation of the turbulent kinetic energy is equal to the mean-vorticity arising from the velocity fluctuations

times the molecular viscosity. To be able to make the definitions above, one must assume high Reynolds number flow where local isothophy in the small scale fluctuations prevails. (That the large scale turbulence and the small scale turbulence are so much apart in the spectrum that any anisotrophy in the large scale turbulence doesn't affect the smallest eddies).

The k and ϵ equations are modelled as follows (*Rodi 1980*)

$$\frac{\partial}{\partial x_i}(\rho U_i k) = \frac{\partial}{\partial x_i}\left[\frac{\mu_t}{\sigma_k}\frac{\partial k}{\partial x_i}\right] + \mu_t \frac{\partial U_i}{\partial x_j}\left[\frac{\partial U_i}{\partial x_j}+\frac{\partial U_j}{\partial x_i}\right] - C_D \rho \varepsilon \qquad (2.16)$$

convection = diffusion + production − destruction

$$\frac{\partial}{\partial x_i}(\rho U_i \varepsilon) = \frac{\partial}{\partial x_i}\left[\frac{\mu_t}{\sigma_\varepsilon}\frac{\partial \varepsilon}{\partial x_i}\right] + C_1 \mu_t \frac{\varepsilon}{k}\frac{\partial U_i}{\partial x_j}\left[\frac{\partial U_i}{\partial x_j}+\frac{\partial U_j}{\partial x_i}\right] - C_2 \rho \frac{\varepsilon}{k}\varepsilon \qquad (2.17)$$

convection = diffusion + production − destruction

The parameters σ_ϵ, σ_k, C_1, C_2, C_D and C_μ are regarded as constants in the sense that they do not change within the calculation (*Nallasamy 1987*). The values are found to (*Launder et al. 1974*)

$$C_\mu = 0.09,\ C_1 = 1.44,\ C_2 = 1.92,\ \sigma_k = 1.0,\ \sigma_\varepsilon = 1.3,\ C_D = 1.0$$

The determination of the model and its constants are discussed in detail by e.g. *Launder et al. 1974, Rodi 1980.*

Equation (2.16) to (2.18) constitutes the k,ϵ turbulence model for high Reynolds numbers (i.e. fully turbulent flow) and the use of it has been quite successful in engineering types of flow. The validity of the equations are restricted to regions away from no-slip boundaries. This problem is normally dealt with by calculating the velocity outside the boundary-layer and impose this velocity as boundary condition for the momentum and turbulence equations (this topic will be discussed in the next chapter). This approach is of course valid only if the flow is fully turbulent. If, on the other hand, the flow show signs of being influenced by viscous effects e.g. in boundary-layer flow, low Reynolds number (LRN) effects in transitional flow or if one needs to determine the velocities in the near-wall region

for use in heat transfer calculation, the high Reynolds number k,ϵ-model is difficult to use. This fact has promoted a series of LRN proposals of the k,ϵ-model where the viscous forces are taken into account. *Patel et al. 1985* reviewed several forms of LRN k,ϵ-model. Some differences were recorded but the models of *Launder and Sharma 1978, Chien 1982, Lam and Bremhost 1981* and *Wilcox and Rubesin 1980* yielded comparable results and were performing considerably better than the rest.

In the calculations in this thesis the Launder-Sharma version of the Jones-Launder model is used. The model takes following form

$$\mu_t = \rho C_\mu f_\mu \frac{k^2}{\tilde{\varepsilon}} \tag{2.18}$$

$$\tilde{\varepsilon} = \varepsilon - 2\frac{\mu}{\rho}\left[\frac{\partial}{\partial x_i}\left[\frac{\partial \sqrt{k}}{\partial x_j}\right]\right] \tag{2.19}$$

$$\frac{\partial}{\partial x_i}(\rho U_i k) = \frac{\partial}{\partial x_i}\left[\frac{\mu_t}{\sigma_k}\frac{\partial k}{\partial x_i}\right] + \mu_t \frac{\partial U_i}{\partial x_j}\left[\frac{\partial U_i}{\partial x_j} + \frac{\partial U_j}{\partial x_i}\right] - C_D \rho \tilde{\varepsilon} \tag{2.20}$$

convection = diffusion + production - destruction

$$\frac{\partial}{\partial x_i}(\rho U_i \tilde{\varepsilon}) = \frac{\partial}{\partial x_i}\left[\frac{\mu_t}{\sigma_\varepsilon}\frac{\partial \tilde{\varepsilon}}{\partial x_i}\right] + C_1 f_1 \mu_t \frac{\tilde{\varepsilon}}{k}\frac{\partial U_i}{\partial x_j}\left[\frac{\partial U_i}{\partial x_j} + \frac{\partial U_j}{\partial x_i}\right] - C_2 f_2 \rho \frac{\tilde{\varepsilon}}{k}\tilde{\varepsilon} + C_3 \frac{\mu \mu_t}{\rho}\left[\frac{\partial}{\partial x_i}\left[\frac{\partial U_j}{\partial x_k}\right]\right]^2 \tag{2.21}$$

convection = diffusion + production - destruction

As seen is the low Reynolds number version of the k,ϵ-model similar in form to the high Reynolds number model. The models are identical if the flow is fully turbulent.

The low Reynolds number effects are introduced via a set of functions with values in the interval 0-1. The set of functions is determined by looking at the behavior of the turbulent boundary-layer flow (section 1.2.2). The parameters σ_ϵ, σ_k, C_1, C_2, C_D and C_μ has the same values as in the high Reynolds number version. C_3 is equal to 2.

The function f_μ mimics the direct effects of the molecular forces by adapting the

turbulent viscosity (i.e. the turbulent stress) to the appropriate level according to the distance to the wall. f_μ is a function of the turbulent Reynolds number, $R=\rho k^2/\mu\,\tilde{\epsilon}$, going from 0.033 to 1

$$f_\mu = \exp\left[\frac{-3.4}{\left(1+\frac{R}{50}\right)^2}\right] \tag{2.22}$$

The function f_1 is together with the extra source term in (2.21) is increasing the $\tilde{\epsilon}$-level. The extra source term is introduced because of the substitution of the dissipation variable ϵ to $\tilde{\epsilon}$. This shift is chosen because it offers computational advantages in the $\tilde{\epsilon}$ boundary condition (*Jones et al. 1972*). However the shift has the effect that $\tilde{\epsilon}$ decreases very rapidly when approaching the wall and consequently the solution may be grid dependent (*Patel et al. 1985*). f_1 is equal to 1 in the model proposed by Launder, Jones and Sharma which means that all the viscous dissipation in the near-wall region is added via the extra source term.

The last function, f_2 in (2.21) is determined by experiments and incorporates LRN effects in the destruction term. The function is constructed so that the decay of isotropic grid turbulence in a shear free flow corresponds to the measured decay rate (*Jones et al. 1972*).

$$f_2 = 1 - 0.3\exp\left(-R^2\right) \tag{2.23}$$

2.3 Closure

In this chapter some aspects of turbulent air flow has been discussed. On the basis of statistical turbulence theory a mathematical model for the time-averaged velocity field is established. The model uses the Boussinesq approximation for the Reynolds stresses which introduces an apparent turbulent viscosity. To calculate this turbulent viscosity the k,ϵ-model is derived from the momentum equations using physical reasoning. The k,ϵ-model is presented both in a high Reynolds number version for use in fully turbulent flow away from boundary-layers and in a LRN version for application at lower Reynolds numbers and in boundary-layer or transitional flow.

The mathematical model is too complicated for a general theoretical solution so

one must look a particular numerical solution. This is the topic of the next chapter.

2.3.1 The governing equations in general form

All the equations in the mathematical model are transport equations (except the equation for mass conservation). Equations of this form can be expressed in a general form which is more comprehensive for the numerical discretisation

$$\frac{\partial}{\partial x_i}(\rho U_i \Phi) = \frac{\partial}{\partial x_i}\left[\Gamma_\Phi \frac{\partial \Phi}{\partial x_i}\right] + S_\Phi \tag{2.24}$$

where Φ, Γ_Φ and S_Φ is shown in table 2.1. and the constants in table 2.2.

Equation	Φ	Γ_Φ	S_Φ
Continuity	1	0	0
U	U	μ_{eff}	$-\frac{\partial\left[P+\frac{2}{3}\rho k\right]}{\partial x_i}+\frac{\partial}{\partial x_j}\left[\mu_{eff}\left[\frac{\partial U_i}{\partial x_j}+\frac{\partial U_j}{\partial x_i}\right]\right]$
V	V	μ_{eff}	
W	W	μ_{eff}	
k, high Re	k	μ_t/σ_k	$\mu_t\frac{\partial U_i}{\partial x_j}\left[\frac{\partial U_i}{\partial x_j}+\frac{\partial U_j}{\partial x_j}\right]-C_D\rho\varepsilon$
k, low Re	k	μ_t/σ_k	$\mu_t\frac{\partial U_i}{\partial x_j}\left[\frac{\partial U_i}{\partial x_j}+\frac{\partial U_j}{\partial x_j}\right]-C_D\rho\tilde{\varepsilon}$

ϵ, high Re	ϵ	μ_t/σ_ϵ	$C_1\mu_t\frac{\varepsilon}{k}\frac{\partial U_i}{\partial x_j}\left[\frac{\partial U_i}{\partial x_j}+\frac{\partial U_j}{\partial x_i}\right]-C_2\rho\frac{\varepsilon}{k}\varepsilon$
ϵ, low Re	$\tilde{\epsilon}$	μ_t/σ_ϵ	$C_1 f_1\mu_t\frac{\tilde{\varepsilon}}{k}\frac{\partial U_i}{\partial x_j}\left[\frac{\partial U_i}{\partial x_j}+\frac{\partial U_j}{\partial x_i}\right]-C_2 f_2\rho\frac{\tilde{\varepsilon}}{k}\tilde{\varepsilon}+C_3\frac{\mu\mu_t}{\rho}\left[\frac{\partial}{\partial x_i}\left[\frac{\partial U_j}{\partial x_k}\right]\right]^2$

Table 2.1. The definition of the terms Φ, Γ_Φ and S_Φ of (2.24).

The k-ϵ model.	Fully turbulent version.	LRN version.
C_μ	0.09	0.09
$C_{\epsilon 1}$	1.44	1.44
$C_{\epsilon 2}$	1.92	1.92
$C_{\epsilon 3}$	-	2
σ_k	1.0	1.0
σ_ϵ	1.3	1.3
f_μ	1.0	$\exp(-3.4/(1+R/50)^2)$
f_1	1.0	1.0
f_2	1.0	$1-0.3\exp(-R^2)$

Table 2.2. The turbulent model constants and functions. $R = \rho k^2/\mu\,\tilde{\epsilon}$.

CHAPTER 3 - SOLUTION OF THE FLOW EQUATIONS

3.1 Preamble

The equations (2.24), table 2.1 and 2.2 describes the fluid flow under stationary, isothermal and incompressible conditions. The equations are in general inhomogeneous, highly non-linear and strongly coupled. Further are the flow equations in general too complicated to be dealt with by analytical means so numerical solution techniques are the only way to achieve solutions of the equations.

In this chapter a step-by-step discussion of the applied numerical method to obtain approximate solutions of the governing equations is made.

Before choosing the numerical solution algorithm it is essential to look at the characteristics of the set of partial differential equations (PDEs). The governing equations presented in chapter 2 are of elliptic nature, which means that a perturbation in a certain part of the solution domain influences the whole solution domain. This means that in order to have a well posed problem[1] one must provide boundary conditions at all boundaries for all dependent variables. In contrast to e.g. the characteristics of parabolic flow, where it is possible to obtain a local solution in a point immediately adjacent to a boundary by a series expansion, one must in elliptic flow regimes obtain the solution for all variables in the whole flow domain simultaneously.

The next consideration is to choose the discretisation technique. In the field of CFD three different techniques has become very popular : the finite difference method (FD), the finite element method (FEM) and the finite volume method (FV). Other techniques such as e.g. spectral methods is also used but the author is of the opinion that the former three methods still are the most widely used. In this work the FV approach is used. This method implies overall integral conservation of all quantities (mass and momentum) (*Patankar 1980*). In fact this feature is together with its direct physical interpretation the main reason for its popularity. Many of the techniques of deriving the discretisation equations in the FV method are similar to the methods used in FEM, while the appearance of the discretisation equations are similar to the FD approach.

[1] A well posed problem is if a solution exist, is unique and depends continuously on the boundary conditions.

3.2 Solution procedure

Numerical solution of eq. (2.24) involve different steps which will be discussed in this section. The discussion includes only steps which are directly relevant to the numerical procedure used to obtain the results presented in this thesis. If the reader wish to go deeper into the FV-technique for other purposes it is referred to e.g. *Patankar 1980, Launder et al. 1974* or *Gosman et al. 1977.*

Numerical solutions imply that the calculation domain is broken into a finite number of cells (volumes) where all variables are represented by a value located in a gridpoint in the mesh of computational cells. A set of algebraic equations containing information of the all the discrete values is constructed by integrating the governing general equation over a finite three-dimensional space (finite volume). This set of algebraic equations is solved by applying proper boundary conditions, i.e. the obtained numerical solution of the differential equations is not a general solution but a particular solution involving particular boundary conditions.

3.2.1 Integration and discretisation

The general equation (2.24) is integrated over a control volume (cell) in the solution domain (for notation se fig. 3.1)

$$\int_V \frac{\partial}{\partial x_i}\left(\rho U_i \Phi\right) dV - \int_V \frac{\partial}{\partial x_i}\left[\Gamma_\Phi \frac{\partial \Phi}{\partial x_i}\right] dV = \int_V S_\Phi dV \tag{3.1}$$

In the FV technique it is assumed that the variable Φ is piecewise linear between the gridnodes and that the fluxes over the surfaces are constant over the whole surface. If the dependent variable further is treated one-dimensional, it is possible to obtain following coefficient equation (for a more comprehensive derivation se appendix 3.1)

$$\Phi_P\left(a_E+a_W+a_N+a_S+a_D+a_U\right) =$$
$$\Phi_E a_E+\Phi_W a_W+\Phi_N a_N+\Phi_S a_S+\Phi_D a_D+\Phi_U a_U+\left(S_P\Phi_P+S_C\right)\Delta x\Delta y\Delta z \Rightarrow$$

$$\Phi_P a_P = \sum_K \Phi_K a_K + S_C \Delta x \Delta y \Delta z \tag{3.2}$$

Where the coefficient is defined as follows

$$a_E = (\Gamma_\Phi)_e \frac{A_e}{\delta_e} - A_e \frac{(\rho U)_e}{2} \quad , \quad a_W = (\Gamma_\Phi)_w \frac{A_w}{\delta_w} + A_w \frac{(\rho U)_w}{2} \tag{3.3}$$

$$a_N = (\Gamma_\Phi)_n \frac{A_n}{\delta_n} - A_n \frac{(\rho V)_n}{2} \quad , \quad a_S = (\Gamma_\Phi)_s \frac{A_s}{\delta_s} + A_s \frac{(\rho V)_s}{2} \tag{3.4}$$

$$a_D = (\Gamma_\Phi)_d \frac{A_d}{\delta_d} - A_d \frac{(\rho W)_d}{2} \quad , \quad a_U = (\Gamma_\Phi)_u \frac{A_u}{\delta_u} + A_u \frac{(\rho W)_u}{2} \tag{3.5}$$

It is important to notice that the coefficients are equal to the sum of mass flow and the diffusion conductance over a cell face. This will be used to introduce boundary conditions (sec. 3.2.5).

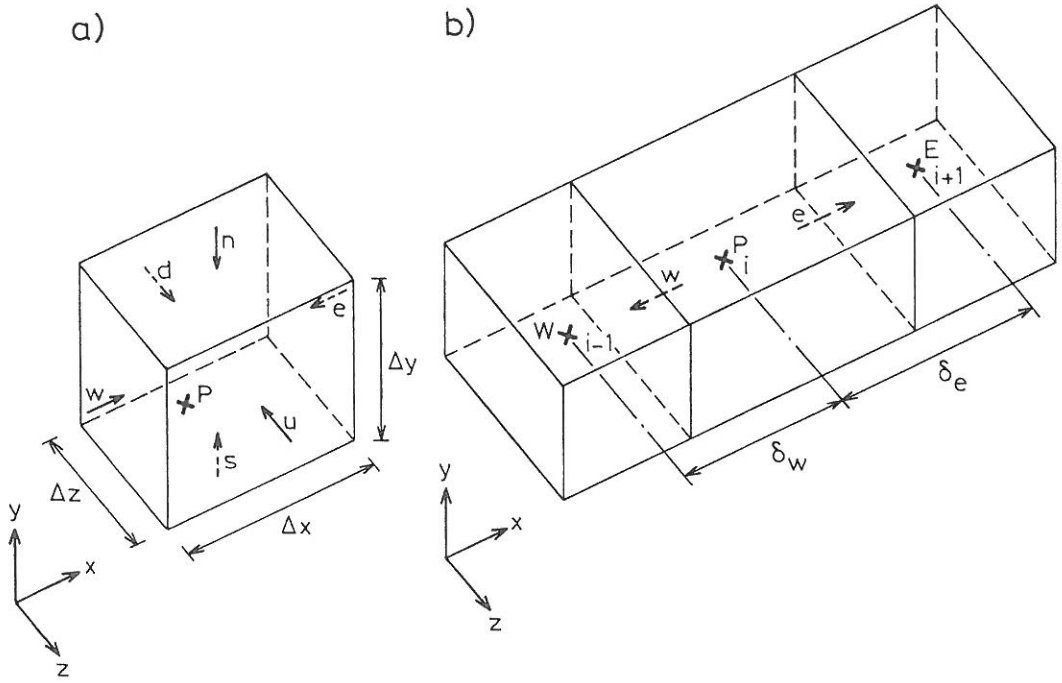

Figure 3.1. Computational cell with grid information. a) A single three-dimensional volume. b) A x-array of three-dimensional volumes.

3.2.2. Differencing schemes

If the coefficients in (3.3)-(3.5) are examined it is noticed that the coefficients may become negative if the absolute value of the Peclet number (which in isothermal flow correspond to the cell Reynolds number) defined as

$$Pe = Re_{cell} = \frac{\delta_e(\rho U)_e}{\Gamma_\Phi} \tag{3.6}$$

is greater that 2. This occurrence violates one of the main rules in the FV technique, namely the Scarborough criterion (*Patankar 1980*) which says that

$$|a_P| \leq \sum_K |a_K| \quad (must\ be\ < in\ at\ least\ one\ eq.) \tag{3.7}$$

The criterion is a sufficient condition for convergence of a numerical problem with at least one solution method (the Gauss-Seidel method). Although this method isn't applied in this work fulfillment of the criterion will still be required.

The coefficients in (3.3)-(3.5) arises from a gradient interpolation over a cell border (appendix 3.1) of the form

$$\left[\frac{\partial \Phi}{\partial x}\right]_e = \frac{\Phi_E - \Phi_P}{\delta_e} \Rightarrow \Phi_e = \frac{1}{2}(\Phi_E + \Phi_P) \tag{3.8}$$

This approximation of the differential quotient is known as central differencing (CD). The scheme can be shown to be second order accurate in terms of truncation errors (*Skovgaard 1988*), but it has big limitations in high Reynolds number flows if one requires the criterion in eq. (3.7) fulfilled.

In order to improve the numerical stability of the differencing procedure a lot of work have been done to develop more stable methods to approximate the gradient term. Among the schemes which is used as alternatives in present work is the power-law scheme PLDS (*Patankar 1980*), the hybrid scheme HYB (*Patankar 1980*) and quadratic upstream weighted interpolation for convective kinematics QUICK

(*Leonard 1979*).

The general equation (2.24) can be solved analytically for the one-dimensional convection-diffusion (advection-dispersion) case. This solution is introduced in the equation and is integrated over a volume. If the total flux over the cell is modelled by this exact solution it results in a discretisation equation which describes the behavior of the one-dimensional convection-diffusion problem (see appendix 3.2). This scheme - the exponential scheme - is nevertheless not very widely used. First of all it is only exact for the one-dimensional case mentioned and secondly it is rather expensive to compute. But the knowledge from the behavior of the variable can be used to construct a more easy to use approximation scheme.

The first scheme is the HYB scheme which approximate the curve of the exact one-dimensional solution in three different intervals by three straight lines.

$$\text{For } (Pe)_e < -2 : \quad a_E = -A_e \frac{(\Gamma_\Phi)_e}{\delta_e} (Pe)_e$$

$$\text{For } |(Pe)_e| \leq 2 : \quad a_E = A_e \frac{(\Gamma_\Phi)_e}{\delta_e} \left[1 - \frac{(Pe)_e}{2} \right]$$

$$\text{For } (Pe)_e > 2 : \quad a_E = 0$$

The scheme can be expressed in a more compressed and for the numerical use a more comprehensive form

$$a_E = A_e \frac{(\Gamma_\Phi)_e}{\delta_e} MAX \left[-(Pe)_e \, , \, 1 - \frac{(Pe)_e}{2} \, , \, 0 \right] \tag{3.9}$$

The PLDS scheme gives an even better approximation of the exact solution. The improvements of introducing the PLDS scheme is mainly in the Pe range around 2 where the HYB scheme has the biggest deviation from the exact solution

$$For\ (Pe)_e<-10:\quad a_E = -A_e\frac{(\Gamma_\Phi)_e}{\delta_e}(Pe)_e$$

$$For\ -10<(Pe)_e<0:\quad a_E = A_e\frac{(\Gamma_\Phi)_e}{\delta_e}\left(\left(1+0.1(Pe)_e\right)^5-(Pe)_e\right)$$

$$For\ 0<(Pe)_e<10:\quad a_E = A_e\frac{(\Gamma_\Phi)_e}{\delta_e}\left(1-0.1(Pe)_e\right)^5$$

$$For\ (Pe)_e>10:\quad a_E = 0$$

Which in the more compressed form can be expressed

$$a_E = A_e\frac{(\Gamma_\Phi)_e}{\delta_e}MAX\left[0\ ,\ \left(1-(Pe)_e\right)^5\right] + A_e\frac{(\Gamma_\Phi)_e}{\delta_e}MAX\left[0\ ,\ -(Pe)_e\right] \qquad (3.10)$$

The last scheme used in this thesis is the QUICK scheme. The aim with this scheme is to have a scheme which is as accurate as the CD scheme but more stable. The method fits the Φ variable on the volume interface by a second order polynomial. Different schemes has been proposed e.g. *Hodge et al. 1979* or *Leonard 1979*. The scheme proposed by Leonard is used in this work. The scheme can be interpreted as a central differencing scheme with a stabilizing upstream weighted curvature correction arising from the second order polynomial fit.

$$\Phi_e = \frac{1}{2}(\Phi_E+\Phi_P) - \frac{\delta_e^2}{8}CURV_e$$

If the grid is uniformly distributed the above equation can be written

$$For\ \Phi_e>0:\ \Phi_e = \frac{1}{2}(\Phi_E+\Phi_P) - \frac{1}{8}(\Phi_W-2\Phi_P+\Phi_E)$$

$$For\ \Phi_e<0:\ \Phi_e = \frac{1}{2}(\Phi_E+\Phi_P) - \frac{1}{8}(\Phi_P-2\Phi_E+\Phi_{EE})$$

If the grid on the other hand isn't uniformly distributed the calculation is more tiresome and therefore left out her (for detail of the derivations is referred to *Skovgaard 1988, Huang 1986* or *Davidson 1989*). For non-uniform grid the QUICK scheme is as follows

$$For\ \Phi_e>0:\ \Phi_e = \Delta_3\Phi_W+\Delta_1\Phi_P-\Delta_2\Phi_E \tag{3.11}$$

$$For\ \Phi_e<0:\ \Phi_e = \Delta_1\Phi_P-\Delta_2\Phi_E+\Delta_3\Phi_{EE}$$

$$\Delta_1 = \frac{\delta_1\delta_3(\delta_1+\delta_2)}{\Delta_4}$$

$$\Delta_2 = \frac{\delta_2\delta_3(\delta_2-\delta_3)}{\Delta_4}$$

$$\Delta_3 = \frac{\delta_1\delta_2(\delta_1+\delta_2)}{\Delta_4}$$

$$\Delta_4 = \delta_2\delta_3(\delta_2-\delta_3) - \delta_1\delta_3(\delta_1+\delta_3) + \delta_1\delta_2(\delta_1+\delta_2)$$

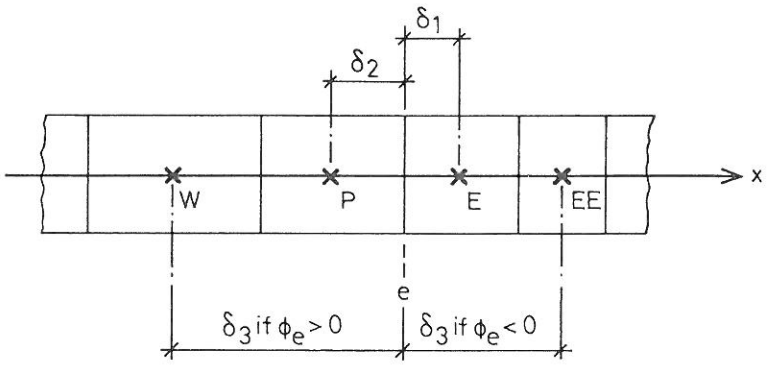

Figure 3.2. One-dimensional grid information for derivation of the QUICK scheme.

In the presentation of the three different schemes only the east coefficients are shown. Similar expressions can be derived at all other cell faces.

If a comparison between the three schemes is made it is noticed that the QUICK scheme in most cases will be the most accurate but has the drawback that it is more tiresome to implement that the others. The computing costs is also considerably bigger than the two others mostly because it yields slower convergence of the numerical procedure. The PLDS scheme is also rather costly to compute compared to the HYB scheme. The PLDS and the QUICK scheme are therefore used in the two-dimensional calculations and the HYB scheme is used for all three-dimensional calculations.

3.2.3 Treatment of the source terms

As described in eq. (3.2) is it necessary to linearize the source terms (S_Φ in table 2.1).

$$S_\Phi = S_C + S_P \Phi_P \tag{3.12}$$

This linearization may be done in several ways and this section is devoted to a discussion of the problem and recommend how to linearize the source terms in the model.

One basic rule is that all coefficient (including a_P) must be positive which again means that S_P always must be less or equal to zero (*Patankar 1980*).

In many of the governing equation the source terms are always positive, but with both negative and positive parts (i.e. destruction and generation terms). Further are the source terms often large compared to the other terms in the equations. It is therefore crucial to model the source terms in the right way. Some work has been done trying to linearize the source terms in the right way in the LRN version of the k,ϵ-model (which is the most sensitive model to this topic). The author found that following linearization is recommendable.

Momentum equations

$$S_P = 0 \ , \ S_C = S_\Phi \tag{3.13}$$

k-equation (by use of eq. 2.19)

$$S_P = -C_\mu F_\mu \rho^2 \frac{k^*}{\mu_t} \ , \ S_C = \mu_t \frac{\partial U_i}{\partial x_j}\left[\frac{\partial U_i}{\partial x_j}+\frac{\partial U_j}{\partial x_i}\right] \tag{3.14}$$

ϵ-equation

$$S_P = -C_2 F_2 \rho \frac{\varepsilon^*}{k} \ , \ S_C = C_1 f_1 \frac{\varepsilon^*}{k}\mu_t \frac{\partial U_i}{\partial x_j}\left[\frac{\partial U_i}{\partial x_j}+\frac{\partial U_j}{\partial x_i}\right] + C_3 \frac{\mu\mu_t}{\rho}\left[\frac{\partial}{\partial x_i}\left[\frac{\partial U_j}{\partial x_k}\right]\right]^2 \tag{3.15}$$

* correspond to the value from the previous iteration.

3.2.4 The staggered grid and pressure correction technique

In the source terms of the momentum equation one of the involving terms is the pressure gradient. This means that in order to be able to calculate the velocity field the pressure field must be known. An assumption of how to approximate the pressure gradient must be made and an additional expression of how to resolve the pressure field from the velocity field has to be established.

The pressure gradient term is integrated over a finite volume

$$-\int_V \frac{\partial P}{\partial x_i} = (P_w - P_e)\Delta y \Delta z = \frac{1}{2}(P_W - P_E)\Delta y \Delta z \tag{3.15}$$

This approximation of the pressure gradient term may result in a "wavy"pressure field which is felt like a uniform pressure field by the momentum equations because the pressure difference is taken between two alternate grid points and not between two adjacent (*Patankar 1980*). This phenomenon is called the checkerboard phenomenon. A similar effect is occurring in the continuity equation if the velocity

gradients are approximated in a similar manner. A way to overcome this phenomenon is to stagger the location of the velocity variables and the corresponding grid and computational volumes (fig. 3.3) (*Harlow et al. 1965* and *Patankar 1980*). The benefits of doing this is that it eliminates the risk of "wavy"velocity and pressure fields but the trade-off is that it requires extra computer storage and an additional interpolation effort.

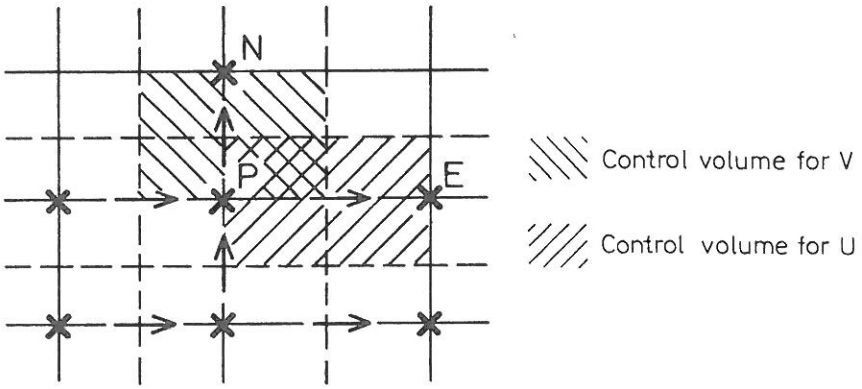

Figure 3.3 Staggered grid layout in the x and y directions.

The staggered location of the velocity variables means that the discretisation equations has to be rewritten in the following way (instead of eq. (3.2))

$$a_e U_e^* = \sum_{nb} a_{nb} U_{nb}^* + S_\Phi \Delta x \Delta y \Delta z + \left(P_P^* - P_E^*\right)\Delta y \Delta z$$

$$a_n V_n^* = \sum_{nb} a_{nb} V_{nb}^* + S_\Phi \Delta x \Delta y \Delta z + \left(P_P^* - P_N^*\right)\Delta x \Delta z \qquad (3.16)$$

$$a_u W_u^* = \sum_{nb} a_{nb} W_{nb}^* + S_\Phi \Delta x \Delta y \Delta z + \left(P_P^* - P_U^*\right)\Delta x \Delta y$$

The equations is written for all three directions because the staggering results in three "new" staggered control volumes.

This set of equations can be solved only if the pressure field is known or guessed (* denotes the intermediate or the guessed value of the pressure). Solution of these

equations result in an intermediate or starred velocity field.

The pressure field is now split up in an intermediate (or guessed) part and an additional correction part

$$P = P^* + P' \tag{3.17}$$

The velocity field corresponding to the pressure correction P' is written similar to (3.16)

$$a_e U'_e = \sum_{nb} a_{nb} U'_{nb} + S_\Phi \Delta x \Delta y \Delta z + \left(P'_P - P'_E\right)\Delta y \Delta z$$

$$a_n V'_n = \sum_{nb} a_{nb} V'_{nb} + S_\Phi \Delta x \Delta y \Delta z + \left(P'_P - P'_N\right)\Delta x \Delta z \tag{3.18}$$

$$a_u W'_u = \sum_{nb} a_{nb} W'_{nb} + S_\Phi \Delta x \Delta y \Delta z + \left(P'_P - P'_U\right)\Delta x \Delta y$$

The final velocity field is now found by the pressure correction formulas

$$U_e = U_e^* + \frac{1}{a_e}\left(P'_P - P'_E\right)$$

$$V_n = V_n^* + \frac{1}{a_e}\left(P'_P - P'_N\right) \tag{3.19}$$

$$W_u = W_u^* + \frac{1}{a_e}\left(P'_P - P'_U\right)$$

It is seen that the summation term of the neighbor coefficients is omitted. This can be done because solution scheme employed isn't fully implicit (se section 3.2.7) (*Patankar 1980*).

The task is now to formulate an equation for the pressure correction. This is done

by integrating the equation for mass conservation over a control volume and substitute eq. (3.19) into the integrated equation.

$$a_P P'_P = \sum_K a_K P'_K + S^* \tag{3.20}$$

where the coefficients are

$$a_E = \rho_e \frac{(\Delta y \Delta z)_e}{a_e} \Delta y \Delta z \ , \quad a_W = \rho_w \frac{(\Delta y \Delta z)_w}{a_w} \Delta y \Delta z$$

$$a_N = \rho_n \frac{(\Delta x \Delta z)_n}{a_n} \Delta x \Delta z \ , \quad a_S = \rho_s \frac{(\Delta x \Delta z)_s}{a_s} \Delta x \Delta z$$

$$a_U = \rho_u \frac{(\Delta x \Delta y)_u}{a_u} \Delta x \Delta y \ , \quad a_D = \rho_d \frac{(\Delta x \Delta y)_d}{a_d} \Delta x \Delta y$$

$$a_P = a_E + a_W + a_N + a_S + a_U + a_D$$

$$S^* = \left((\rho U^*)_e - (\rho U^*)_w\right)\Delta y \Delta z + \left((\rho V^*)_n - (\rho V^*)_s\right)\Delta x \Delta z + \left((\rho W^*)_u - (\rho W^*)_d\right)\Delta x \Delta y$$

3.2.5. Implementation of boundary conditions

As mentioned earlier boundary conditions are required along all the domain boundary, because of the elliptic nature of the governing equations. In this work four types of boundary conditions are used:

i) Prescribed value
ii) Symmetry plane
iii) Wall
iv) Outlet

In the following each kind of boundary specification is considered separately.

i) Prescribed value

There is two ways to ensure that a desired value in a computational cell remains unchanged during the process of solving the equations. One way is simply to do no work in the cell where the value is wanted unchanged. However, this method isn't very flexible because some programming has to be done in each case. Another way is to make use of the source term in the discretization equation for the considered variable

$$a_P\Phi_P = \sum_k a_k\Phi_k + (S_\Phi + S_P\Phi_P)\Delta x\Delta y\Delta z$$

If the value if the cell is wanted to be Φ_b then

$$S_C + S_P\Phi_P = \lambda\Phi_b - \lambda\Phi_P \qquad (3.21)$$

where λ is a large number.

ii) Symmetry plane

On a symmetry plane all gradients normal to the surface are equal to zero and the velocity normal to the surface is prescribed zero. If e.g. the south side of a computational cell is required to be a symmetry plane the required condition can be fulfilled by setting $a_S=0$ for normal components and $\Phi_{i,j,k}=\Phi_{i,j+1,k}$ for other components.

iii) Wall

The way to specify the wall boundary condition (i.e. the no-slip condition) is different for the standard k,ϵ-model and for the LRN version of the model. This is because the standard model is valid for fully turbulent flow only, and hence cannot be used in the near wall region, while the LRN version of the model has been developed for this purpose.

In the standard model a wall function method is used to incorporate the near wall

behavior into the computational cell nearest the wall. (fig. 3.4) (*Launder et al. 1974*). The method presumes that the near-wall flow can be described as a one-dimensional boundary-layer (section 1.2.2).

The shear force on the wall is expressed (fig. 3.4)

$$F_s = \delta_e \tau_o \tag{3.22}$$

which according to chapter 1.2.2 can be expressed in the following way.

For $y^+ < 11.7$:

$$F_s = \delta_e \tau_0 = -\delta_e \mu \frac{\partial U}{\partial n} = -\delta_e \mu \frac{(U_P - U_S)}{y_P} = -\delta_e \mu \frac{U_P}{y_P} \tag{3.23}$$

For $y^+ > 11.7$:

$$F_s = \delta_e \tau_0 = -\delta_e U_\tau^2 \rho = -\delta_e \rho U_\tau \frac{U_P}{U^+} = -\delta_e \rho \frac{(C_D C_\mu)^{\frac{1}{4}} k_P^{\frac{1}{2}}}{\frac{1}{\kappa} \ln \left[E\rho \frac{(C_D C_\mu)^{\frac{1}{4}} k_P^{\frac{1}{2}}}{\mu} y_P \right]} U_P \tag{3.24}$$

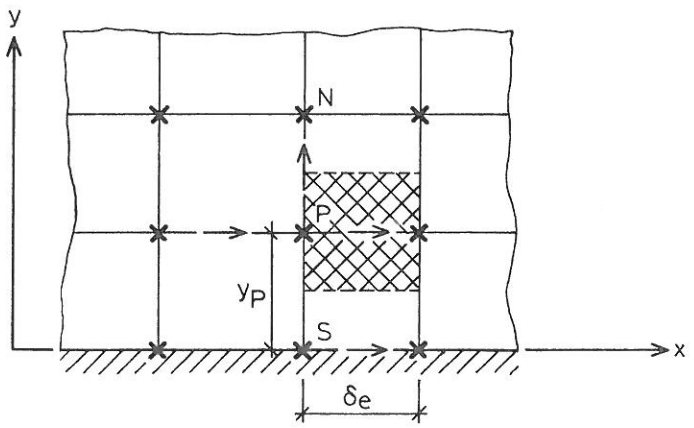

Figure 3.4. The structure of the grid near the wall.

The appropriate shear force according to the y^+-value in the first gridnode is introduced in the source term S_P.

The location of the first gridnode is important because the validity of the "laminar" wall expression is better the nearer the first grid node is to the wall. On the other hand is the validity of the turbulent log-law better for y^+-values around 30. This means that there is regions where the determination of U_P is poorer that in other regions. This fact has promoted development of more-layer model (*Nallasamy 1987*) but these aren't considered in this work.

Another issue is when the wall functions is used in connections with wall-jet flows. In this case the boundary layer deviates from the boundary layer on a flat plate already at y^+-values around 100 so the first point must be in the interval $30 < y^+ < 100$ in order to be able to capture the peak velocity of the jet.

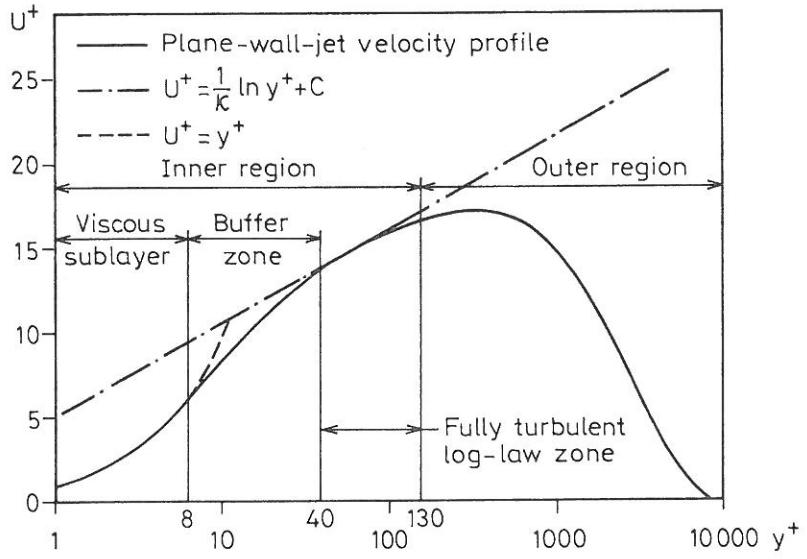

Figure 3.5. Velocity profiles in the turbulent boundary layer over a smooth flat plate.

For k is the boundary conditions zero normal gradient and the dissipation is calculated from (*Nallasamy 1987*)

$$\varepsilon_P = \frac{u_\tau^3}{\kappa y_P} = \frac{\left[\left(C_D C_\mu\right)^{\frac{1}{4}} k_P^{\frac{1}{2}}\right]^3}{\kappa y_P}$$

In the LRN version of the k,ϵ-model, which is valid throughout the laminar, semi-laminar and fully turbulent region, the wall boundary condition is implemented in the easiest way by prescribed zero velocity. Further due to the shift in the dissipation variable k and ϵ are also prescribed to zero in the Launder-Sharma LRN model.

iv) Outlet

In return openings all gradients in the outflow plane are set to zero. The velocity perpendicular to the outflow plane is set to fulfill the overall continuity of mass. If e.g. the inlet is located in the z-plane the boundary conditions is described

$$\Phi_{out,uniform} = \frac{\int_{y_1}^{y_2}\int_{x_1}^{x_2} \Phi_o(x,y)\partial x \partial y}{A_{out}} \tag{3.25}$$

3.2.6 Solution of the algebraic discretization equations

The governing equations have now been integrated over the finite volume, brought onto a linearized form and the proper boundary conditions has been applied. All these actions is resulting in a set of linear algebraic equations on the form

$$a_P \Phi_P = \sum_K a_K \Phi_K + S_C \tag{3.26}$$

It is now possible to assemble all the discretized algebraic coefficient equations on a matrix form and solve the system directly. However, this approach is very time consuming and an iterative method is much more comprehensive. One of the easiest

and a quite effective method is the Tridiagonal-Matrix Algorithm (TDMA) extended to three dimensions by iteration. The method works at one plane at the time and in this plane the equations are solved along a chosen line. All values except the value in the actual cell is assumed known. The method is straight forward and is repeated until a converged solution is obtained in all cells. (For a fully comprehensive explanation see *Patankar 1980*).

Because of the iterative nature of the method some remarks must be made regarding the solution strategy because the spread of information in the grid structure is depending of this strategy. In fully elliptic problems it would be the best to alternate the sweep directions from iteration to iteration because the solution in every point in the domain is depending on the boundary conditions all around the domain boundary (chapter 2). This procedure would also prevent areas where larger errors may build up. But on the other hand if the flow has parabolic nature (in any elliptic flow domain there may be found areas with parabolic flow characteristics) the coefficient will be larger upstream the main flow direction and therefore the solution strategy should take this into account.

3.2.7 The overall solution procedure and under relaxation.

Previous sections has been concerned with the numerical discretization and solution of the general governing equations. This section deals with the overall solution of the whole system of governing equations.

As described in chapter 2 the set of partial differential equation is strongly coupled and unlinear which means that some sort of iterative procedure initiated by a guess must be used to solve the system of equations.

In the FV technique different guess-and-correct procedures have become popular. Different algorithms employe different techniques of handling especially the velocity-pressure coupling, because this coupling has a significant impact on the effectivity of the algorithm (i.e. convergence rate). The convergence rate insured by different methods varies from problem to problem and more advanced algorithms as SIMPLER and PISO have shown to be more effective than the SIMPLE algorithm (*Patankar 1980*) used in this work. However, the effects of the pressure-velocity handling seems to decrease in more complex turbulent flows where the pressure forces plays a minor role as driving force. This means that the advantages of the methods with enhanced pressure-velocity handling are smaller and the use

may indeed be a subject of discussion because they imply a lot more computational work (*Huang 1986, Leschziner 1991*).

The main solution steps of the SIMPLE algorithm used to solve the equations in table 2.1 can be summarized in the following way

1. Initialize the variable Φ^*
2. Calculate Γ_Φ^*

3. Assemble coefficient for U^*-momentum
4. Impose boundary conditions for U^*-momentum
5. Solve for U^* by the TDMA technique

6. Assemble coefficient for V^*-momentum
7. Impose boundary conditions for V^*-momentum
8. Solve for V^* by the TDMA technique

9. Assemble coefficient for W^*-momentum
10. Impose boundary conditions for W^*-momentum
11. Solve for W^* by the TDMA technique

12. Assemble coefficient for P^*-momentum
13. Impose boundary conditions for P^*-momentum
14. Solve for P^* by the TDMA technique

15. Obtain P,U,V,W from pressure correction formulae

16. Assemble coefficient for k^*-momentum
17. Impose boundary conditions for k-equation
18. Solve for k by the TDMA technique

19. Assemble coefficient for k-equation
20. Impose boundary conditions for ϵ-equation
21. Solve for ϵ by the TDMA technique

22. If not converged goto 2. and set $U^*=U$, $V^*=V$ etc.

The SIMPLE procedure with its pressure-correction technique is prone to diverge if the changes of the variables isn't slowed down from iteration to iteration. This is

done by introducing a set of relaxation factors, α

$$\frac{1}{\alpha_\Phi} a_P \Phi_P^i = \sum_k a_k \Phi_k^i + S_C^i \Delta x \Delta y \Delta z + \frac{1-\alpha_\Phi}{\alpha_\Phi} a_P \Phi_P^{i-1} \tag{3.27}$$

and in the pressure correction

$$P = P^* + \alpha_P P' \tag{3.28}$$

The under-relaxation parameters are in the interval from 0 to 1. There is no way to choose a general set of optimum relaxation factors because the value depends on the problem, the computational grid (spacing and number) and other things. In fact, the author is of that opinion that the task of choosing the relaxation parameters are one of the drawbacks of this method.

Another issue is when to stop the iteration procedure and to determine when the solution is a converged solution. This topic is discussed in the next section.

3.2.8 Convergence criterion

When the solution don't change from iteration to iteration we say that the iterative process has converged. In practice this will never happen (or is dependent of the computer and the problem) so we need to establish a sufficient criterion for convergence of the iterative procedure.

In each iteration we are able to calculate the residual in the following way

$$R_\Phi = \sum_{P=1}^{N} \left(\sum_{nb} a_{nb} \Phi_{nb} + S_C \Delta x \Delta y \Delta z - a_P \Phi_P \right)$$

When the iterative process have converged R_Φ will of course be zero. So a way to give a convergence criterion would be to terminate the iterative procedure when R_Φ is small. But how small ? The answer is that it has to be determined in each case because R_Φ is dependent of the problem which again means that a large R_Φ in one

problem can cover a nearly converged solution while a small R_Φ in another problem does not guarantee a converged solution. A way to overcome this will be to normalize the residual. For e.g. the momentum equations we have

$$R_\Phi = \frac{\sum_{P=1}^{N}\left(\sum_{nb} a_{nb}\Phi_{nb} + S_C\Delta x\Delta y\Delta z - a_P\Phi_P\right)}{inflow-momentum} \tag{3.29}$$

The residual is now relatively independent of the problem and can be used as a measure for convergence. The stop criterion is around 10^{-4} to 10^{-6}.

Because the method will be used to predict air flow pattern in ventilated spaces we are equally interested in the overall flow pattern as well as in the solution in a single point (e.g. the maximum velocity in the occupied zone) which means that eq. (3.29) must be used with care. A small value of R_Φ could cover a relatively large residual in a small number of cell masked by a very small residual in the majority of the cells. A way to overcome this could be to compare the Φ^i directly with Φ^{i-1} in a RMS way (*Page 1991*). However this will require storage for at least one set of Φ. In this thesis the convergence criterion in eq. (3.29) is used bearing the above mentioned in mind.

3.3 Closure

In this chapter the discretization and the numerical solution technique have been discussed. The outline of the discretization process of the governing second order, unlinear, inhomogeneous and coupled partial equations can be summarized in following way.

General description	Used technique
Look into the physical nature of the governing equations and select discretisation technique	Finite volume, implicit method
Perform the numerical discretisation	Integrate over a finite volume, linearization of the equations and the source terms and decoupling of the equations
Improve the stability by selecting the proper differencing scheme	HYB : good stability, easy to compute PLDS : good stability, more accurate than HYB around Pe=2, easy to compute QUICK : less stable - not bounded (can produce overshoots), best accuracy, more complex to compute, lower rate of convergence
Solve the pressure-velocity coupling by appropriate scheme	SIMPLE : handles the pressure-velocity coupling in a crude way but due to the complex turbulent flow is the gain of a more enhanced procedure limited.
Impose boundary conditions	Four different boundary conditions is presented : prescribed value, symmetry, wall and outlet.
Solve the system of equations	TDMA is used to solve the algebraic equation and an iterative under-relaxation technique is used to solve the set of coupled equation

The described structure is essential the TEACH structure (*Gosman et al. 1973*) with additions and improvements.

CHAPTER 4 - PREDICTION OF FULLY TURBULENT FLOW IN A VENTILATED ROOM.

4.1 Preamble

The content of this chapter is devoted to a relatively simple CFD prediction of the three-dimensional velocity distribution in a room ventilated by the mixing principle. The simulations are meant to be an introductory study to later and more complicated applications of CFD in the field of ventilation in rooms (chapter 6 and 7).

The traditional way to design a ventilation system for mixing ventilation is, as explained in the introduction, to describe the resulting flow near the inlet by a two or three dimensional wall-jet and then make use of the equation (1.1) and (1.7)-(1.10).

This chapter will therefore as a starting point for evaluation of the performance of the numerical predictions look upon specific areas such as decay of the velocity in the jet-zone and the maximum velocity in the occupied zone in relation to the simplified models.

4.2 CFD prediction of the velocity distribution in a room ventilated by a single jet

The simulations presented in the following are made in a room ventilated by a single jet resulting from a rectangular inlet. The room dimensions are chosen to be the same as the test room used in the international research work performed by 12 countries within the International Energy Agency (IEA), Annex 20: "Air flow within buildings" (*Lemaire 1989*).

4.2.1 Test case

The dimensions of the test case are shown in fig. 4.1 and in table 4.1. Three different inlet geometries are simulated, each for three different air-change-rates.

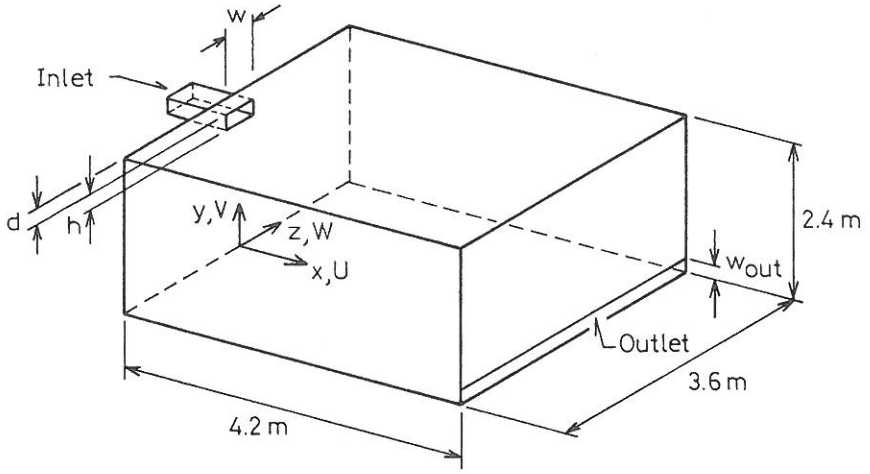

Figure 4.1. The geometry of the test case.

Case	L*H*W	d	w	h	a_0
1	4.2*2.4*3.6	0.075	0.6	0.275	0.165
2	4.2*2.4*3.6	0.075	0.6	0.175	0.105
3	4.2*2.4*3.6	0.075	0.6	0.07	0.042

Table 4.1. Data for the test case with reference to fig. 4.1.

4.2.2 Boundary conditions and computational details

The numerical predictions are obtained by a numerical solution of the time averaged Navier-Stokes equations and the continuity equation. For the description of the turbulence the standard high Reynolds number k,ϵ-model is used (table 2.1).

The computational domain is divided into a non-uniform 15*20*11 mesh giving 3300 finite volumes. The equations are discretised to a set of linear homogeneous equations (chapter 3). A staggered grid is used for the dependent variables U,V and W to avoid the checkerboard phenomenon (chapter 3.2.4)and the hybrid differentiation scheme (chapter 3.2.2) is used. The solution of the unlinear set of equations is done by the SIMPLE pressure relaxation method (chapter 3.2.7) and the equations are solved by a TDMA - ADI solution technique (chapter 3.2.6).

The boundary conditions are:

Inlet: A prescribed plug profile for U-velocity determined by the required air-change-rate. V and W are prescribed zero. The turbulence intensity is set to 5%.

Outlet: The outlet conditions described in chapter 3.2.5 is used.

Wall: The no-slip condition on all the walls are indirectly introduced by wall functions which either can be of the logarithmic or of the linear (Couette) type depending on the value of y^+ value at the first gridnode (chapter 3.2.5).

Symmetry: The flow is assumed symmetrical and all the gradients are forced to zero across the symmetry plane (chapter 3.2.5).

Approx. 3000 iterations of 1 s/it. ($8x10^{-5}$ s/it/node/eq.) each are required to obtain a fully converged result on a Sony workstation with a RISC 3000 processor (fig 4.2).

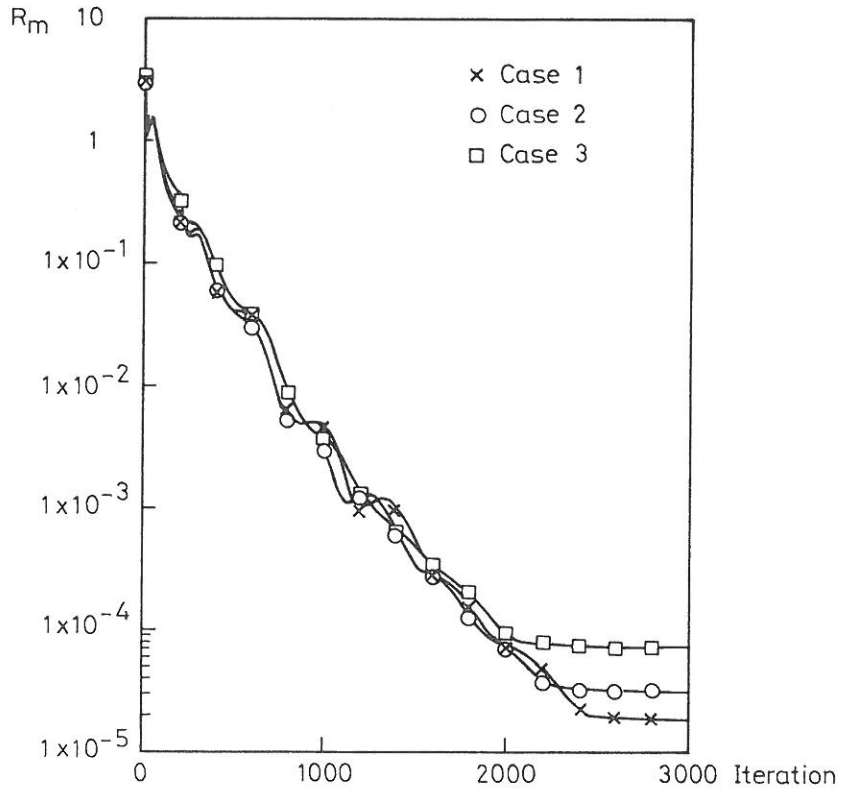

Figure 4.2. Convergence history for the normalized mass-residual in the three test cases in table 4.1.

4.2.3 Results and discussion

One of the major forces of CFD is that it gives detailed qualitative information of the velocity field in a room. From fig. 4.3, 4.4 and 4.5 the three-dimensional nature of the flow is evident and it is interesting to observe that the maximum velocity in the "return flow" is not located in the centre but instead closer to the side walls. It is also seen that the location of the outlet creates a stagnation point near the floor in the occupied zone. The Coanda effect is also observed[1].

To evaluate the result more specific it is chosen to see how the simulation of the flow field with the standard turbulence model performs versus some of the well known and extensively used simplified relations for wall-jets and maximum velocities in the occupied zone (chapter 1).

Case	U_0	Q_0	I_0	$I_0^{½}$	U_{rm}	n
1a	0.11	0.0219	0.0024	0.049	0.02	1.81
1b	0.35	0.0696	0.0244	0.16	0.075	5.75
1c	0.61	0.121	0.0740	0.27	0.135	10.0
2a	0.16	0.0202	0.00324	0.057	0.025	1.67
2b	0.48	0.0607	0.0292	0.17	0.09	5.02
2c	0.96	0.121	0.117	0.34	0.18	10.00
3a	0.45	0.0228	0.0102	0.10	0.06	1.88
3b	1.2	0.0607	0.0729	0.28	0.16	5.02
3c	2.0	0.101	0.202	0.45	0.28	8.35

Table 4.2. Computed data for the two test cases.

Equation (1.8) is a well known relation for fully turbulent flow conditions. The relation states that the maximum velocity in the occupied zone is proportional to the air-change-

[1] Coanda effect - The jet created from the inlet is entraining air from the ambience. The ceiling make it impossible to entrain air from above and this consequently decreases the pressure level compared to the surroundings. This lower pressure level is deflecting the jet towards the ceiling where the flow will attach. Further downstream the jet is obtaining the characteristic velocity profile of a wall-jet.

rate. In fig. 4.5 simulated data for U_{rm} is plotted against the air-change-rate. It is seen that U_{rm} is proportional with the air-change-rate. The slope of the curve which correspond to C_1 is different for the three cases which

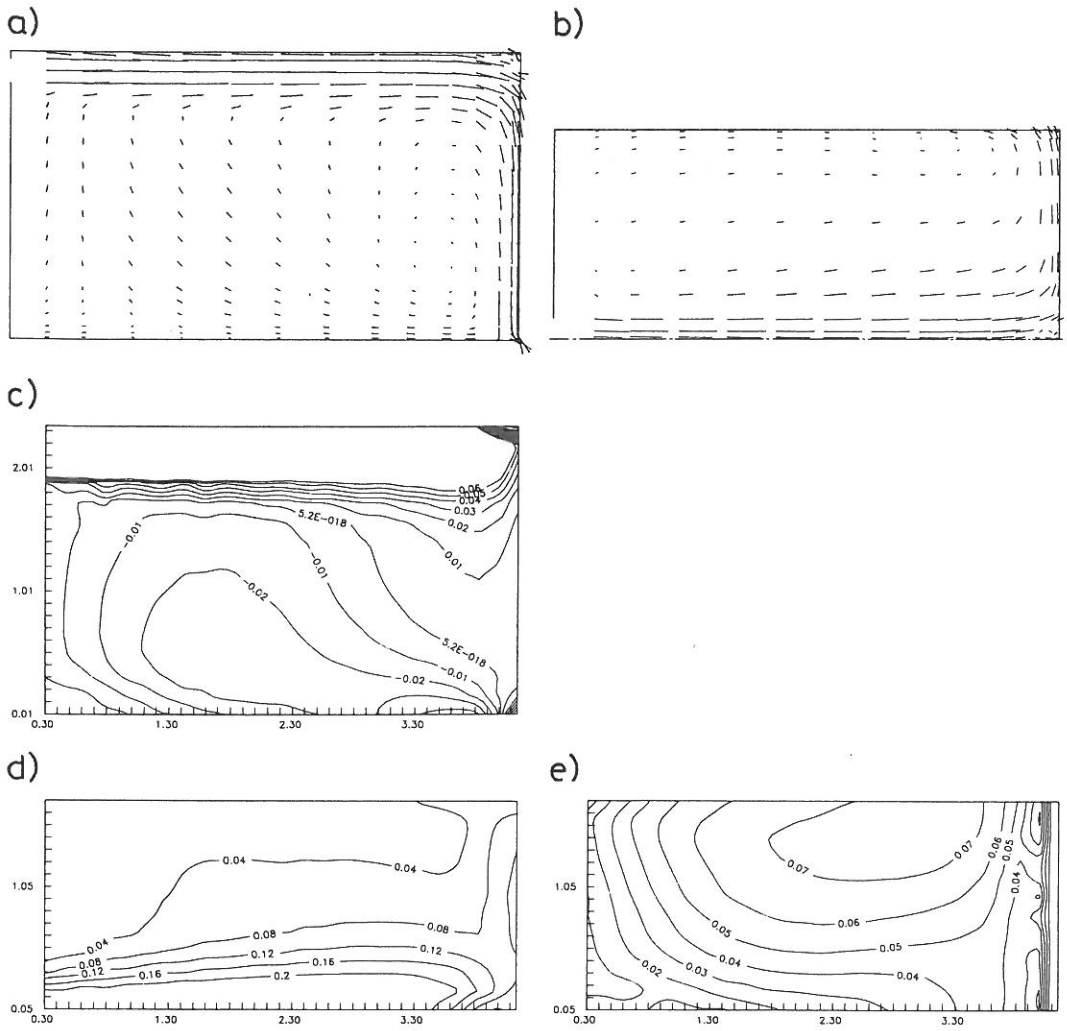

Figure 4.3 Computed velocity distribution for test case 1b. a) velocity vectors for z=0.0m. b) velocity vectors for y=2.35m. c) U-velocity isolines for z=0.0m. d) speed isolines for y=2.35m. e) speed isolines for y=0.05m.

means that the coefficient C_1 at least is a function of the inlet geometry. If we instead investigate eq. (1.9), which expresses that the maximum velocity in the occupied zone is proportional to the momentum flow in the inlet, we can from fig. 4.6 see that C_2 is much

less a function of the inlet geometry. This result is interesting because it means that we are able to predict the magnitude of the maximum velocity of U_{rm} just by the exact information of the momentum flow through the inlet. So, if we know the connection between the inflow momentum and U_{rm} for one single case (e.g. through full scale

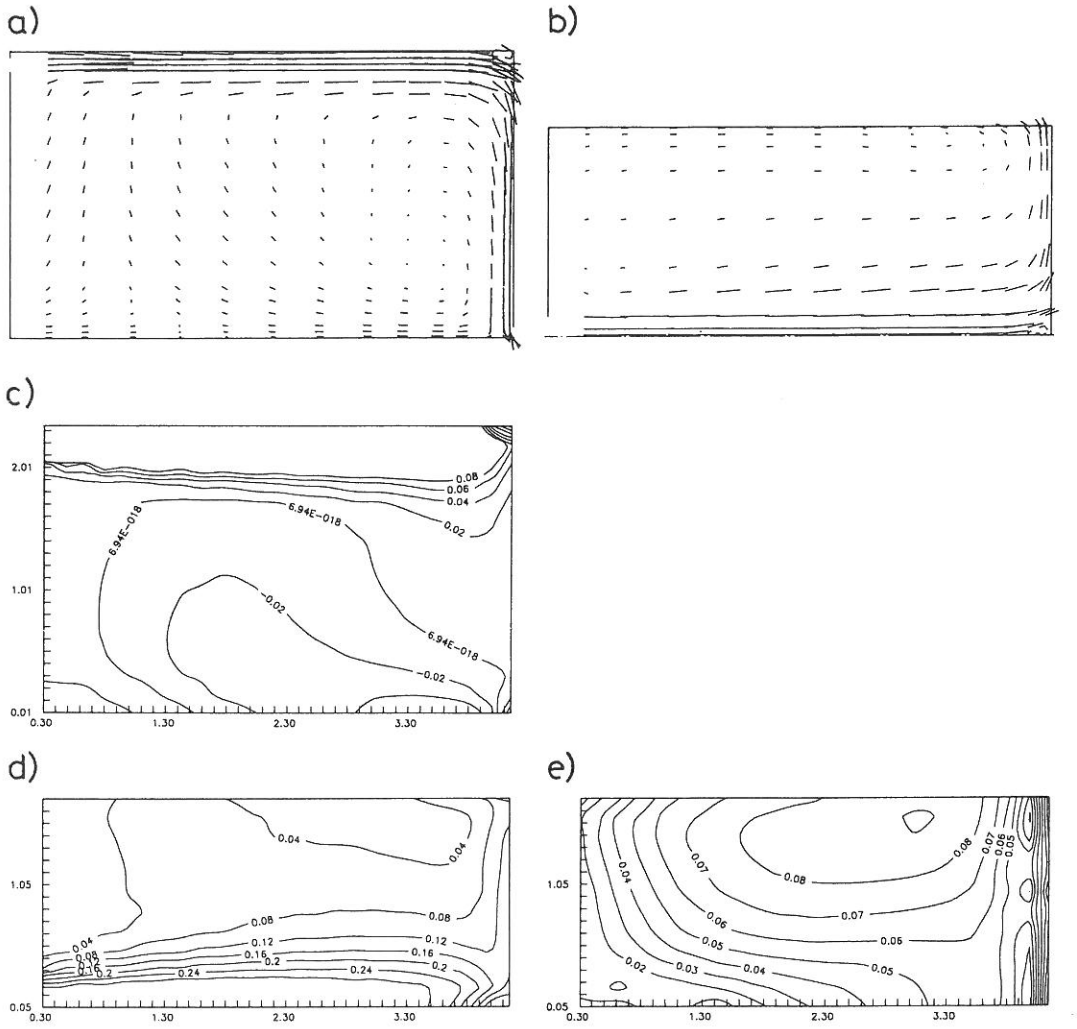

Figure 4.4 Computed velocity distribution for test case 2b. a) velocity vectors for z=0.0m. b) velocity vectors for y=2.35m. c) U-velocity isolines for z=0.0m. d) speed isolines for y=2.35m. e) speed isolines for y=0.05m.

or numerical experiments) we are able to give a qualified guess at the maximum velocity in the occupied zone even for another inlet device of the same type (same K_a -factor). The two coefficients C_1 and C_2 will of course be functions of the room geometry and inlet

velocity (chapter 6). In many modern inlet devices the inlet velocity isn't fully turbulent. This means that the inflow momentum is different from expected assuming fully turbulent conditions (the velocity profile over the inlet is dependent on the inlet Reynolds number). This means that the constant C_1 is now a function of the air-change-rate. In Chapter 5 and 6 this phenomenon is investigated further.

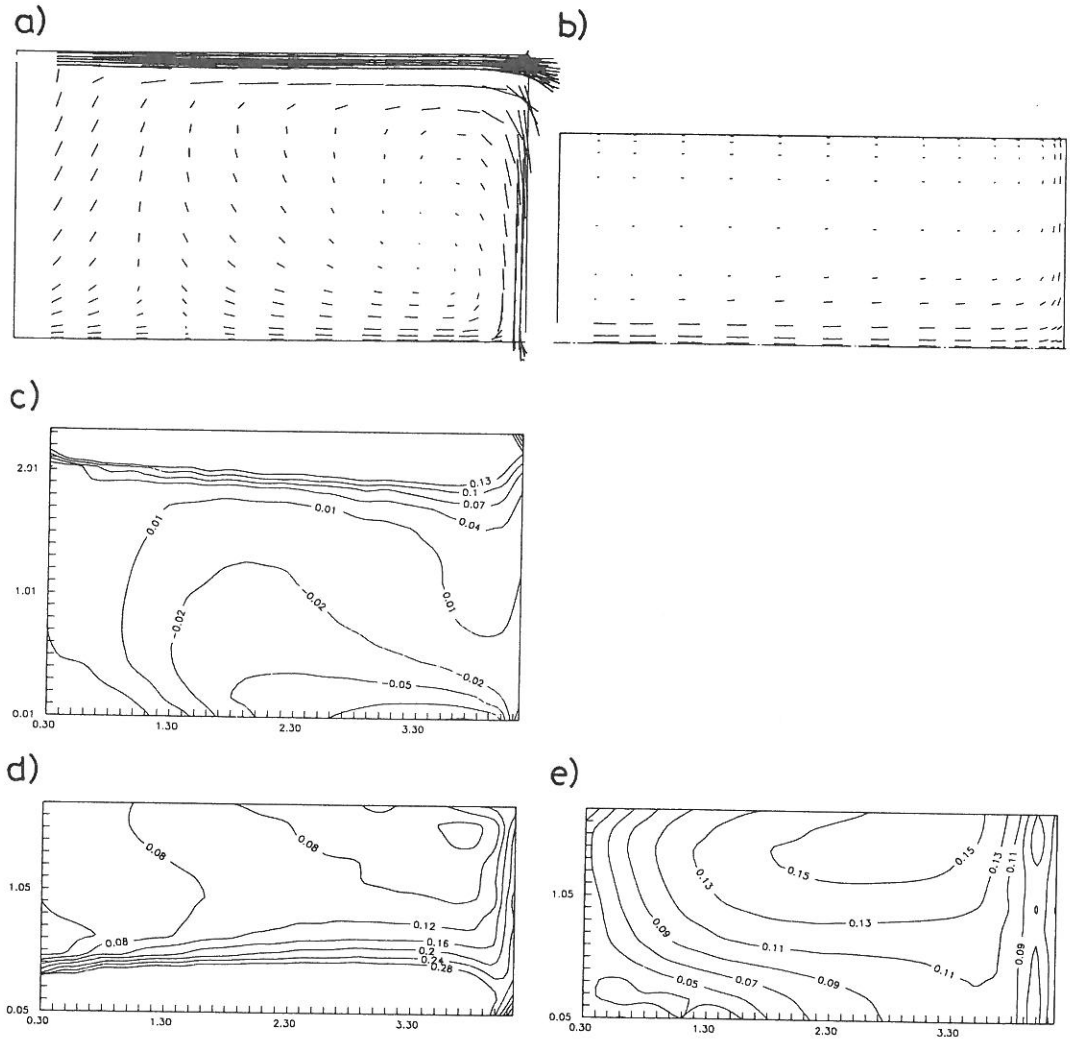

Figure 4.5 Computed velocity distribution for test case 3b. a) velocity vectors for z=0.0m. b) velocity vectors for y=2.35m. c) U-velocity isolines for z=0.0m. d) speed isolines for y=2.35m. e) speed isolines for y=0.05m.

If the jet region below the ceiling is observed (fig, 4.8, 4.9 and 4.10) it is seen that there is a zone with small decay, a zone with linear decay and a region where the decay in

under influence of the wall. In the first zone, the core of the jet, should have been without any decay at all. The decay which is present in this region may be due to numerical diffusion arising from the truncation error in the approximation of the velocity gradients. In order to overcome this one must have a large number of cells in the region near the inlet which will increase the computational time dis-proportionately from an engineering point of view. The decay in the second region (the characteristic decay region) is dependent on the jet type and the room

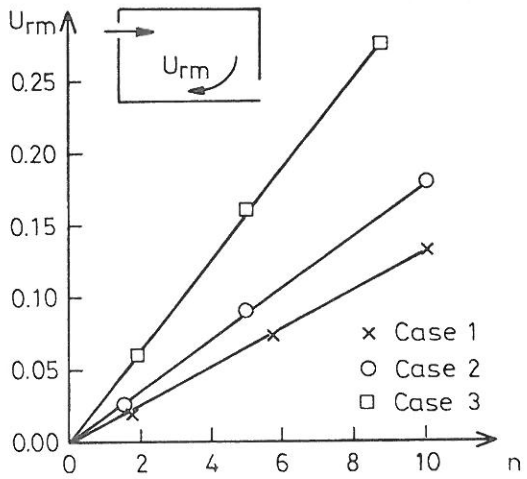

Figure 4.6. The maximum velocity in the occupied zone as a function of the air-change-rate for case 1, 2 and 3.

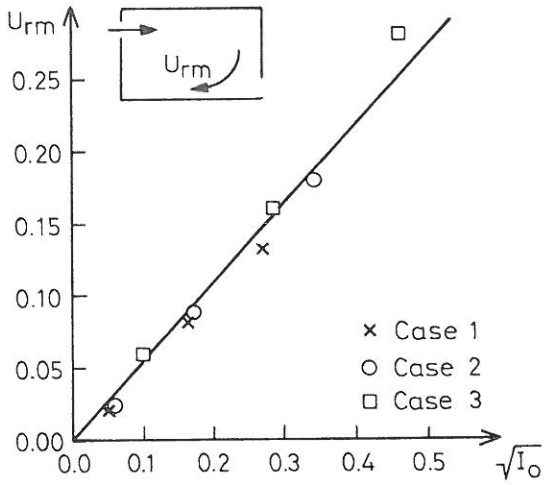

Figure 4.7. The maximum velocity in the occupied zone versus the momentum flow in the inlet for case 1, 2 and 3.

length. If the room length is large compared to the inlet height and the jet flow is three-dimensional then the velocity will first decay proportional to $x^{½}$ (the two-dimensional region) and later proportional to x^{-1} (the three-dimensional region). It is in this last region where the factor K_a may be determined. As it is seen from the three figures the room length is too small compared to the inlet height to obtain fully developed three-dimensional jet flow character and it is not possible to determine the K_a factor. In order to investigate relation (1.10) which is the ratio between the velocity at the end wall and the maximum velocity in the occupied

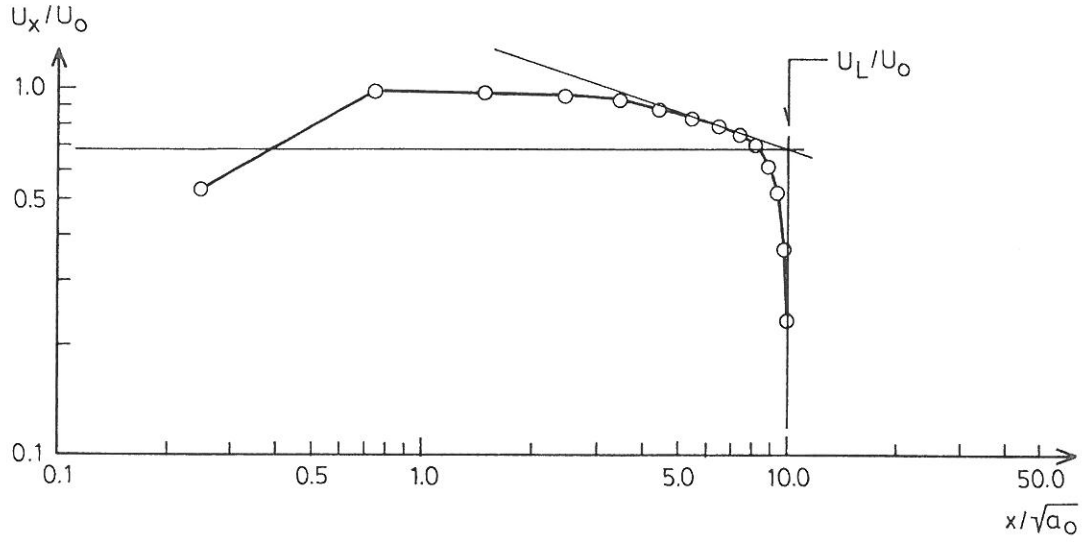

Figure 4.8. The decay of the center line velocity in the wall-jet for case 1.

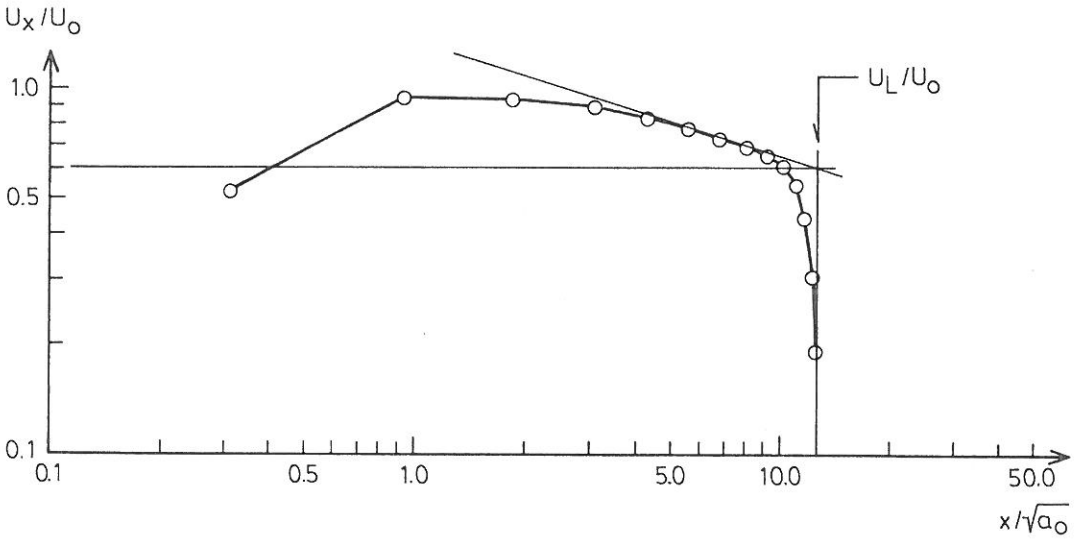

Figure 4.9. The decay of the center line velocity in the wall-jet for case 2.

zone one must determine the velocity in the jet at x=L. This is done in table 4.3. *Hestad 1974* did also investigate the relation and concluded that it is a function of the jet width at the end-wall (*SBI 128 1981*). Table 4.3 shows that the value of f_1 is approximately 0.3 which is the same value *Hestad 1974* has measured for three-dimensional flows. However, the test cases are quite similar and it can be difficult to throw the benefit of eq.(1.10) into relief but because the use of relation f_1 isn't limited to the very same room and therefore is more universal is the relation and certainly worth while to examine in more detail.

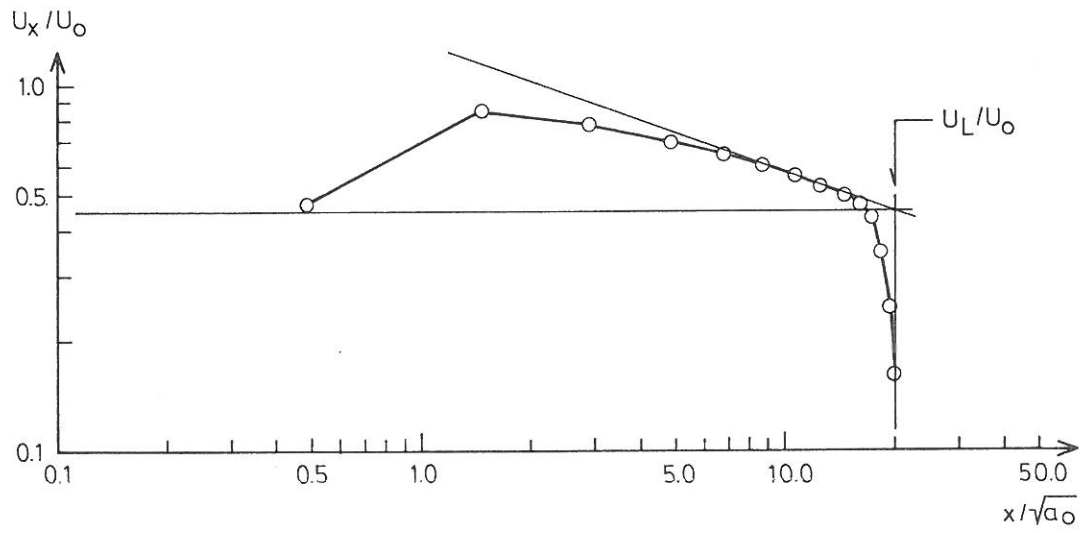

Figure 4.10. The decay of the center line velocity in the wall-jet for case 3.

Case	U_0	U_{rm}	U_L	f_1
1a	0.11	0.02	0.074	0.27
1b	0.35	0.075	0.238	0.32
1c	0.61	0.135	0.414	0.33
2a	0.16	0.025	0.099	0.25
2b	0.48	0.09	0.298	0.30
2c	0.96	0.18	0.595	0.30
3a	0.45	0.06	0.194	0.31
3b	1.2	0.16	0.54	0.30
3c	2.0	0.28	0.9	0.31

Table 4.3. Calculation of the function f_1 in relation (1.10) for case 1, 2 and 3.

4.3 Closure

This chapter has dealt with evaluation of CFD used to predict a relatively simple three-dimensional flow field in a room ventilated by the mixing principle. The code used is based on the time-averaged momentum equations, the continuity equation and the standard k,ϵ-model. This code is referred to as the standard CFD code in the following concluding remarks

The performance of the standard CFD code which presume fully turbulent flow conditions, gives additional valuable knowledge of the flow pattern (e.g. gives the location of the maximum velocity) and supports the prediction by the simplified models.

The standard CFD code is a good additional analysing tool to obtain detailed information of flow phenomena in ventilated rooms of different geometries.

If low Reynolds number effects are present, (which often is the case) such as Reynolds number dependent effective inlet area or low Reynolds number effects in the room, special actions need to be taken. These special actions could be implementations of empirical data or another model than the standard k,ϵ-model for description of the turbulence.

When the simplified models are used in the design process of a ventilation plant, CFD could be used at an early stage to obtain knowledge of the relations or to make a schedule for an experimental investigation.

CHAPTER 5 - EXPERIMENTAL INVESTIGATION OF INLET CONDITIONS AND LOW REYNOLDS NUMBER PHENOMENA.

5.1 Preamble

The aim of the experiments is first of all to improve the knowledge of the general flow pattern in a room ventilated by the mixing principle. Investigations have shown that the general flow pattern in a room ventilated by the mixing principle changes with the air-change-rate (*Nielsen et al. 1985*, *1988a* and *Heiselberg 1990*). When the air-change-rate is dimished, that is, when the inlet velocity through the inlet device decreases, the airflow patterns and e.g. the maximum velocity in the occupied zone deviate from what one may expect under fully turbulent conditions. This behavior will in the following be termed low Reynolds number (LRN) effects. These effects seem to arise both directly at the inlet and within the room (*Larsen et al. 1988*). This means that in order to study and later to be able to predict the velocity distributions in a ventilated room investigations of the LRN effects must be made experimentally both with respect to reveal the sources of the LRN effects and with respect to the relevance of these effects to flows encountered in real situations.

5.2 Experimental setup

The experimental investigations are carried out in a full-scale clima chamber at the University of Aalborg, Institute of Building Technology. The size and the inlet device is the same as used in the international research work made in the International Energy Agency, Annex 20: "Air Flow Pattern within Buildings" during 1988 to 1991 (*Lemaire 1989*).

5.2.1 The test chamber

The test chamber is placed in a laboratory hall and the dimensions of the chamber are:

Height	2.4m
Length	4.2m
Width	3.6m

These values give a floor area of 15.12m^2 and a cubic content of 36,29m^3. The chamber is built upon a wooden sceleton with walls made of 0.019m Douglas plates. It is possible to observe the foregoings in the room through one of the sides of the room where double glassed windows are installed. The ventilation system has a capacity of up to 7-10 h^{-1} in terms of air-change-rate depending of the resistance in the supply installation. The inlet air may be cooled or heated 10K. A photography of the test chamber is shown in fig. 5.1.

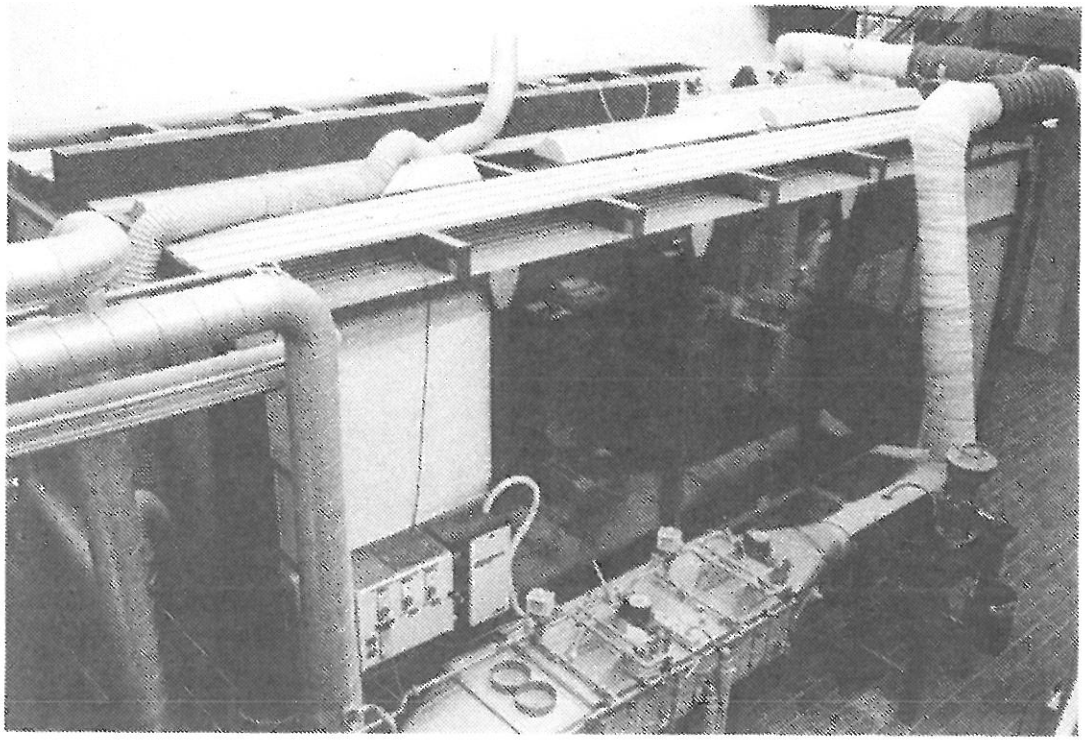

Figure 5.1. The test chamber. In front is the fully equiped ventilation plant seen.

The installed inlet device is the HESCO - type KS4W205K370 (*Nielsen 1988b*). The diffuser consist of 4 rows with 21 nozzles which can be adjusted independently to different directions giving any kind of three-dimensional flow structure. This feature is typical for modern inlet device design. For this purpose all the nozzles have been adjusted to an angle of 40° from horizontal towards the ceiling (fig. 5.3). The inlet is located 0.2m below the ceiling and the outlet is located 0.6m below the ceiling and has the dimension of 0.3x0.2m^2.In order to obtain an even velocity distribution over the inlet the installation arrangement shown in fig. 5.4 is used.

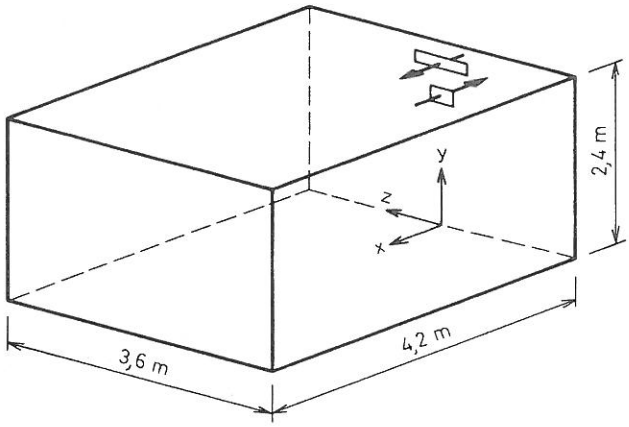

Figure 5.2. Sketch of the room geometry.

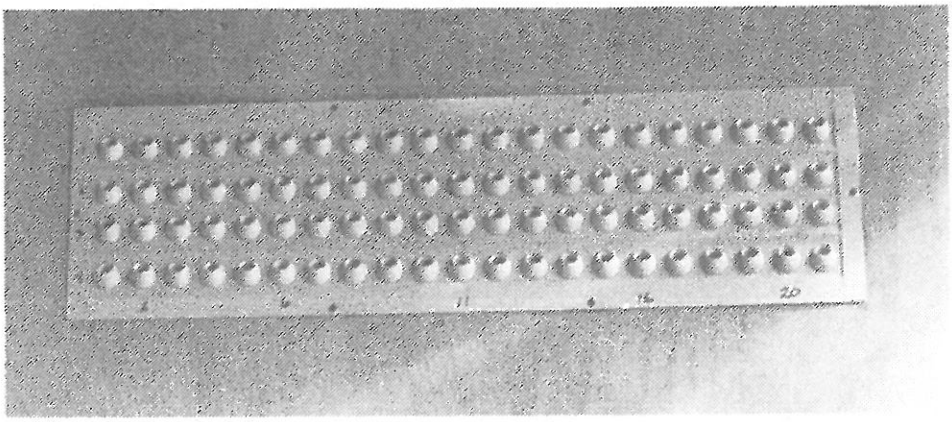

Figure 5.3. Close-up of the inlet device.

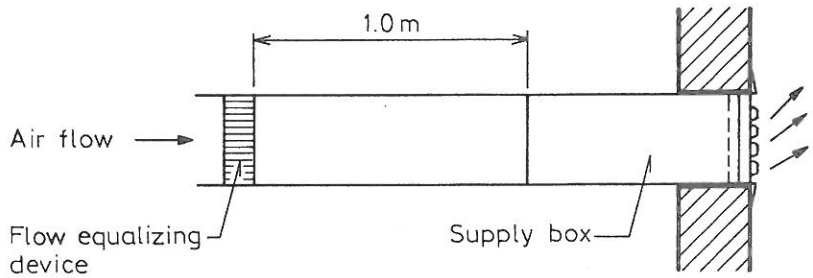

Figure 5.4. The installation of the air supply terminal.

5.2.2 Velocity measurement and calibration

The velocity is measured with two different types of low velocity measurement systems.

Velocity measurements in the inlet nozzles and in the region below the ceiling

In the wall-jet and in the region around the inlet device the Dantec multichannel Flow Analyser (type 54N10) together with a software package (type 54G301) is used. With this equipment it is possible to measure mean velocity and RMS-value and to present it in a crude graphical manner on a PC. The probes (type 54R10) are of the omnidirectional type. This means that they in theory should be independent of the flow direction (at least do they not provide any information of the flow direction). The probe consist of two spheres - a flow sensor which is heated and a sphere which adapts the temperature of the bulk and compensate for the temperature difference.

The probe is adjusted and calibrated when the system is delivered from the Dantec factory. This adjustment may, however, change quite significantly so one must always calibrate the system before (and after) use. This calibration must be done with the probe oriented in the direction in which it is used in order to take, the self convection[1] and other effects which may not be independent of the flow direction, into account.

Velocity measurements in the occupied zone

In the occupied zone where the velocity level is lower and the turbulence level is expected to be higher a single hotwire probe in connection with a temperature compensated bridge (Dantec 56C14) is used. The analogue voltage output from the bridge is passed through different electrical devices (amplifier, linearizer, RMS-unit and mean-value unit) and it is now possible to measure the mean velocity and the standard deviation (which is equal to the RMS value for large samples).

---

[1] The self convection caused by the heated sphere cannot be expected to be independent of the flow direction. *Kofoed 1991* has made comprehensive investigations of the impact of the self convection and he concludes that "*calibration must be done in a flow with the same flow direction as in the investigated flow to ensure accurate measurements*".

Contrary to the ball probe the single wire anemometer is strongly influenced by the flow direction, one must therefore investigate the direction of the flow e.g. by smoke before the velocity measurements are carried out. This direction sensitivity in addition to the self convection make the remarks made in the previous concerning the calibration procedure just as or even more important here.

In the velocity measurements made during this work the primary interest is steady-state values for the mean velocity and the standard deviation to represent the turbulent fluctuations. This means that the collection of data has to prevail until a representative ensemble of the different turbulent scales (or frequencies) has been recorded. In other words this means that the measurements must proceed until reproducible values for the mean velocity and the standard deviation is obtained. The integration time is dependent of many factors e.g. the time constant of the measurement device, the scale of turbulence and the magnitude of the mean velocity. Preliminary tests were carried out and two different integration periods were chosen. 90s for the measurements with the ball probes in the region below the ceiling and 960s for the measurement with the hotwire in the occupied zone.

5.2.3 Temperature measurements

One of the objectives for the measurements is to detect and investigate LRN phenomena under isothermal conditions. These effects are of course occurring when the velocities are low. This means that the influence of the self convection may be rather significant if it isn't considered in the calibration procedure described in the previous section. Another phenomenon which could influence the flow is a small temperature difference which would cause small, but due to the low velocity level, significant buoyancy forces. In order to overcome this the vertical temperature gradient is measured on all four walls. The temperature difference between inlet and exhaust is also measured. The temperature measurements are made with thermocouples in connection with a constant cold junction (KAYE Icepoint Thermocouple Reference System). The accuracy of the set-up is < 0.2K (*Kofoed 1991*). It is decided to require the temperature gradient $dT/dx < 0.125$K/m.

5.2.4 Data processing

The invention of the microprocessor and later the PC has made collection of large amounts of measured data much easier. This means that the tedious tasks in the

measurering procedure can be handled numerical. This procedure has also the advantage that the data acquisition can be handled on-line so experiments which have unexpected results or e.g. if the sufficient isothermal conditions aren't present can be done over again. Unfortunately the equipment used here for the velocity measurements is of such a character that collection of the analogue output isn't possible which again means that only mean-values can be calibrated correctly. Therefore, if one push it to extremes, the measured turbulence values are only valid in this room made with this specific apparatus. So to leave any doubt behind about the velocity measurements and the tendencies they might show the analysis in the following chapter is made over the mean-values only.

5.2.5 Test series

The velocity measurements are performed in three parts of the test chamber where the important ventilation parameters occur and where the LRN phenomena are expected to arise. Further the experimental investigation is carried out in preparation for boundary conditions in a numerical simulation of the flow field.

The regions are:

i) Measurements of the effective inlet area
ii) Wall-jet measurements
iii) Measurements in the occupied zone

i) Measurements of the effective inlet area

The effecive inlet area is defined:

$$a_0 = \frac{Q_0}{U_0} \tag{5.1}$$

In fully turbulent flow eq. (5.1) is approximately equal to the geometrical inlet area which is $0.0095m^2$. As the inlet velocity decreases the flow is becoming more and more "laminar" and the effective inlet area is decreasing due to the change in the velocity profile over the single nozzle.

U_0 is measured in the centre of 10 different nozzles distributed over the inlet

device. U_0 is measured for n=0.5, 1.0, 1.5, 2.0, 3.0, 4.0, 5.0, 6.0, 7.0, 8.0, 9.0 h^{-1}.

ii) Wall-jet measurements

The flow from the inlet which is directed 40° upwards is impinging on the ceiling and creates a flow similar to a wall-jet of three-dimensional character. The velocity profiles are measured in the centre plane and at radii of 1.0 and 1.5m from the inlet. (The exact location of the measurements is shown in figure 5.1).

x	y[1]	z	num. of measurem.	air change rate	integ. time	ref.
0.6	2.365-1.575	0.0	80	1,2,3,4,6,8	90	1
1.4	2.365-1.575	0.0	80	1,2,3,4,6,8	90	2
2.2	2.365-1.575	0.0	80	1,2,3,4,6,8	90	3
3.0	2.365-1.575	0.0	80	1,2,3,4,6,8	90	4
4.0	2.365-1.575	0.0	80	1,2,3,4,6,8	90	5
0.71	2.365-1.575	-0.71	80	1,2,3,4,6,8	90	6
1.0	2.365-1.575	0.0	80	1,2,3,4,6,8	90	7
0.71	2.365-1.575	0.71	80	1,2,3,4,6,8	90	8
1.06	2.365-1.575	-1.06	80	1,2,3,4,6,8	90	9
1.5	2.365-1.575	0.0	80	1,2,3,4,6,8	90	10
1.06	2.365-1.575	1.065	80	1,2,3,4,6,8	90	11

1) In addition to these measurement the maximum velocity of the profile is measured.

Table 5.1. Information about the velocity measurement in the wall-jet region.

iii) Measurements in the occupied zone

The occupied zone is characterized by recirculating flow and relatively low velocity level. The velocity profiles are measured at different locations in the centre plane and the symmetry of the flow is measured. (Table 5.2 gives the exact information of the measurements in the occupied zone).

x	y	z	num. of measurem.	air change rate	int. time	ref
3.6	0.0-0.25	0.0	23	1,1.5,2,3,4,6,7,8	960	12
3.0	0.0-0.25	0.0	23	1,1.5,2,3,4,6,7,8	960	13
2.4	0.0-0.25	0.0	23	1,1.5,2,3,4,6,7,8	960	14
1.8	0.0-0.5	0.0	23	1,1.5,2,3,4,6,7,8	960	15
1.2	0.0-0.5	0.0	23	1,1.5,2,3,4,6,7,8	960	16
In addition to the mesurements listed above an investigation of the symmetry of the flow in the occupied zone made is carried out.						

Table 5.2. Information about the velocity measurement in the occupied zone.

5.3. Closure

In this chapter several aspects of full-scale experimental techniques have been discussed. Full-scale measurements in the field of ventilation require accurate equipment with a high resolution because the gradients often are small and e.g. the velocity level is low. Side effects from the equipment, which cannot be observed when measurering high velocities, may be important in the actual case and special procedures must be used (e.g. influence of flow direction in the calibration etc.).

The outcome of the experimental investigations will be used in the next chapter where comparisons between the full-scale measurements and CFD predictions are made.

CHAPTER 6 - COMPARATIVESTUDY BETWEEN CFD PREDICTIONS AND FULL-SCALE MEASUREMENTS OF THE FLOW PATTERN IN A ROOM VENTILATEDBY THE MIXING PRINCIPLE

6.1 Preamble

As stated in chapter 1 and 2 the field of ventilation engineering has started to look upon CFD as a design and analyzing tool because it offers a radical change in available analytical tools by which the engineer is able to predict the impact of a particular design of an air conditioning system. This is traditionally done by a simplified approach as mentioned in chapter 1 and 2. But in contrast to most test carried out with CFD (e.g. the example in chapter 4) real building and air conditioning systems are often very complex in terms of building - and air supply geometry (fig 1.4) which give rise to complex flow phenomena.

The scope of this chapter is to look into the influences of a modern complex supply terminal used in the mixing type of ventilation. This is done by reporting and by investigating the results from the full-scale experiment outlined in the previous chapter and secondly by simulating the very same case by the method described in chapter 3. Hereafter is it possible to make comparisons between the experimental and the numerical results.

Some of the ideas used in establishing proper boundary conditions for the numerical simulation may just as well be used in other areas were the presence of large gradients demands a large number of computational volumes to resolve the changes.

6.2 Comparisons between CFD predictions and measurements

The purpose of following sections may be summarized: to give a general idea of the flow field in the room and to evaluate the simplified radial approach mentioned in chapter 1, to evaluate and detect isothermal flow dependence of the Reynolds number (LRN effects) (section 6.2.2and 6.2.5) and to investigate different ways to model the inlet device (section 6.2.2,6.2.3 and 6.2.4).

6.2.1 Computational details

The numerical solutions are obtained with the standard k,ϵ-model presented in chapter 2 eq. (2.16)-(2.17). A three-dimensional derivative of the TEACH-T code developed partly at the Imperial College, UK and partly at the University of Aalborg, DK based on the method given in chapter 3. A 32x31x16 (15872 volumes) non-uniform grid is used. A finer grid in the near-wall region and in the area around the inlet, where the false diffusion is distinct due to high level of cell-diagonal velocity, is used. The code is using the SIMPLE solution scheme and the HYBRID differencing scheme. The equations are solved by the TDMA technique.

From 6000 to 9000 iterations are required to obtain reduction of the mass-residual from $1x10^{1}$ to $1x10^{-4}$ based on the criterion in eq. (3.29). Fig. 4.2 shows the convergence history for the mass-residuals.

All simulations are performed only in one half of the room because symmetric flow is assumed.

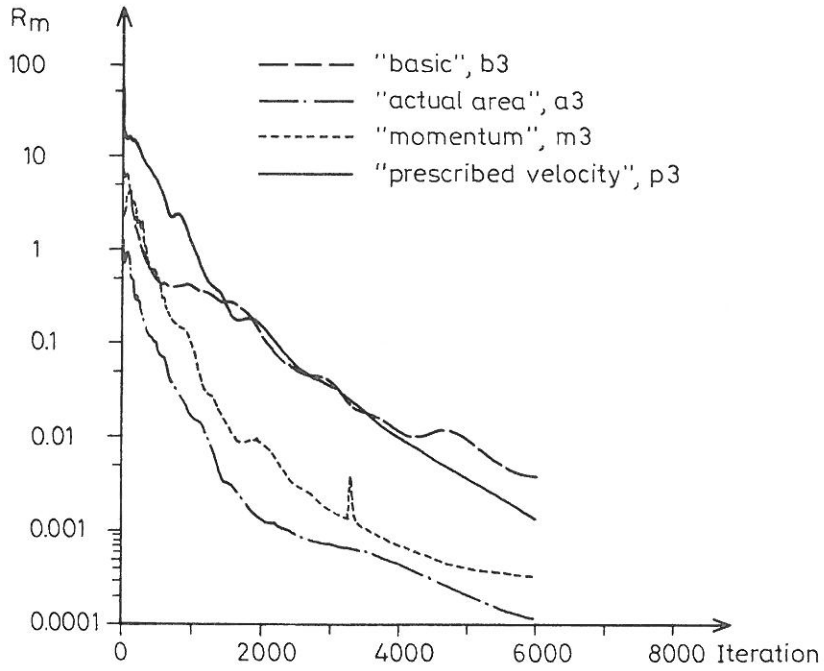

Figure 6.1 Convergence history for the mass-residual in each of the four test cases.

6.2.2 Boundary conditions

It is well known that the velocity level in a room ventilated by a mixing type of ventilation is strongly influenced by the supply conditions *(Nielsen 1976)* and that

it is the momentum flow of the inlet which has the major impact of the flow pattern in the room (except maybe for very low inlet velocities). It is also known that the impingement of the inlet-jet upon the ceiling decreases the momentum in the jet (*Mc Ree et al. 1967*). It is therefore important that the model of the inlet is able to produce the wall-jet momentum after the impingement. This may be done by a model of the inlet device and then calculate the impingement or by use of empirical data. In the following several inlet models is proposed and tested.

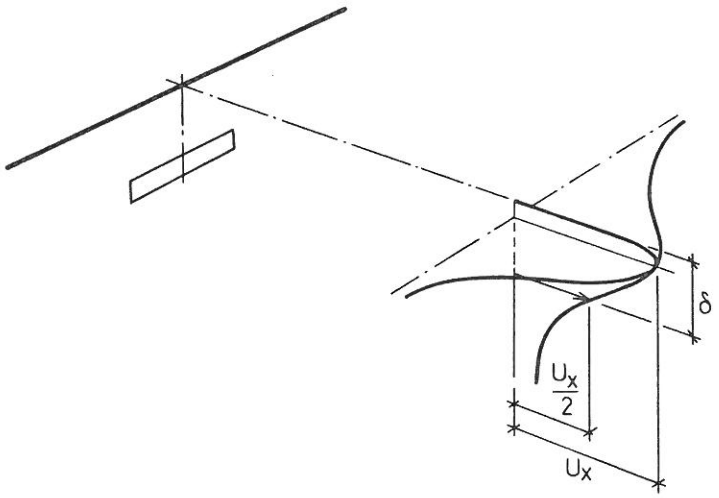

Figure 6.2. Typical flow from a wall mounted diffuser.

Fig. 6.2 shows a typical mounting of an inlet device in a wall. The flow from the inlet creates a wall-jet type of flow in a certain distance from the inlet, either because the inlet flow is directed upwards or because it is influenced by the Coanda effect. An attempt to model the inlet directly would in most cases require too much computational effort to be realistic. Another more comprehensive way would be to prescribe the actual conditions in a volume where the flow has adopted wall-jet character. Such a method implies that device specific data are available.

6.2.2.1Inlet conditions

The complex inlet device used in the present test case is chosen to give a complicated flow pattern around the inlet and is therefore a realistic test of the CFD method. The present inlet device is difficult to model directly because the many small nozzles are distributed, over a fairly large area and are directed upwards in an angle of 40°. It is therefore decided to try several approaches to represent the inlet flow conditions.

i) The "basic" method

The assumptions for this method are that the momentum flow in the jet created around the inlet should be represented by a simple model. The distributed nozzles are simulated by a single rectangular opening having the same effective inlet area, the same aspect ratio (h/w) and a flow rate equal to the measured and therefore the same momentum flow as the actual diffuser. The centre of the inlet is situated 0.285m below the ceiling and 1.80m from the sidewalls.

The first problem is to establish the right a_0 for different inlet velocities, as this generally will be a function of the inlet Re number unless the flow is fully turbulent. Measurements are made to investigate the Re-number depence on the inlet device. The result is depicted in fig 6.3.

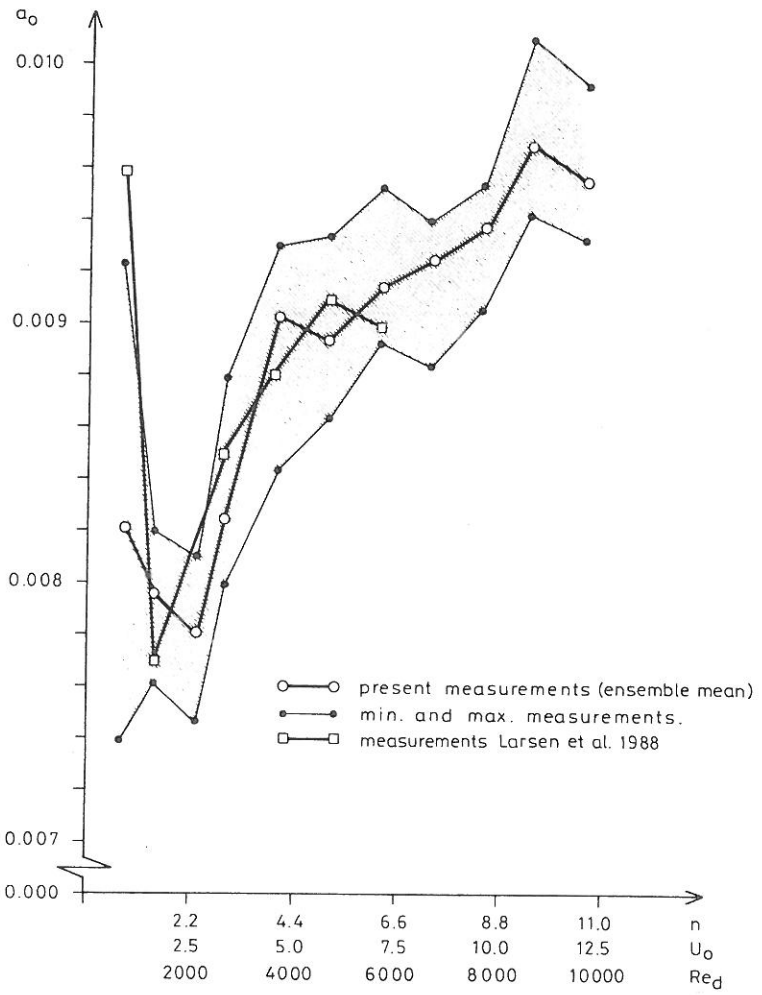

Figure 6.3. The effective inlet area as a function of the inlet velocity

As it can be seen the a_0 area is not a constant, but an increasing function of the Reynolds number due to the transition from laminar to turbulent flow through the nozzles. The curve has a minimum which is referring to the transition point. This transition is seen at Re_d equal to 2000 which correspond to the assumed $Re_{critical}$ for a tube. The large a_0 value for $n = 0.5\ h^{-1}$ may be explained by asymmetric flow in the opening or geometrical effects within the diffuser.

From fig. 6.3 it may be concluded that the flow even though it is turbulent has a dependency of the supply velocity which can be interpreted as an initial laminar effect.

Fig 6.3 gives following effective areas for air change rates 1, 3 and 6 h^{-1}:

$a_o = f(u_o)$

for $n = 1 : 0.008\ m^2$

for $n = 3 : 0.00855\ m^2$

for $n = 6 : 0.009\ m^2$

Which gives following inlet conditions

case	w	h	U_{inlet}	V_{inlet}	W_{inlet}	I_0	n
b1	0.18	0.045	0.903	0.757	0.0	0.012	0.93
b3	0.18	0.048	2.71	2.2	0.0	0.13	3.0
b6	0.18	0.05	5.42	4.54	0.0	0.54	6.3

For k and ϵ are used:

$k_0 = 1.5*I^2U_{inlet}^{\ 2}$, $I = 0.1$

$\epsilon_0 = C_\mu^{3/4}k_0^{3/2}/l$, $l = h/10$

ii) The "actual area" method

The method is based upon the essence of fig. 4.7 which says that the maximum velocity in the recirculation zone (i.e the occupied zone) is a linear function in the inflow momentum. The diffuser is modelled by a single rectangular opening with the same aspect ratio as the diffuser but the size of the perimeter of the inlet device

which means that the momentum flow is distributed over a surface similar to the real condition. The centre of the inlet is 0.285m from the ceiling and 1.80m from the sidewalls. The method do not decouple the boundary conditions for the momentum equations and the continuity equation and consequently the inlet mass flow is different from the real mass flow.

The assumptions give following inlet conditions:

case	w	h	U_{inlet}	V_{inlet}	W_{inlet}	I_0	n
a1	0.70	0.20	0.229	0.19	0.0	0.013	3.5
a3	0.70	0.20	0.68	0.57	0.0	0.13	11.3
a6	0.70	0.20	1.37	1.15	0.0	0.54	19.0
U_{inlet} is also used as boundary condition for the continuity equation which is the reason for the high air-change-rate.							

For k and ϵ are used:

$k_0 = 1.5*I^2U_{inlet}^2$, I = 0.1
$\epsilon_0 = C_\mu^{3/4}k_0^{3/2}/l$, l = h/10

iii) The "momentum"method

The method is a development of the previous method. The method separates the boundary conditions for the momentum equations and the continuity equations (the method has previously been used by *Chen et al. 1991* and *Heikkinen 1992*). The correct mass flow is set as boundary condition in the inlet opening and the correct momentum flow is ensured by an extra source term introduced after the mixing of the many small jets. The distance of mixing is observed from smoke experiments to be 0.05-0.06m from the inlet.

For k and ϵ is used:

$k_0 = 1.5*I^2U_{inlet}^2$, I = 0.1
$\epsilon_0 = C_\mu^{3/4}k_0^{3/2}/l$, l = h/10

The assumptions give following inlet conditions after the extra momentum source:

case	w	h	U_{inlet}	V_{inlet}	W_{inlet}	I_0	n
m1	0.70	0.20	0.229	0.19	0.0	0.013	1.0
m3	0.70	0.20	0.68	0.57	0.0	0.13	3.0
m6	0.70	0.20	1.37	1.15	0.0	0.54	6.0
For boundary conditions for the continuity equations is the correct air-change-rate - converted to U-velocity - used.							

iv) The "prescribed velocity" method

In this model the boundary conditions are given as a simple opening which is the size of the outline of the inlet device (as in ii) and iii)). The mass flow corresponds to the required air-change-rate. The fulfillment of the momentum requirements are obtained by prescribing the boundary conditions in a imaginary box in front of the diffuser (fig. 6.4) at a location where the wall-jet type of flow is established and where the flow characteristic is of parabolic nature.

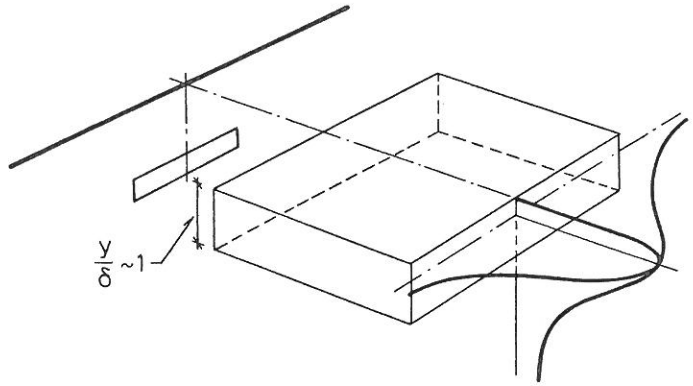

Figure 6.4. The location of the imaginary box in front of the inlet device.

The method utilizes that the velocity in the established jet can be described by

$$U_r = K(\theta)\, U_0 \frac{\sqrt{a_0}}{x+x_0} \tag{6.1}$$

The $K(\theta)$, a_0 and x_0 functions are determined (see A.6.1 or *Skovgaard et al. 1990b*). a_0 as a function of U_0 is depicted in fig 6.3, $K(\theta) = K(40,\theta)$ and x_0 is evaluated in appendix A.6.1. In addition to the anemometer measurements reported in A.6.1 additional smoke-visualisation experiments are carried out (fig. 6.5) so $K(\theta)$ can be established more accurate.

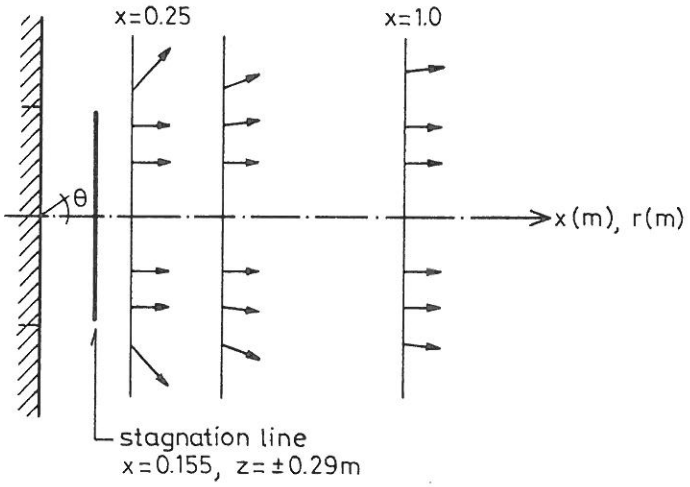

Figure 6.5. The flow field in front of the diffuser visualized by smoke (Nielsen 1991).

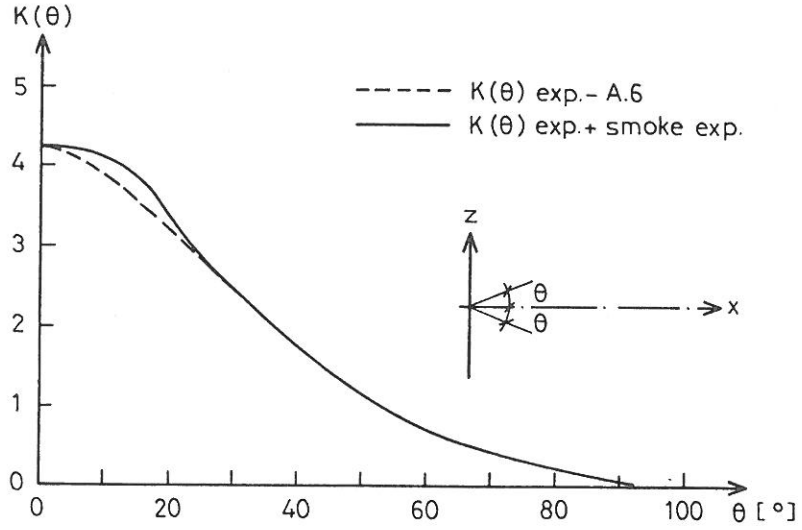

Figure 6.6. K(θ) interpolated from the velocity experiments in A.6 and the smoke experiments in fig. 6.5.

Fig 6.6 shows two different shapes of the $K(\theta)$ factor. The dotted line is the outcome of an interpolation from the anemometer measurements (fig. A.6.6). Later and more detailed flow experiments revealed a zone with parallel flow (fig. 6.5).

This parallel flow is taken into account by holding K(θ) constant in this area. This approach leads to the full line in fig. 6.6. The K(θ) is implemented in the program in the following way

$$K(\theta) = 4.2 - 0.975\theta - 8.206\theta^2 + 7.828\theta^3 - 2.088\theta^4$$

θ is in rad and $\theta << 1$ for $z < 0.2$m.

U and V are calculated from

$U = \cos\theta U_r$
$V = \sin\theta U_r$

U and V profiles are self similar up to a distance of $y/\delta = 1.0$ under the ceiling (*Nielsen 1989b*). The following wall-jet profile is assumed (*Verhoff 1963*)

$$f\left[\frac{y}{\delta}\right] = 1.4794\left[\frac{y}{\delta}\right]^{\frac{1}{7}}\left[1-erf\left[0.6775\left[\frac{y}{\delta}\right]\right]\right]$$

and δ is taken from A.6.1

$$\delta(x) = 0.08(x+0.45)$$

The assumptions give following inlet conditions:

case	w	h	U_{inlet}	V_{inlet}	W_{inlet}	I_0	n
p1	0.70	0.20	0.072	0.0	0.0	pres.	1.0
p3	0.70	0.20	0.216	0.0	0.0	vel.	3.0
p6	0.70	0.20	0.432	0.0	0.0		6.0
The level of momentum flow is given through prescibing the velocity in the wall-jet.							

For k and ϵ are used:

$k_0 = 1.5*I^2U_{inlet}^2$, I = 0.1
$\epsilon_0 = C_\mu^{3/4}k_0^{3/2}/l$, l = h/10

6.2.2.2Outlet boundary conditions

All gradients in the outflow plane are zero as well as the pressure. Outlet U-velocity is set to fulfil the overall continuity according to eq. (3.25).

6.2.2.3Wall boundary conditions

Because of the validity range of turbulence model (fully turbulent region) the no-slip boundary conditions have to be introduced indirectly by wall functions in the source term at the first gridnode. This approach has also the advantage that it reduces the number of gridnodes in the near wall region. However, this method can be difficult to use in areas where the maximum velocity is found close to the surface (e.g. the wall-jet region).

The boundary conditions are given by the shear force at the wall and the velocity parallel to the surface in the first gridnode according to eq. (3.23) and (3.24). Boundary conditions for k and ϵ is set according to section 3.2.5-iii.

6.2.3 Predicted flow patterns

The overall flow patterns for the four simulated cases are shown in fig. 6.7-6.10.

Predictions with the basic model show that the radial jet below the ceiling, fig. 6.7g, has a component of very high velocity directed against the upper downstream corners. The velocity distribution below the ceiling in the other cases (fig. 6.8-6.10) has a characteristic "peak" along the centre line (fig. 6.8g-6.10g). This is also observed in the experiments as a area with parallel flow (fig. 6.5). Measurements by *Heikkinen 1991* have also shown this combination of three-dimensional jet flow and radial jet-flow. The flow pattern in the occupied zone is very similar for the "actual area" model and the "prescribed velocity" model (fig. 6.8h and 6.10h) while the velocity level in the "basic" model is too high. In the "momentum" model the

velocity in the centre plane is too low and the maximum velocity is located closer to the sidewalls than in the other simulations. This may in the "basic" model be due to the spread of the jet and the low mixing of the concentrated jet and in the "momentum" method due higher numerical diffusion because the momentum source is introduced in only one layer of computational cells (hereafter called one sheet) in front of the inlet. It is also noticed that neither of the "actual area" or the "momentum" model has established a characteristic wall-jet character. Also the entrainment of the surrounding air in the "basic" and the "momentum" model is considerably different that in the other two.

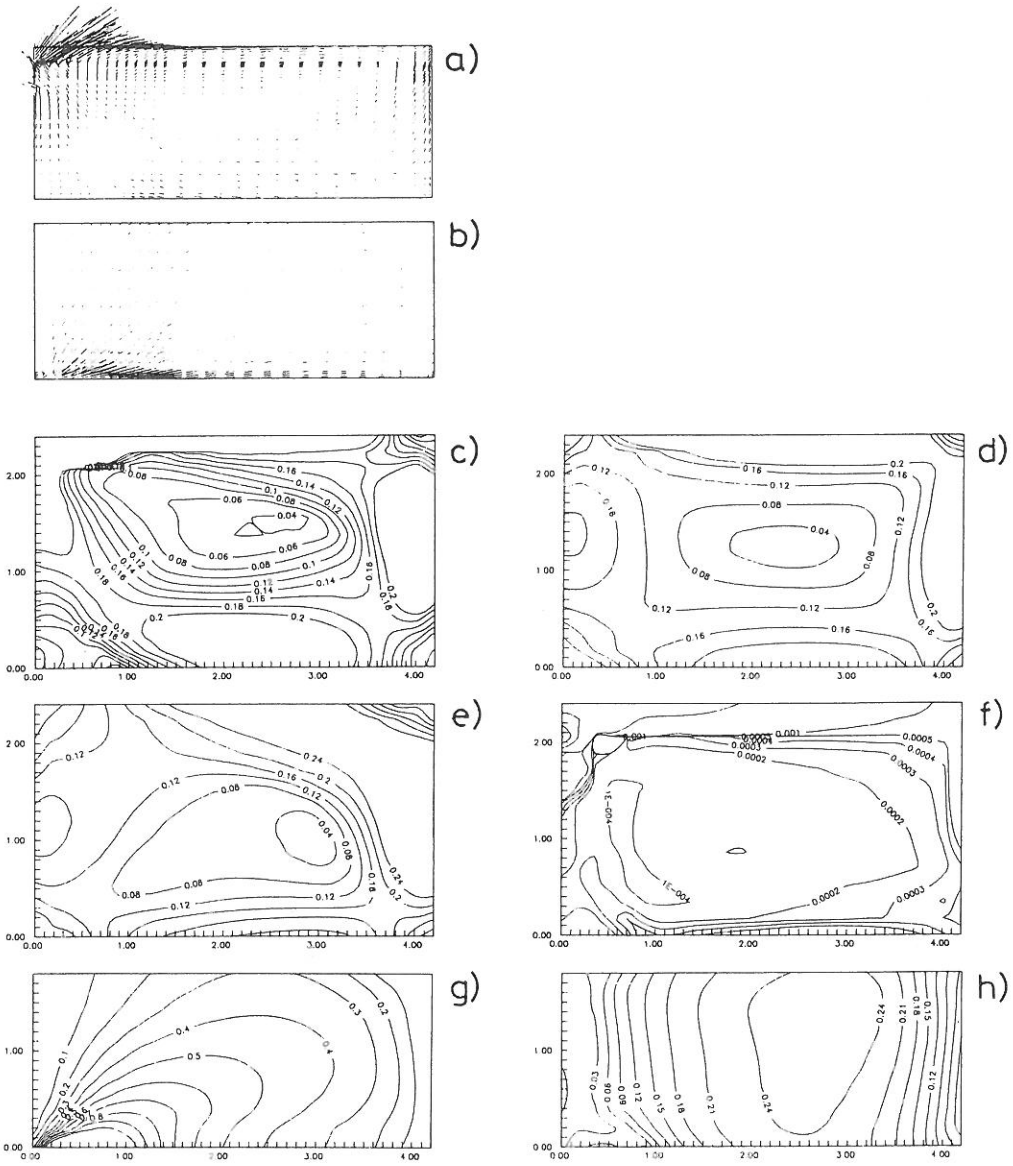

Figure 6.7. Air flow patterns from the basic model (b3). a) Velocity vectors in the centre line. b) Velocity vector in a plane 0.04m below the ceiling. c)-e) Speed contours in the

planes z = 0.02, 1.0 and 1.7m. f) Iso-kinetic energy in plane z = 0.02. g)-h) Speed contours in y = 2.36 and y = 0.05.

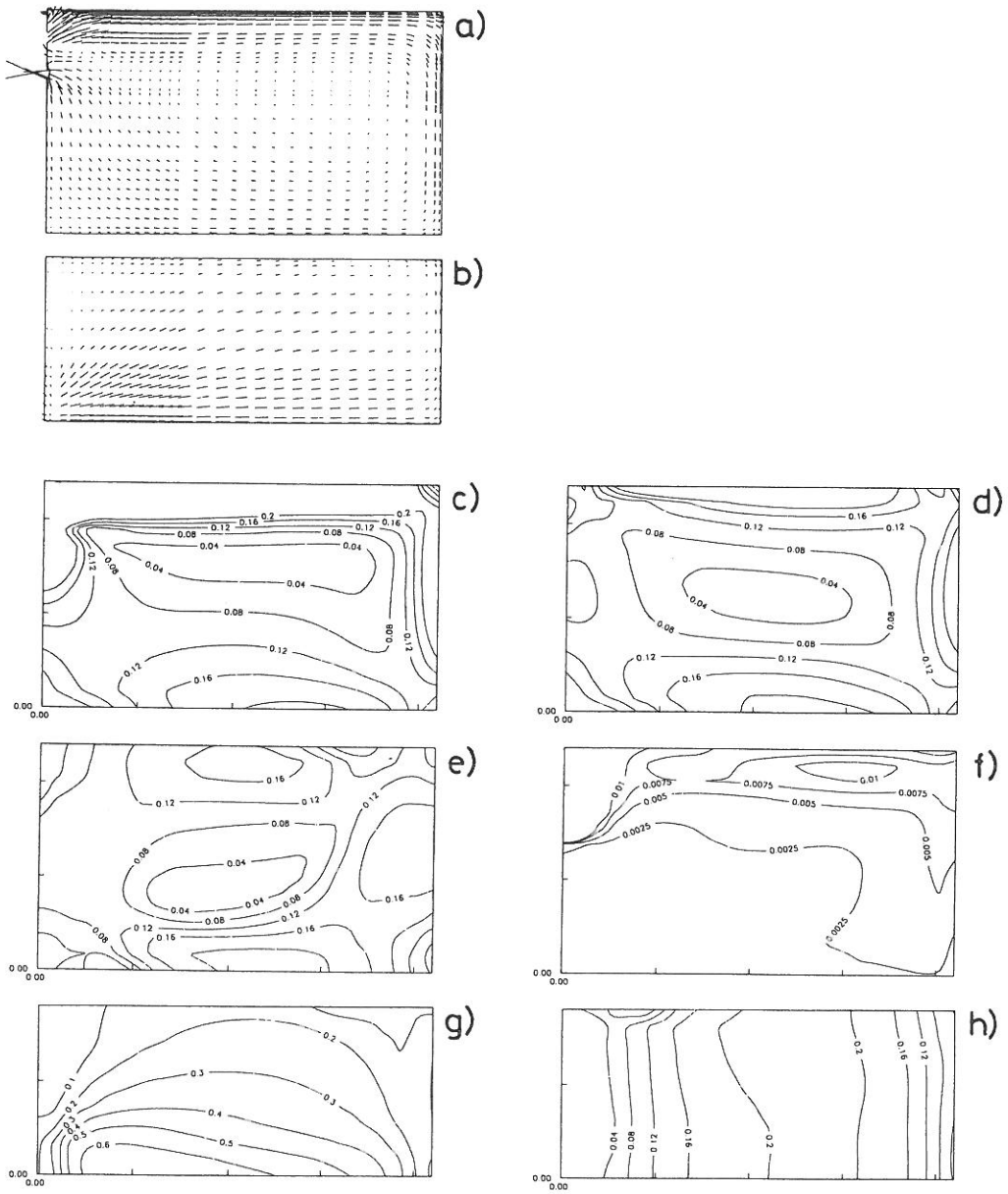

Figure 6.8. Air flow patterns from the "actual area" model (a3). a) Velocity vectors in the centre line. b) Velocity vector in a plane 0.04m below the ceiling. c)-e) Speed contours in the planes z = 0.02, 1.0 and 1.7m. f) Iso-kinetic energy in plane z = 0.02. g)-h) Speed contours in y = 2.36 and y = 0.05.

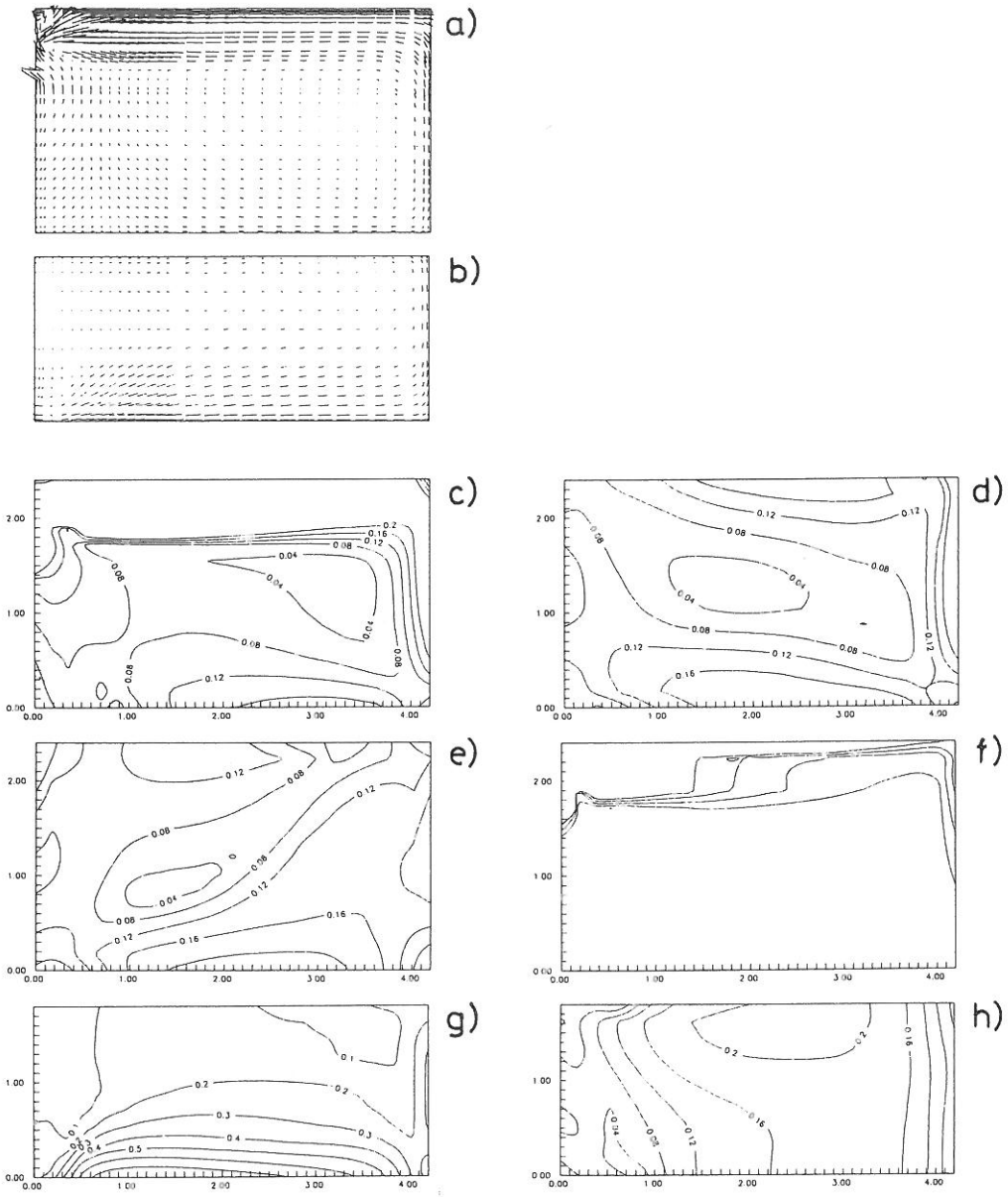

Figure 6.9. Air flow patterns from the "momentum" model (m3). a) Velocity vectors in the centre line. b) Velocity vector in a plane 0.04m below the ceiling. c)-e) Speed contours in the planes z = 0.02, 1.0 and 1.7m. f) Iso-kinetic energy in plane z = 0.02. g)-h) Speed contours in y = 2.36 and y = 0.05.

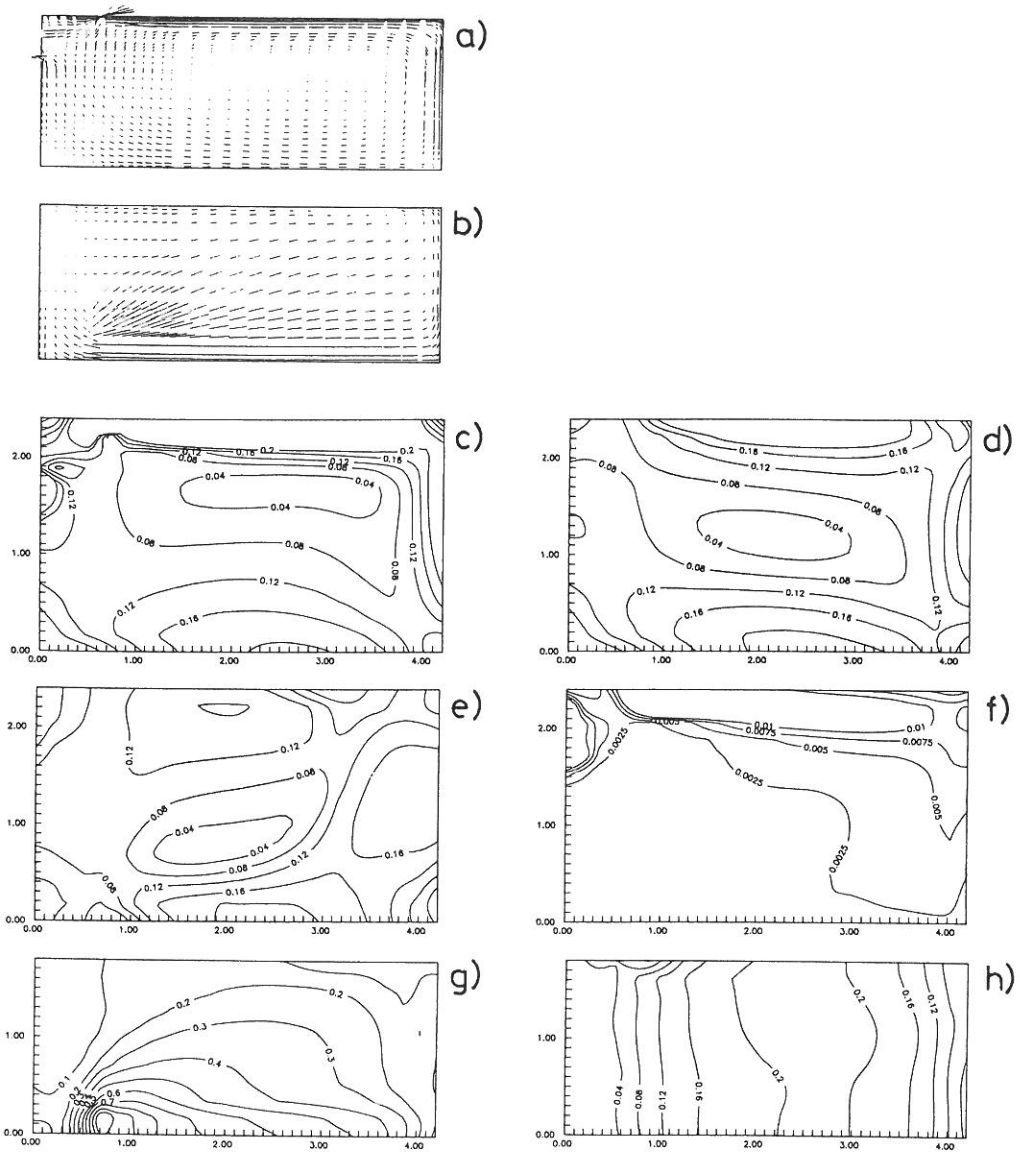

Figure 6.10. Air flow patterns from the "prescribed velocity" model (p3). a) Velocity vectors in the centre line. b) Velocity vector in a plane 0.04m below the ceiling. c)-e) Speed contours in the planes z = 0.02, 1.0 and 1.7m. f) Iso-kinetic energy in plane z = 0.02. g)-h) Speed contours in y = 2.36 and y = 0.05.

The area with the maximum velocity, U_{rm}, in the occupied zone is located very close to the wall opposite the supply opening (fig. 6.15). The predictions are not able to reproduce this location.

6.2.4 Comparisons in the jet region

The results in fig. 6.11-6.13 relate the measured data (A.6.1) to the simulated. Fig. 6.11 depicts the decay of the centre line velocity. x_0 is measured to 0.45 m behind the inlet. $a_o^{1/2}$ is again taken from the measured data in fig. 6.3.

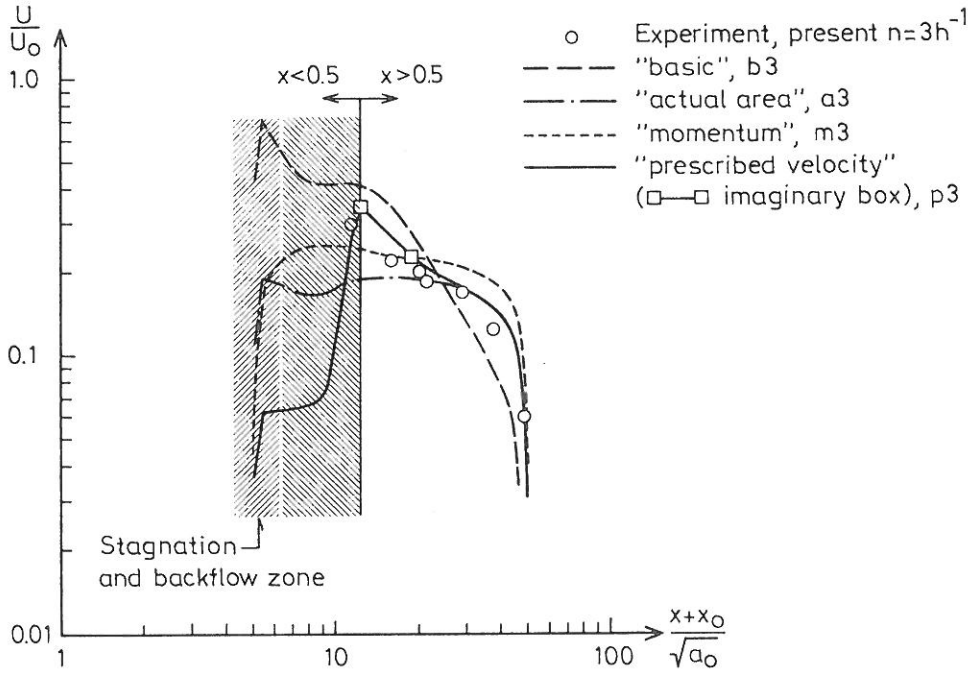

Figure 6.11. Measured and simulated decay of peak centre line velocity.

It is seen that discrepancies are found in all simulations due to the very complex flow structure in the real case. In the "basic" case, the peak velocity decreases too rapidly caused by the flow going outwards towards the corners. The "actual area" and the "momentum" method have totally different shapes because the flow under the ceiling haven't developed a wall-jet structure. However the "actual area" model performs better than the "momentum" method. If one focus on the "prescribed velocity" model it is seen that although discrepancies are present the velocity decay after the imaginary box is simulated with good accuracy.

The width of the jet in the centre plane, which is depicted in fig. 6.12, has a close connection to the results shown in fig. 6.11. It is seen that the spread of the jet simulated by the "prescribed velocity" method is close to the measured values while the "basic" case shows a similar rate of decay but with another virtual origin. The "actual area" method gives the same level of velocity and the right shape of the

wall-jet profile in the region near the end wall of the room and yields therefore the same velocity pattern in the occupied zone as the "prescribed velocity" method (fig. 6.8h and 6.10h).

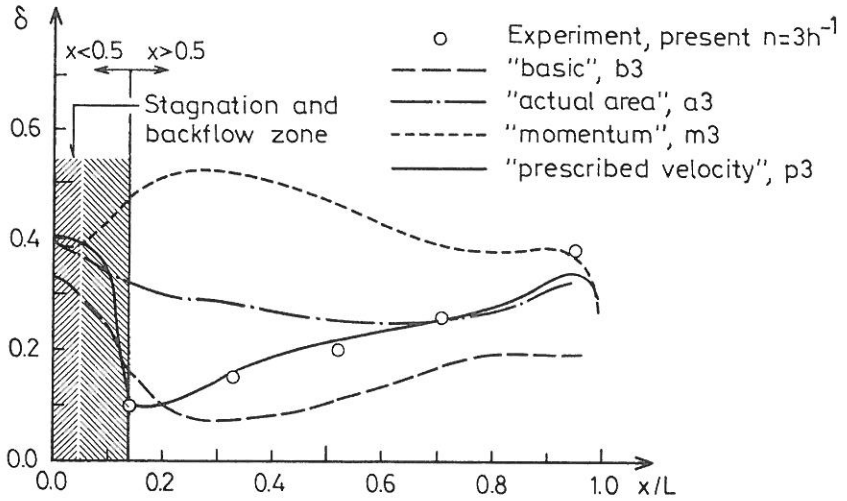

Figure 6.12. Spread of the wall-jet in the centre plane.

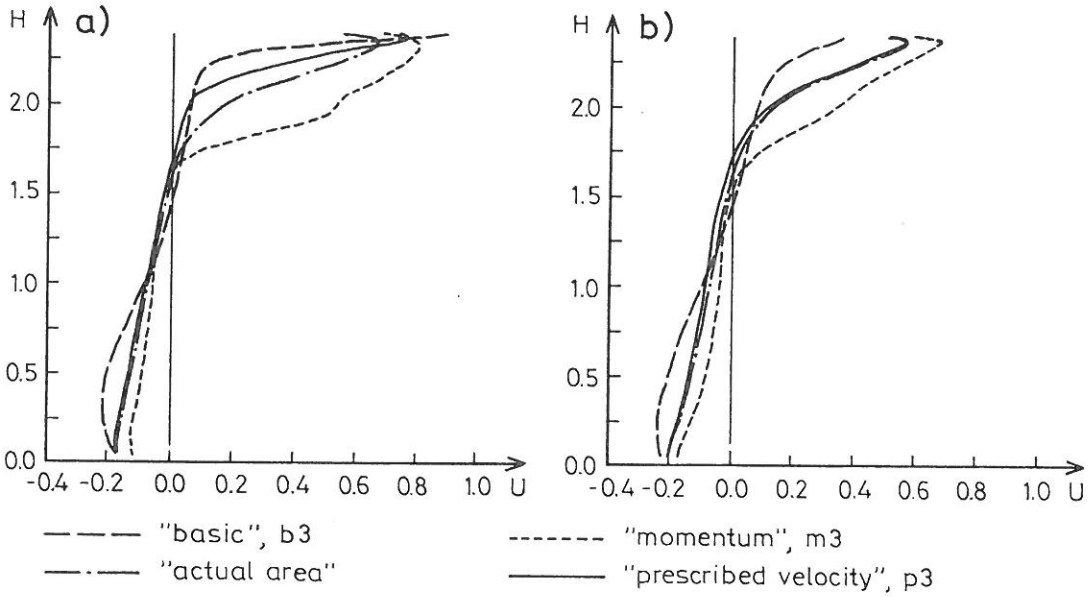

Figure 6.13. Simulated U-velocity profiles in the plane z=0.02. a) x/H=0.33 and b) x/H=0.67.

Fig 6.13 shows simulated U-velocity profiles in the centre plane of the room. The figure supports the results from the other two figures. The "basic" model gives too

narrow profiles and the velocity decays too rapidly due to the spread of the velocity towards the corners of the room. The "actual area" and the "momentum" models result in profiles of a different shape than the "prescribed velocity" model. It is again seen that the velocity profile resulting from the "actual area" method is adapting the right shape in the "downstream" end of the room.

The predictions indicate that a good description of the boundary conditions especially a good representation of the inlet momentum, both in term of the correct total inlet level and the right distribution, is a necessary requirement for the prediction of fully turbulent flow patterns with acceptable accuracy.

6.2.5 Comparisons in the occupied zone

One of the main purposes of a design process is from a comfort point of view to predict the velocity distribution and especially maximum velocity in the occupied zone. Fig. 6.14 shows the measured and the predicted maximum velocity U_{rm}. The figure shows that the "prescribed velocity" method is giving the best estimate of U_{rm}. But it can also be seen that the performance is poor for n = 1 in all the models because the low Reynolds number effect has a pronounced effect on the flow at low velocities.

Several authors have made studies of this phenomenon (see e.g. *Skovgaard et al. 1990a*, *Murakami 1983* or *Restivo 1979*) but it has not led to any prediction of it because the use of the standard k,ϵ-model presumes a fully turbulent flow. The low Reynolds number effect i fig. 6.14 arises partly from the supply device and partly from the flow in the room (appendix A.6.2). The "basic" model can incorporate the change in the effective area, a_o and the "prescribed velocity" model can in addition to this also include variations in the prescribed volume up to a distance of x=1.35m. The effects are not obvious in any of the predictions. This is partly because the change in K(θ) as a function of air-change-rate isn't taken into account in the "prescribed velocity" model (it is chosen to apply a mean-value of the K(θ)-function). But it is also because low Reynolds effects are generated inside the flow and therefore cannot be described by the boundary conditions. Further investigations in this specific area is made in the next chapter.

Another thing which was revealed in the experiments was symmetrical flow in the jet region under the ceiling (which is why it was decided to make symmetrical simulations), but in the occupied zone further investigations showed a strong asym-

metrical flow (fig. 6.15).

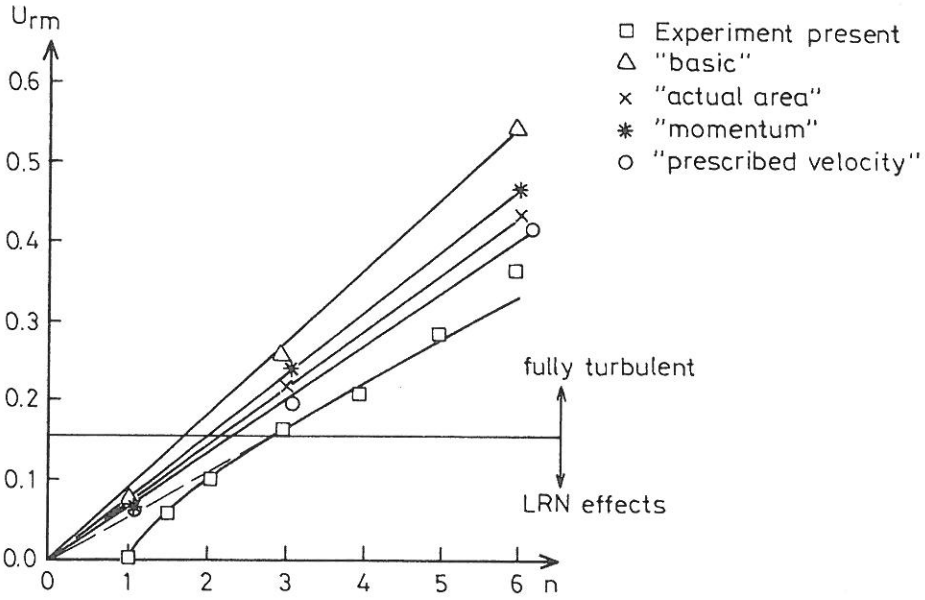

Figure 6.14. U_{rm} as a function of air change rate.

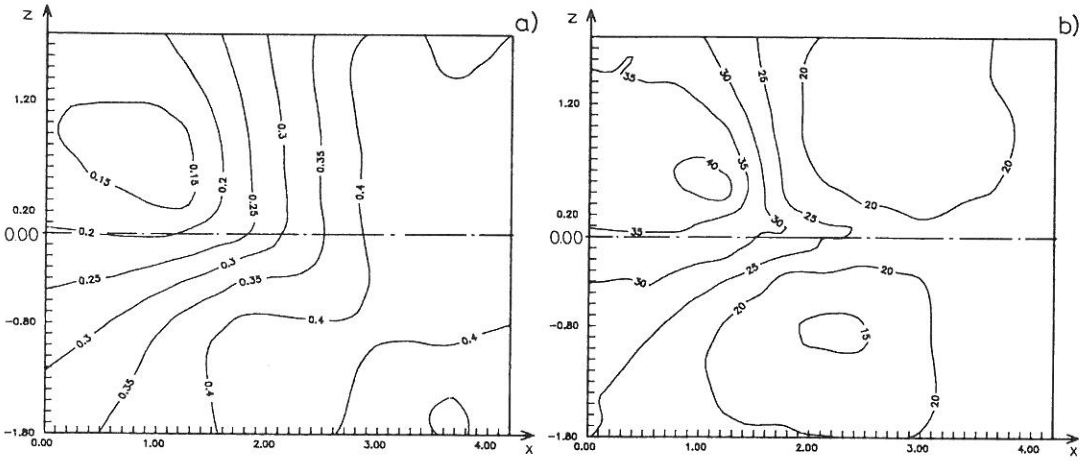

Figure 6.15. Hotwire measurement of the velocity in the occupied zone. Asymmetrcal flow is observed. a) mean velocity. b) turbulence level.

The figure shows that the jet is deflected towards one corner and runs diagonally across the floor. Figure 6.15b shows the turbulence level in percent. The figure shows clearly that turbulence is a generated/dissipated phenomenon but the relevance of including transport mechanisms is apparently also of great importance.

The flow asymmetry is not predicted in the simulations because of the symmetrical boundary conditions. A necessary cure for this is to simulate the whole flow domain in situations like the one investigated.

As previously mentioned one of the major benefits using CFD analysis of flow fields is the very detailed knowledge of the velocity, turbulence and thermal parameters in the room. These data can be used in a comfort analysis of the room or the occupied zone. In fig.6.15such an application is shown where the PD index (percent dissatisfied) is calculated.

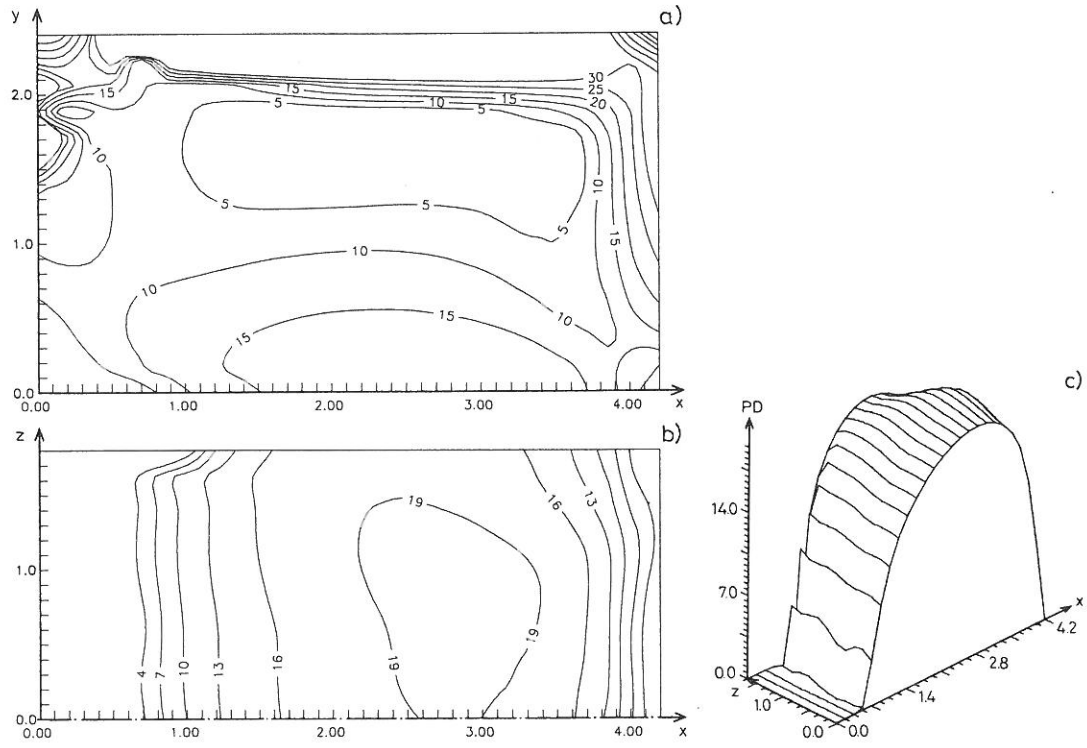

Figure 6.16. Calculated PD index. a) z = 0.02. b) foot height, 5 cm above the floor.

The calculation is given as an example and the same equation is therefore used for the full room and for the foot level, although it is known that the draft tolerance is higher at foot level than at the average of the body. The comfort equation mentioned in the introduction is used (eq. (1.11) (*Fanger et al. 1989*)).

6.3 Closure

From the simulations made in this chapter it can be concluded that CFD simulations of airflow patterns in ventilated enclosures result in valuable detailed information of comfort parameters and therefore are useful as analyzing and design tools.

The simulations carried out includes an oblique impingement on the ceiling of the jet created by the inlet device, which is not uncommon in real ventilation problems, but which is complicated to measure and to calculate.

The main conclusion is that a good representation of the boundary conditions is a necessary requirement for prediction of the boundary conditions. The most important property is the inlet momentum. Four different inlet models are tested and the most accurate is the "prescribed velocity" method which make use of measured data to ensure the momentum in the jet is exactly as in the real situation both with respect to direction and amount. By this method it is possible to predict the overall flow pattern, the velocity decay in the jet and the maximum velocity in the occupied zone with satisfactory accuracy. The second-best model is the "actual area" model which gives a good description of the inlet momentum flow but a far to large mass flow rate. This higher mass flow rate has no influence on the velocity level and the maximum velocity in the occupied zone is predicted reasonably well. This result is useful because it means that the method can give a idea of the flow pattern and the velocity level very quickly. The result may also be used to set up scale-model experiments without making an completely exact and very detailed model of a complicated inlet device. The other two models yields rather unsatisfactory results e.g. is the "basic" model is not even able to reproduce the overall flow pattern correctly.

In preliminary predictions the result showed significant traces of numerical diffusion especially around the inlet where the gradients were large. This diffusion is strongly grid dependent and it is necessary to use a finer grid near the inlet as the one applied in this chapter.

The experiments revealed two phenomena which the simulations fail to predict: the asymmetry in the occupied zone and LRN effects.

In order to be able to predict the asymmetry of the flow the symmetric approach must be abandoned and it is possible that true time-dependent simulations must be carried out if the phenomenon is a matter of instability of the jet-flow.

The other aspect is the LRN effects which the experiments indicate to arise partly from the inlet and partly within the room. The effects comming from the inlet can be incorporated in the numerical model presented in this chapter but the effect is rather small. It seems that the major source of the LRN effects is deriving from the room and where the velocity is below 0.15-0.20m/s (see appendix A.6.2). This kind

of low Reynolds effects cannot be simulated by the standard k,ϵ-model because it presumes fully turbulent conditions. The next chapter is devoted to a more detailed examination of the low Reynolds number phenomenon.

CHAPTER 7 - INVESTIGATION OF LOW REYNOLDS NUMBER EFFECTS

7.1 Preamble

In the previous chapter it was concluded that the flow patterns occurring in mechanically ventilated spaces give rise to many complications when one wants to describe them theoretically and/or predict them numerically. Chapter 6 was dedicated to detect these complications and to simulate some of the complications, which were directly related to the inlet boundary conditions. It was shown that only by careful modeling of the inlet boundary conditions the flow characteristics could be simulated satisfactory. But such phenomena as transitional effects in the resulting jets and low Reynolds number effects in the room could not be simulated by the used standard k,ϵ-model.

Some studies of the LRN effects have recently been carried out - both numerically (e.g. *Skovgaard et al. 1991a, Murakami, 1983* and *Chen 1990)* and experimentally (e.g. *Nielsen et al. 1988a, Skovgaard et al. 1990b, Heiselberg et al. 1987* and *Restivo 1979).*

This chapter reports work done on the low Reynolds number flows near the wall and in the transitional jet regime. Both areas are important when one wish to predict flow patterns in a ventilated room because the velocity level in a room is strongly influenced by the inlet momentum flow and - at lower velocities - by the boundary layer flow (as stated in chapter 1).

7.2 Numerical investigation of low Reynolds number effects

The numerical investigations of the LRN effects are done with a low Reynolds number k,ϵ-model - the Launder-Sharma version of the Jones-Launder model which is presented in chapter 2 eq. (2.18)-(2.21). This particular model is chosen because the damping functions f_μ, f_1 and f_2 include no irrelevant distances from the wall and are functions of the local turbulent Reynolds number only. It is therefore possible that this model may be able to predict LRN effects in recirculating flows in areas where the local Reynolds number is small.

The simulation of the LRN effects is done in three different cases. The first case serves as a test of the turbulence model in the near-wall region, which is the region

for which the model is developed. The second case is a two-dimensional geometry similar to the test case used by *Nielsen 1978* and others. The test case is chosen to determine whether it is possible to obtain reasonable agreement by the model and the measured data at a relevant Re-number. In the last test case the model is used to simulate transitional flow over a backward facing step in the Reynolds number range typical for room air flows.

The test cases are chosen to cover similar LRN phenomena as all the phenomena mentioned in the preamble.

The two-dimensional elliptic flow solver TEAM *(Huang 1986)* which has been extensively used and validated is used to obtain the flow solutions. The code is using the finite volume technique to solve the equations mentioned in chapter 2 employing the staggered grid layout to overcome the checkerboard phenomenon. The solution scheme is SIMPLE and the differencing scheme is QUICK for convective terms in the momentum eq.s and PLDS for other terms and variables. This differencing procedure has shown to work well when dealing with low Reynolds number models (*Davidson 1989* and *Ince et al. 1989*). A non-uniform grid is used to achieve a finer grid in the near wall region and in the shear layers. In fact the solution is rather sensitive to the grid layout especially the region $5 < y^+ < 30$ due to the shift in the dissipation variable. The equations are solved by the TDMA technique in an ADI - iterative manner. As expected the convergence is rather slow because of the slow diffusive processes in the boundary layer and because of the fine necessary grid.

7.2.1 Near-wall turbulence - test of the LRN k,ϵ-model

To validate the performance of the model it is chosen to apply it to fully developed channel flow. Primarily because a wide range of data is available for comparison and secondly because the fully developed U, k and ϵ profile will serve as inlet conditions in the later application.

The case is solved one-dimensionally with fixed dP/dx, in the u - momentum eq. In this way it is only necessary to solve for U, k and ϵ. 35 gridnodes are used in the cross stream direction. Boundary condition for u, k and ϵ is set to zero on the walls.

Fig. 7.1a depicts the mean velocity up through the boundary layer for Re_{bulk} =

50,000. As seen the U^+ values in the sub-layer are in good agreement with the RSM

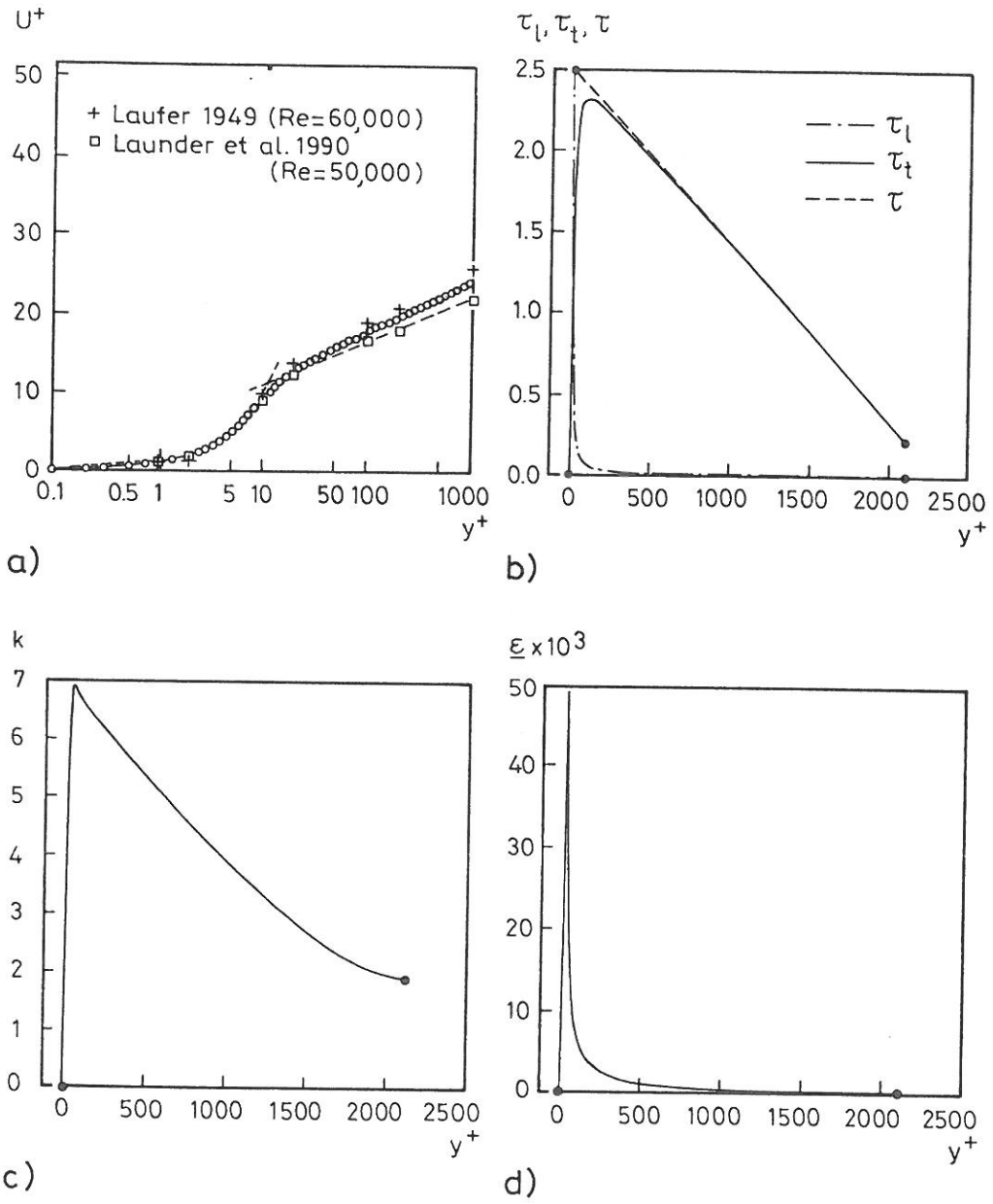

Figure 7.1. Simulated data from the straight channel flow. Experimental data by Laufer 1949. RSM data by Launder and Tselepedakis 1990. a) U^+ *values as a function of* y^+ *(o), b) shear stress profiles, c) k profiles and d)* ϵ *profiles.*

data (*Launder et al. 1990*) and the experimental data of *Laufer 1949*. In the outer fully turbulent region the U^+ values are too high compared to the log. law and the RSM data. *Patel et al. 1985* concludes that it is caused by the source term $C_{\epsilon 3}$..... which increases the dissipation level in the shear layer giving a too low k level. The three other pictures in fig 7.1 correspond well to the overall characteristics of a

channel boundary layer (fig. 1.3).

7.2.2 Test of the turbulence model in a confined two-dimensional enclosure

In this section the turbulent isothermal flow pattern in a simple two-dimensional room geometry is calculated with the low Reynolds number model. This particulary geometry has been used by several authors to validate different computer codes and models because of the availability of measurements made by the laser Doppler anemometry technique and because of the absence of imposed complications (e.g. complicated inlet geometry, LRN effects (except for the near-wall region) and any pronounced three-dimensional structure).

The geometry of the test case is L/H=3.0, h/H=0.056 and t/H=0.16 (see fig. 7.2) and the actual dimensions used in the present simulation are H=3.0m, L=9.0m, h=0.168m and t=0.48m. As pointed out in the specification the inlet opening is rather large compared to practical diffusers (it can be mentioned that the ratio $a_0^{1/2}/H$ is equal to 0.035 in the three-dimensional test case in the previous chapter). In the present case where a low Re number k,ϵ-model is used it is necessary to use

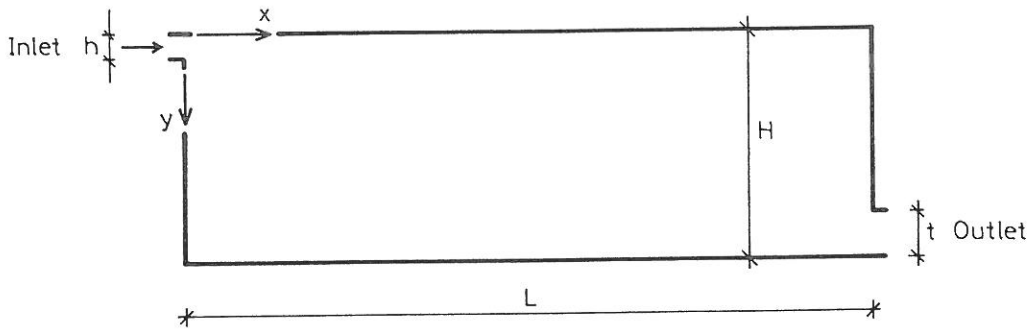

Figure 7.2. The geometry of the two-diensional test case.

a fine grid in the opening because of the inlet is located close to the ceiling. The grid used is 38 in the flow-direction and 78 in the cross-stream direction.

The test case and the experimental data are described in detail in the internal IEA-annex 20 report by *Nielsen 1990*.

The boundary conditions for the test case are:

Inlet : $U_0=5000\mu/(\rho h) = 0.455$ m/s
$V_0=0.0$
$k_0=1.5(0.04U_0)^2$
$\epsilon_0=k_0^{1.5}/(h/10)$

Outlet : $U_{out}=U_0h/t = 0.159$ m/s
$dV/dx=d\epsilon/dx=dk/dx=0.0$

Wall : $U=V=\epsilon=k=0.0$

Comparisons with LDA measurements

Figure 7.3 shows the predicted velocity field and the distribution of turbulent kinetic energy.

Fig. 7.4 shows the comparison between the computed velocity and kinetic energy profiles.

As seen the overall agreement is very good. It is seen that the inlet conditions for k_o have very little effect on the turbulence level in a distance from the inlet, which again means that the turbulence is created mainly in the shear layer. The $k^{1/2}$ level can be compared to the measured level of $(u^2)^{1/2}$ (*Nielsen 1990*). It is noted that the decay of U_{max} is slightly higher than in the measurements which becomes more evident in fig. 7.6.

In fig 7.5. results from two cross sections in the y-direction are compared with measured data.

The effect from the shear layer outside the potential core of the jet is seen. It is seen that the recirculating flow recorded in the measurements in both cross sections is predicted well in the simulation, although the magnitude of the counter flow is too low. The maximum velocity in the occupied zone is well predicted both with respect to location and to magnitude.

The decay of the maximum velocity and the downstream growth of the jet width are depicted in fig 7.6 and 7.7. The velocity decay is slightly overpredicted and it can be seen that the faster decay corresponds to a faster growth in the jet width than recorded in the experiments (fig. 7.7). No investigation of grid dependency of the

solution has been carried out which means it is possible that some numerical diffusion may be present.

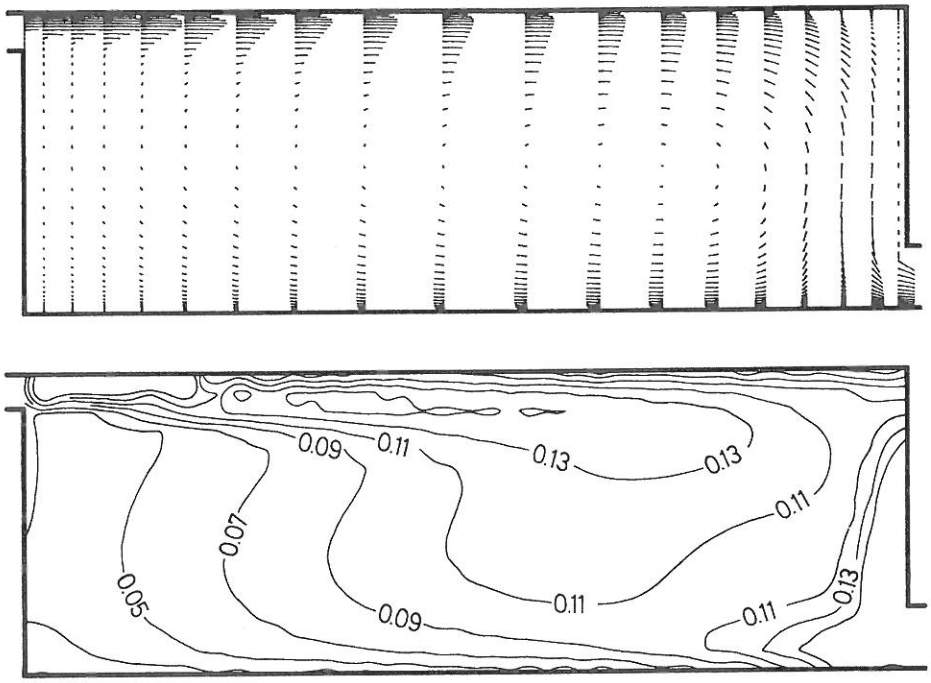

Figure 7.3. The predicted velocity field U/U_o and the distribution of turbulent kinetic energy $k^{1/2}/U_o$.

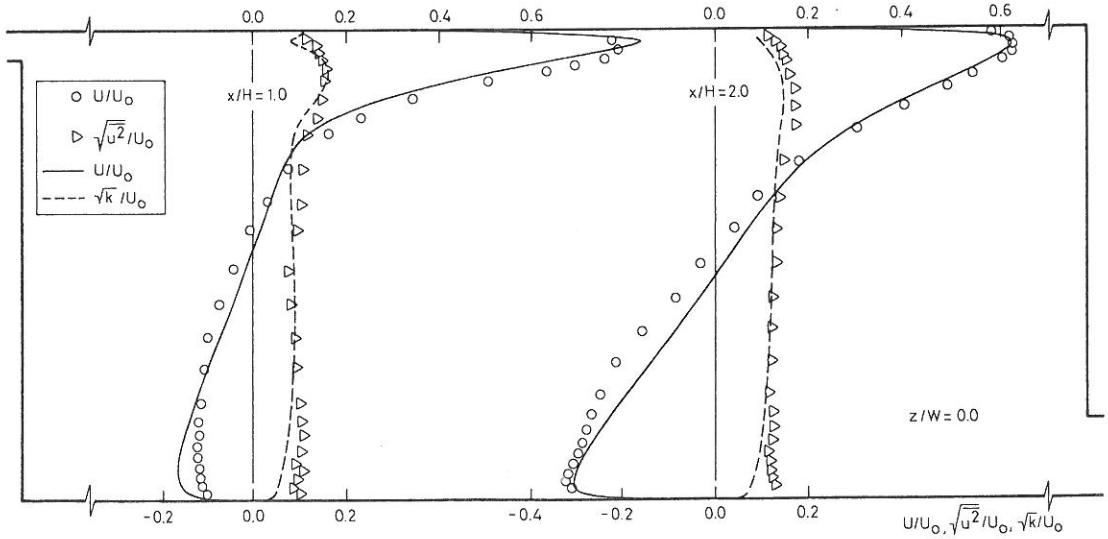

Figure 7.4. Measured and simulated flow profiles. The discrete points are measurements made by Restivo 1979.

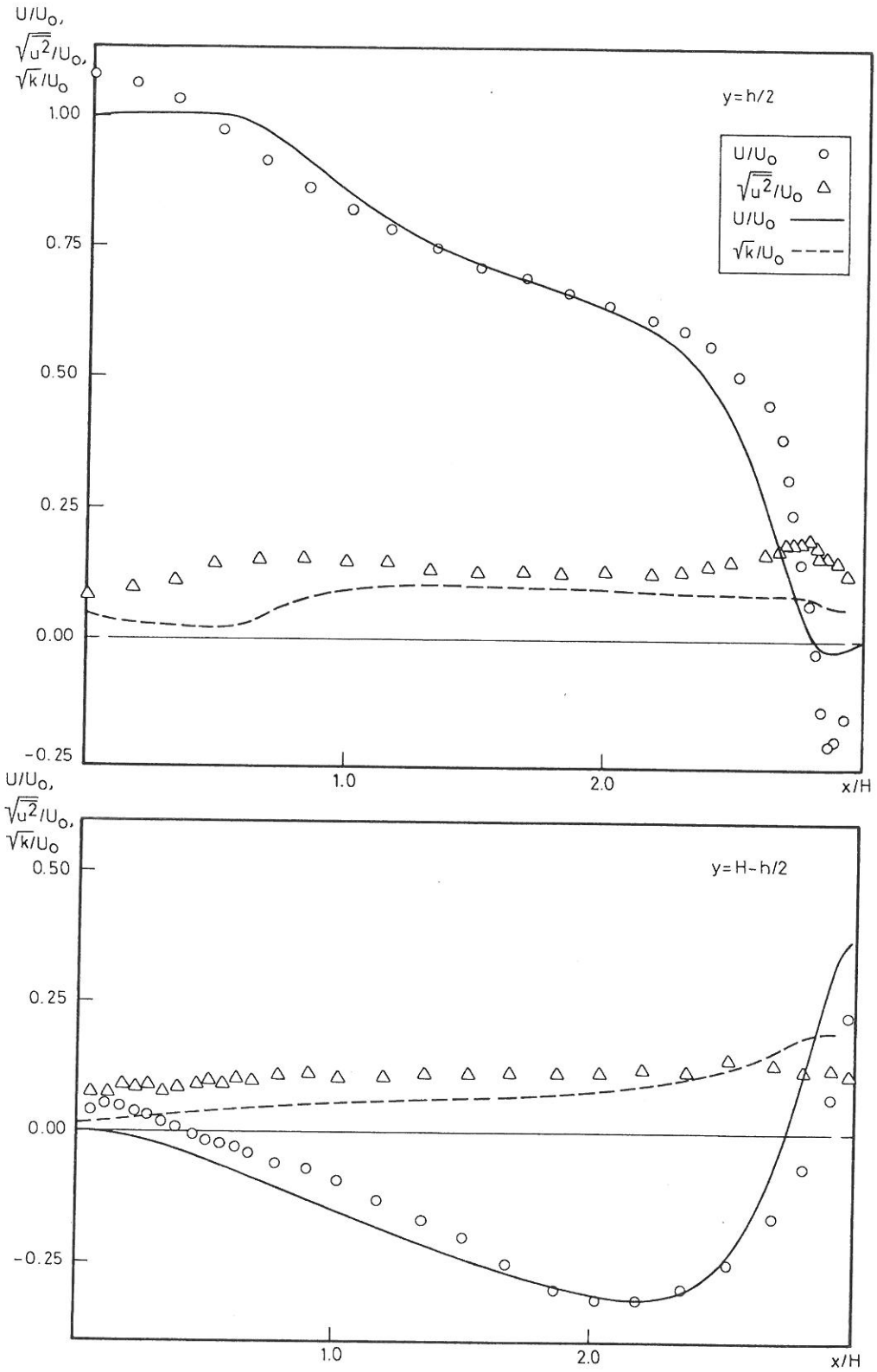

Figure 7.5. Comparison between predicted and measured values in cross section y=h/2 and y=H-h/2. The discrete points are measurements made by Restivo 1979.

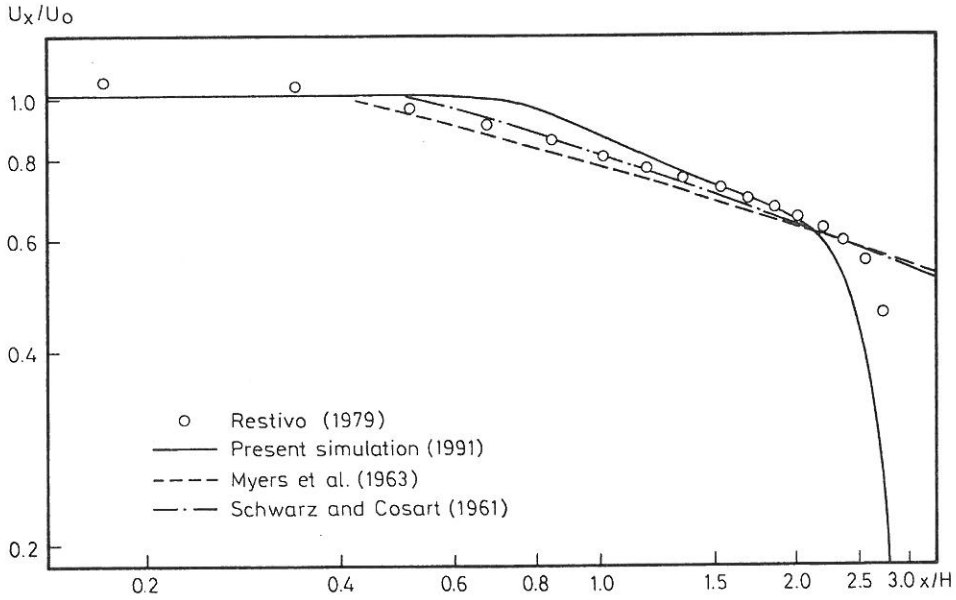

Figure 7.6. Decay of the maximum velocity in the wall-jet.

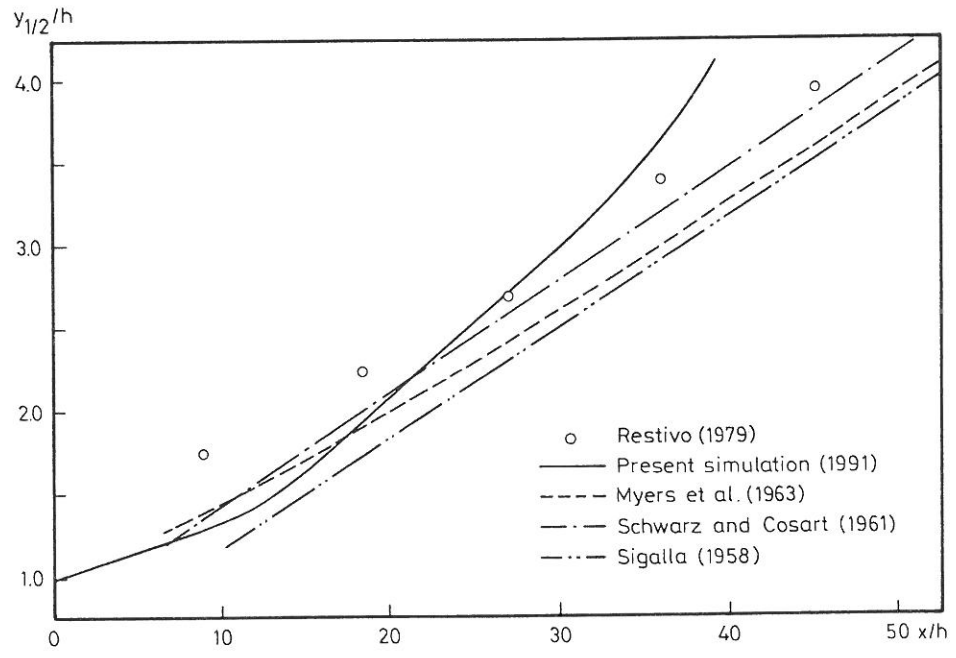

Figure 7.7. The growth in wall-jet width.

Other numerical predictions

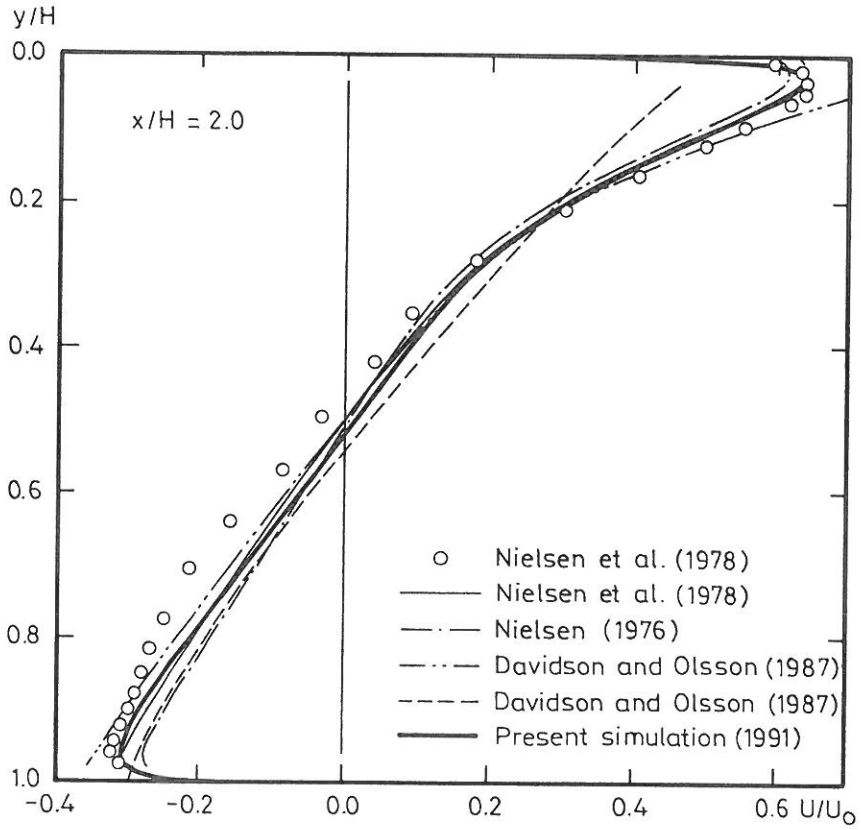

Figure 7.8. Predictions of the velocity distribution in the two-dimensional test case.

Fig. 7.8 shows some other numerical predictions which can be used for comparisons.

One set of predictions is made by the TEACH-T code and a standard k,ϵ turbulence model with wall functions (*Nielsen et al. 1978*). Fig. 7.8 also shows some old predictions made by vorticity-stream function as dependent variables and a k,ϵ-model. The predictions are made at a Reynolds number of 7100 and the inlet conditions are given by a box method.

The predictions by *Davidson and Olsson 1987* are made by a k,ϵ-model and with a one-equation turbulence model. The one-equation model is giving a lower velocity level in the wall-jet below the ceiling (this will generally depend on the prescribed length scale).

As seen all predictions are in good agreement with present simulation although

none of the simulations,except the present, are extended to the near-wall region and all but one underpredicts the maximum velocity in the recirculating flow.

7.2.3 Transitional calculation of a flow over a backward facing step geometry

In the following section the LRN model is applied in a numerical experiment to see whether it is possible to predict the transitional flow over a backward facing step geometry (fig. 7.9) with an expansion ratio of 1/6 (h/H =1/6). The simulation covers a range of Reynolds' number which is typical for room air flows ($100 < Re_{inlet} < 5050$). This is the same range which covers from the transitional regime with evidence of periodicity (flow experiments *Restivo 1979)* to the high velocity regime where the turbulent fluctuations are spread over a wide frequency range and the Reynolds number dependence is insignificant (fully turbulent region). Comparisons with experiments are available from work done by *Restivo 1979.*

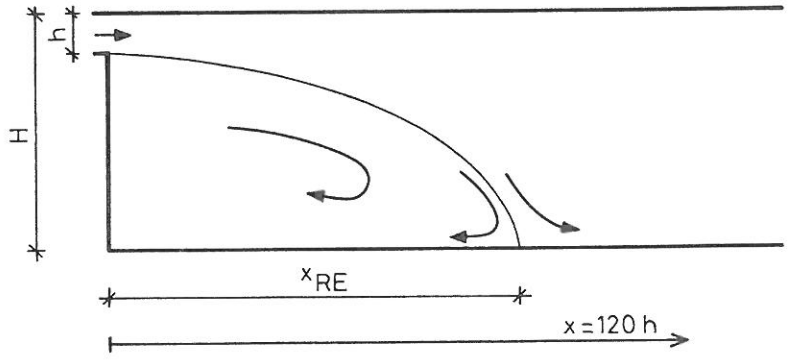

Figure 7.9. Sketch of backward facing step geometry. h/H = 1/6.

The interesting thing about this numerical experiment is to see if it possible to get a solution in the low Reynolds region - which is very important for ventilation engineering. In this region the peak velocity in the jet and the velocity decay are different from the fully turbulent behavior and the turbulent viscosity in the recirculation zone is of the same order of magnitude as laminar viscosity. All those effects are affecting the flow in the whole domain. Another thing which affect the flow is the periodic behavior which the flow might show. However, this is not taken into account in the steady state model.

Numerical approach and boundary conditions

In addition to the numerical procedure already mentioned there are some features which may be important to bear in mind when the results of the numerical experiment are presented.

The scheme is implicit. All calculations are done with the same grid layout which means that the number of nodes in the sub - and buffer layer is not the same for different Re numbers. The grid used for calculation of the inlet boundary conditions (80 in the cross stream direction) is rather coarse.

The boundary conditions are as follows

inlet: U_0, k_0, ϵ_0 - calculated profiles by the method mentioned in section 7.2.1.
$V_0 = 0$

wall: $U = V = k = \epsilon = 0$

outlet: $V = 0$; $dU/dx = dk/dx = d\epsilon/dx = 0$.
The outlet is placed 120h downstream where the flow is expected to be uniform.

Comparisons with LDA measurements

Fig. 7.11 show the results from a simulation with $Re_{bulk} = 5{,}050$ (based inlet height and the mean velocity over the inlet). The velocity and the turbulence profiles shown for different cross sections. The inlet conditions for U - velocity are well predicted and consequently the inlet momentum is exactly the same as recorded in the experiments. The $k^{1/2}/U_o$ values are on the other hand much higher than the experimental values. The predicted inlet values are in the interval from 7 to 13% where the measured ones are from 2 to 6%. This discrepancy - which is significant may be caused by differences in inlet conditions. In the present simulation the inlet condition is strictly two-dimensional where the experimental setup has a contraction in the third dimension which could damp the turbulent fluctuations. But it may also be an indication of the limitation of the model in predicting the right turbulence budget at lower Reynolds numbers. It can also be seen from the values of kinetic energy in the cross section x = 5h that the inlet condition is not important compared to the dominant effect of the shear layer.

If the downstream region is observed it is seen that the mean velocities and the recirculation zone are very well predicted, but again the turbulence level is overpredicted. If e.g. the cross section x = 30h is observed the measured values are in the range of 6 to 11% and the simulated values are in the range of 8 to 15% resulting in a discrepancy of a factor of 2 in the kinetic energy. This significant difference in the turbulence level is unexpected taking the good agreement in the mean velocity into account. Also the previous calculations (section 7.2.2) with the same Re - number in a very similar but confined enclosure have shown that the *Launder-Sharma* model is able to predict the k - level correctly. However one should bear in mind that the relation $u=k^{1/2}$ is depending on the turbulent flow type. *Restivo 1979* also reported that the flow was very unstable and had a periodic tendency which may have influenced the homogenity and isotrophy of the turbulence.

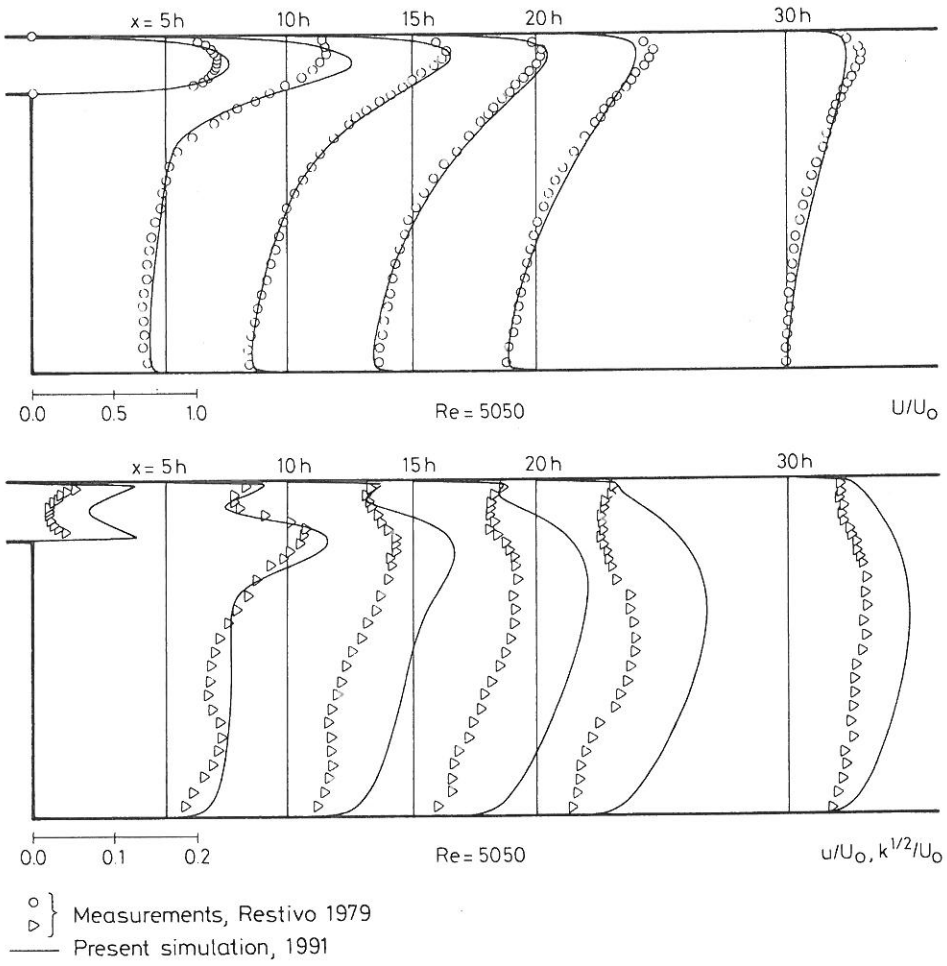

Figure 7.10. Comparisons of present data with experimental values from Restivo. Re=5,050. a) velocity profiles. b) turbulence intensity.

The maximum value of the turbulent fluctuation, u in a fully developed wall-jet is close to $0.22U_x$, where U_x is the peak velocity in the profile at a given distance (*Nelson 1969*). If this assumption is used on the flow in fig. 7.11 it shows that k is underpredicted at x=10h and 15h while it is overpredicted further downstream. All the measurements report a lower level of u compared to the values expected in a fully developed self-similar wall-jet, which could indicate that already at this Re-number LRN are effects present.

Figure 7.11 shows the recirculation length as a function of the Reynolds number.

The figure indicates that the mean flow pattern in the backward facing step case varies substantially for different Re numbers. The behaviour has also been reported by several other authors for geometries with other expansion ratios (e.g. *Armaly et al. 1983*). The figur shows measured data by *Restivo 1979* compared with simulated results. It is seen that all the numerical models fail to follow the measured tendency. If we focus on the LRN simulations specifically it is seen that there is a region where it is impossible to obtain a converged solution which predict a reasonably recirculation length. This may be because the function f_μ is close to zero and consequently the model is equal to the laminar set of equations.

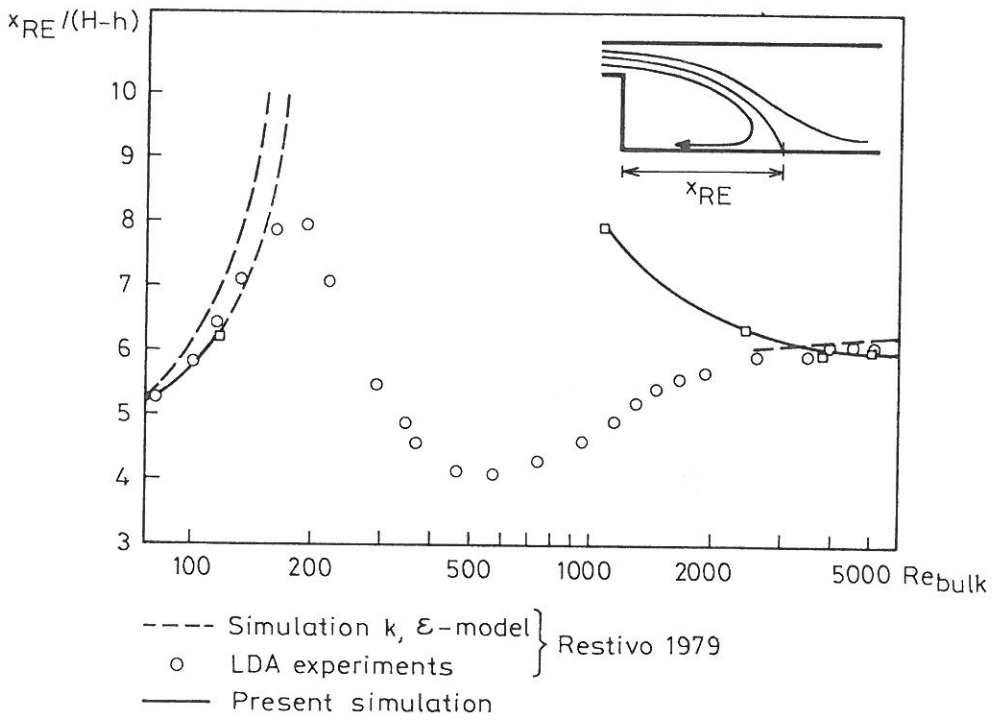

Figure 7.11. Recirculation length vs. Re number for the backward facing step geometry, expansion ratio 1/6.

7.3 Closure

The performance of the Launder-Sharma LRN k,ϵ-model in channel flow is acceptable if the necessary fine grid, which is around 10 points in the y^+ range from 5 to 30, is applied. This again means that it can be used to predict flow close to walls or obstacles and for example to calculate heat transfer coefficients or to calculate velocity distribution in a wall-jet with low Re numbers etc.

Also in the two-dimensional confined test case the performance is good because the Reynolds number is rather high and the LRN effects are restricted to boundary layer flows only.

If we look at the backward facing step test there is still a region in the transitional regime where the LRN model, as well as the high Re number version, fails to give converged results. The explanations of this may be many: The recorded time-dependent behavior of the flow in the transitional regime is not taken into account in the simulation which might be required if we want to calculate transient flow (as already discussed by *Restivo 1979*). The resolution of the grid in the shear layer may need to be higher than in the actual cases where the same grid was used for all Re-numbers. But most likely the reason may be that the LRN turbulence phenomena which we find in the recirculation zone have different character than turbulence in the boundary layer, so in order to capture this the model has to be tuned for these phenomena as well as for the near-wall behavior of the turbulence parameters.

Low Reynolds phenomena, that arises from different sources, and occurs in ventilated spaces is an established fact. In order to be able to predict these effects some theoretical as well as experimental work has to be done in the above mentioned areas to provide a better understanding of the different phenomena.

CHAPTER 8 - GENERAL DISCUSSION AND CONCLUSION

The isothermal flow pattern in rooms ventilated by the mixing principle is investigated experimentally and numerically. The investigations are covering the significant comfort parameters: mean velocity and turbulence. Flow visualization has been used to obtain an idea of the general flow pattern. In the experiments smoke introduced through the inlet or locally has been used and in the numerical work computer graphics, as it is seen on the cover of the thesis, have been applied.

The mathematical model which is used to describe the turbulent air motion is discussed. It is concluded that the best suitable model for prediction of flow patterns in ventilated rooms is an eddy-viscosity model based on the turbulent kinetic energy and it's dissipation. This model is chosen mainly from a computational capability point of view. Other and more advanced models do exist but are still too demanding in terms of computational effort to be used in ventilation engineering.

The discretisation and implementation of the model is discussed and techniques regarding differencing, source term linearizing and strategy of solution of the equations are recommended.

Regarding the experimental investigation the specific problems of measurering isothermal low velocities are discussed - especially self convection, the calibration procedure and the influence of small temperature gradients.

The traditional way to design a ventilation system of the mixing type is by a set of simplified relations assuming that the flow in the vicinity of the inlet may be described as a fully turbulent jet or wall-jet. These well known relations are held up against fully turbulent simulations in an office with one rectangular inlet opening. These investigations showed good agreement between the simplified relations and the simulations. The investigations points out that the significant parameter for the velocity level in the occupied zone is the inflow momentum. The relation U_{rm}/U_L equals approximately 0.3, which corresponds to investigations made by *Hestad 1974*. The relation is important because it offers a way to determine the maximum velocity in the occupied zone from the knowledge of the jet characteristics only.

The full-scale experiments were carried out in a room of the size of a normal office

ventilated by a modern inlet diffuser with a complicated geometrical design. This particular diffuser was chosen to obtain realistic flow patterns. Numerical simulations are performed on the very same case and comparisons are carried out. From these comparisons it is possible to contribute to some important questions:

Is it possible to predict the complex flow created from a modern inlet diffuser?
Is it possible to predict air flow patterns in rooms ventilated by the mixing principle?
Is numerical simulation beneficial in the field of ventilation engineering at present stage of development?

The first two questions are closely connected because the flow pattern in a room ventilated by the mixing principle is depending of the flow created by the diffuser. However, each question will be discussed separately in the following.

The geometry of the diffuser is too complex to model exactly because the grid required to model all the many small nozzles would be too large, which again means that the only way to impose the right boundary conditions is to model the characteristics of the inlet flow bearing in mind that the significant driving parameter is the inflow momentum. Four different approaches were used to simulate the diffuser. The "basic" model do not predict the overall flow pattern because the wall-jet after impingement on the ceiling spreads towards the upper downstream corner. The "momentum" method fails to predict the right velocity profile in the jet region and yields to high velocity level in the occupied zone. The maximum velocity in the occupied zone is located close to the side walls. The "actual area" method gives better results because it adapts the right velocity level in the wall-jet The overall flow pattern is acceptable predicted while the velocity in the occipied zone is a little too high. The best method of the four is the "prescribed velocity" method which predicts the decay in the wall-jet (after the imaginary box), the overall flow pattern (except in the imidiate vicinity of the inlet) and the velocity level in the occupied zone acceptably.

After the summary made above of the different methods by which the diffuser is modelled the first of the questions can be answered by a yes it is possible to model the flow pattern arising from a modern diffuser of complex geometry. But one has to very careful especially to model the momentum flow in accordance with the real situation, because even small deviations in the inflow condition may result in significant deviations in the flow pattern. If careful studies are to be conducted the "prescribed velocity" method is a good way to introduce the boundary condition for

the inlet conditions. If studies of the overall velocity field and trends are to be investigated numerically or by scale models the "actual area" method seems to be a consistent method for this purpose.

Regarding the second question: Is it possible to predict the general flow pattern? The answer have to be more differentiated than in the previous question. The fully turbulent flow pattern can as far as this investigation concerns be simulated satisfactory if a good representation of the inlet conditions is provided. If the "prescribed velocity" method is used then the decay of the velocity in the jet and the velocity level in the occupied zone are predicted with satisfactory accuracy. If the simpler "actual area" method is used the overall flow pattern and the velocity level is acceptably predicted while the velocity level in the occupied is predicted slighty higher than by the former method.

When the supply velocity is decreased the flow through the inlet as well as the flow in the whole room deviates from what may be expected under fully turbulent conditions. The low Reynolds number effects occuring in the inlet can be incorporated in the numerical model. But present k,ϵ turbulence model is not able to capture the low Reynolds number effects in the room.

Investigations of the LRN effects have been carried out based on a low Reynolds number version of the turbulence model. With this model it is possible to predict low Reynolds number boundary flow but the LRN effects occurring in the recirculating flow over a backward facing step in the transitional regime cannot be predicted by the used method. The investigations indicates that some work of both theoretical and experimental character must be done before a suitable model is available for this kind of flow.

The last significant deviation between the experimental study and the numerical simulation is the asymmetric flow in the occupied zone. The asymmtrical behavior was not predicted in the simulation due to symmetric boundary conditions.

On the basis of the discussion above the second question can be answered in the following way: If the flow is fully turbulent it is possible to predict the air-flow pattern in isothermal mixing ventilated room provided careful modeling of the supply conditions are performed. If the low Reynolds number version of the k,ϵ-model is used it is also possible to calculate the near-wall behavior which is significant for non-isothermal flow. Low Reynolds effects occurring in the recirculating flow cannot be predicted by the LRN version of the k,ϵ-model. Further

investigations must be done is this area. Simulations with symmetrical boundary conditions seem to be inadequate because the flow is asymmtric in the recirculating flow.

The previous decades have shown that CFD calculations of two- and three-dimensional flow patterns produces reliable results. The work made in this thesis shows that it is also possible to obtain acceptable results in three-dimensional geometries ventilated by a modern diffuser and complex geometry. This means that it may also be possible to calculate the transport of scalars (like temperature and concentration of non-reactive pollutants) which strongly depends on the velocity distribution. It is also shown that via the detailed knowledge one obtains from the CFD simulations it is possible to produce maps of thermal comfort, which is not possible by the existing analytical methods.

There is no doubt in the authors mind that in the near future the CFD technique is going to be used in the design process of a ventilation plant or in the planning of experiments in practical engineering as we have seen it other areas where fluid dynamic problems are important. But as the work in this thesis shows there are still areas which still needs further investigation e.g. the low Reynolds number flows, thermal boundary-layers and modelling of boundary conditions of other momentum giving sources such as e.g. heat sources.

The author would like to round this discussion of by drawing out a few points which may be described as the main findings - from the authors point of view:

- Careful modeling of the momentum flow near the diffuser necessary for successful use of CFD in the area of mixing ventilation.

- Low Reynolds number effects may be present in rooms ventilated by the mixing principle.

- The low Reynolds number k,ϵ-model used in this thesis is not able to reproduce the observed change in flow pattern over a backward facing step when the velocity level is decreased. (The investigations have only been made under stationary conditions with an implicit solution scheme).

SUMMARY IN DANISH

I denne Ph.D. afhandling er isoterme strømningsforhold i lokaler ventileret efter opblandingsprincippet undersøgt eksperimentelt og v.hj.a. numerisk stømnings-mekanik (CFD). Undersøgelserne er koncentreret omkring de vigtigste komfort-parametre: middelhastighed og turbulens. Visualisering af strømningerne er blevet brugt til at opnå et generelt indtryk af strømningsmønstret. I den eksperimentelle del er anvendt røg, som er blæst ind via indblæsningsarmaturet og lokalt, hvor en større detaljeringsgrad var ønsket. I den numeriske del er computergrafik anvendt, som det fremgår af forside og titelblad.

Den matematiske model der er anvendt til beskrivelse af den turbulente luftbevægelse er diskuteret og det er bl.a. ud fra hensyn til beregningstid og beregningsressourcer konkluderet, at en model baseret på den turbulente kinetiske energi samt dens dissipation er den bedst egnede i øjeblikket. Der findes andre og mere detaljerede modeller men disse skønnes at være for beregningskrævende til brug i ventilationsteknikken.

Diskretiseringen og implementeringen af den matematiske model er diskuteret, og der er bl.a. indenfor approximering af hastighedsgradienter, linearisering af kildeled samt indenfor den iterative løsning af differensligningssystemet foreslået alternative strategier.

Med hensyn til de experimentelle undersøgelser er de specifikke problemer knyttet til isoterme målinger af lave hastigheder diskuteret - specielt områderne egenkon-vektion, kalbreringsprocedure og influens fra små temperatur forskelle.

Den traditionelle måde at dimensionere et opblandingsanlæg er udfra et sæt simpli-ficerede ligninger baseret på tredimensional stråle og vægstråle teori. Disse velkendte relationer er sammenlignet med CFD simuleringer i et kontorlokale med en rektangulær inblæsningsåbning. Sammenligningerne viste, som forventet, god overensstemmelse mellem simuleringerne og de simplificerede ligninger. Et vigtigt resultat fra disse sammenligninger er, at den vigtigste faktor for maksimum hastigheden i opholdszonen er impulsstrømmen i indblæsningsstrålen. Relationen U_L/U_{rm} blev fundet til 0.3. hvilket stemmer overens med andre undersøgelser. Relationen er en vigtig parameter for lokaler ventileret efter opblandingsprincippet, da den gør at man kan bestemme den maksimale hastighed i opholdszonen udfra kendskab til jetkarakteristikken alene.

De eksperimentelle undersøgelser er foretaget i et fuldskala rum af normal kontor størrelse (LxHxB=4,2x2,4x3,6 m^3) der er ventileret v.hj.a. et moderne indblæsningsarmatur bestående af 84 små dyser. Denne form for indblæsningsarmatur er valgt for at opnå strømningsforhold, der er sammenlignelige med, de der forefindes i virkelige situationer. Efterfølgende er der foretaget numeriske simuleringer v.hj.a.CFD teknikken på det samme case. Udfra sammenligninger er det muligt at give et bidrag til bevarelse af følgende vigtige spørgsmål:

Er det mulig at simulere de ofte komplicerede strømningsforhold som et moderne indblæsningsarmetur skaber?
Er det muligt at bestemme/simulere luftstrømningerne i et rum ventileret efter opblandingsprincippet?
Opnås der nogen ekstra viden ved brug af CFD i ventilationsteknik?

De første to spørgsmål er tæt forbundne fordi strømningsmønstret i et lokale ventileret efter opblandingsprincippet er meget afhængigt af de strømningsforhold som skabes af armaturet. I det efterfølgende vil spørgsmålene dog alligevel blive besvaret enkeltvis.

Selve udformningen af det anvendte indblæsningsarmatur gør det umuligt at simulere geometrisk eksakt, fordi alt for mange netpunkter er nødvendige for at modellere alle dyser enkeltvist. Den eneste mulighed er at foreskrive indblæsningsrandbetingelserne ved at beskrive inblæsningsstrålens karakteristika. Fire forskellige metoder er blevet anvendt, for at afsløre hvad der er den vigtigste drivende faktor for det totale strømningsbillede.

"Basic" modellen har samme effektive indblæsningsareal og samme højde/brede forhold som det virkelige armatur. D.v.s.at den resulterende jet har samme masse- og impulsstrøm, men er mere koncentreret end den virkelige strømning. Dette gør, at når jet'en rammer loftet, er stagnationszonen mindre og jet'en spredes mere radialt end i den virkelige strømning. Som et resultat af dette svarer det beregnede totale strømningsmønster ikke til det virkelige.

De næste to metoder benytter resultatet fra de første simuleringer: At den vigtigste parameter for strømningsmønsteret er impulsstrømmen i indblæsningsstrålen. "Actual area" metoden modellerer indblæsningsarmaturet v.hj.a. en rektangulær åbning af samme størrelse som det virkelige armaturs omrids. Impulsstrømmen er den samme, hvilket gør at massestrømmen er større end det luftskifte man ønsker. "Momentum" metoden har som udgangspunkt samme fysiske ræsonnement, men

opdeler randbetingelser for masse og impuls. Massestrømmen er den ønskede og en ekstra impulskilde placeres umiddelbart efter indblæsningen for at opnå den ønskede impulsstrøm. Herved er både impuls- og massestrøm den samme som i den virkelige strømning. De beregnede strømningsbilleder ligner ikke hinanden, da " momentum" metoden ikke formår at beskrive jetzonen så hastighedsfeltet bliver sammenligneligt med det ønskede. Dette skyldes at den ekstra impulskilde kun er foreskrevet i et enkelt lag af beregningsceller, hvilket er for lidt til at have en altafgørende virkning på strømningsfeltet.

Den fjerde metode - "prescribed velocity" metoden - benytter eksperimentelle data til at foreskrive de virkelige forhold i vægstrålen. To hastighedskomposanter er foreskrevet i en imaginær boks placeret under loftet i det parabolske vægstråle område. Størrelsen af denne boks er vigtig, hvis det analytiske udtryk der er brugt i denne afhandling skal gælde. Størrelsen af boksen er $L_{box}=W_{box}=1.0m$ og $H_{box}=y/\delta=0.75\text{-}1.0$. Hastighedsfaldet i strålen efter boksen, hastighedsniveauet i opholdszonen samt det totale strømningsbillede er bestemt tilfredsstillende ved brug af denne metode.

Efter dette denne korte gennemgang af de anvendte metoder til at modellere inblæsningsstrømningen kan det første spørgsmål besvares med: At det er muligt at simulere strømningen skabt fra et moderne indblæsningsarmatur. Men det kræver at den eksakte impulsstrøm og -fordeling som forefindes i den virkelige situation er genskabt i modellen. Hvis meget omhyggelige undersøgelser af strømningsforholdene i et ventileret lokale ønskes udført anbefales "prescribed velocity" metoden anvendt. Hvis der derimod ønskes en undersøgelse af tendenser og det overordnede strømningsfelt enten v.hj.a. CFD eller modelforsøg ser "actual area" metoden ud til at være anvendelig og konsistent.

Spørgsmål nr. to må besvares mere differentieret end nr. et. De undersøgelser der er udført i denne afhandling tyder på at numerisk løsning af en tredimensional turbulent strømning er mulig, hvis indblæsningsforholdene er beskrevet på passende vis f.eks. med en af ovenstående metoder.

Når hastigheden i indblæsningen nedsættes viser de eksperimentelle undersøgelser at der opstår strømningsmønstre, der afviger fra den fuldt udviklede turbulente strømning, hvilket betegnes lavturbulente effekter. Disse effekter opstår både i indblæsningsarmaturet samt i rumstrømningen. De lavturbulente fænomener, der opstår i armaturet, kan inkluderes i de metoder der allerede er præsenteret, hvorimod de lavturbulente effekter der opstår i rumstrømningen ikke er mulige at

forudsige med den standard k,ϵ-model, der er anvendt i simuleringerne. Der er derfor foretaget en undersøgelse af disse lavturbulente effekter v.hj.a en lavturbulent udgave af k,ϵ-modellen. Disse undersøgelser viser, at det er muligt at medtage lavturbulente fænomener, der opstår i grænselaget, hvorimod det ikke er muligt at simulere de lavturbulente fænomener, der opstår i omslagsområdet ved en recirkulerende strømning. Undersøgelserne der er lavet i tilknytning til denne afhandling synes at pege på at de mekanismer, der forefindes i den lavturbulente recirkulerende strømning, ikke er de samme som findes i det lavturbulente grænselag. Ihvertfald tyder undersøgelserne på at teoretisk såvel som eksperimentelt arbejde er nødvendigt for at få større indsigt i disse fænomener.

Den sidste afgørende forskel mellem fuldskala undersøgelserne og de numeriske simuleringer er at eksperimenterne afslørede en asymmetrisk strømning i opholds zonen. Denne asymmetri blev ikke fundet i simuleringerne fordi der blev anvendt symmetriske randbetingelser. Undersøgelserne tyder altså på at den symmetriske praksis må opgives når beregningerne benyttes ved stråleventilation.

Forskningen indenfor dette område har i de sidste par årtier klarlagt et det er muligt at simulere to- og tredimensionale luftstrømninger. Arbejdet i denne afhandling viser hertil, at det er muligt at simulere den tredimensionale strømning i et opblandingsventileret rum med et virkeligt indblæsningsarmatur med en kompliceret opbygning. Dette gør at det også skulle være muligt at beregne transporten af skalarer som f.eks. temperaturer og ikke-reagerende stof, der jo er stærk afhængig af hastighedsfeltet. Der er også påvist, at der v.hj.a.CFD teknikken opnås en detaljeret viden om hele strømningfeltet i et ventileret lokale, hvorudfra det er muligt at f.eks udarbejde "kort" over den termiske komfort, hvilket ikke er muligt i eksisterende analytiske metoder.

Der næres ingen tvivl hos forfatteren om at CFD teknikken i den nærmeste frem tid vil indgå som led i designprocessen af ventilationsanlæg eller i tilrettelæggelsen af en eventuel forsøgsrække ganske som det er set i andre områder, hvor strømningsdynamiske problemer er betydende. Men som det også er kommet til udtryk gennem arbejdet i denne afhandling vil der stadig være områder, hvor mere viden er nødvendig før tilfredsstillende resultater kan opnås. Disse områder er bl.a. lavturbulente fænomener i frie strømninger, termiske grænselag og modellering af randbetingelser ved andre impulsgivende kilder, som f.eks. varmelegemer.

REFERENCES

Armaly , B.F., Durst, F., Pereira, J.C.F and Schönung, B.
Experimental and Theoretical Investigation of Backward Facing Step Flow, Journal of Mechanics, Vol. 127. *1983.*

Beltaos, S.
Oblique Impingement of Circular Turbulent Jets. Journal of Hydraulic Research 14 *1976* no. 1.

Benocci, C. and Skovgaard, M.
Prediction of Turbulent Flow Over a Backward Facing Step". Proc. of 6th Int. Conf. of Laminar and Turbulent Flows. Swansea, UK *1989.*

Chen, Q.
Indoor Airflow, Air Quality and Energy Consumption of Buildings. Ph.D. thesis, the Technical University of Delft, Netherlands. *1988.*

Chen, Q., Suter, P. and Moser, A.
Influence of Air Diffusion. Energy systems laboratory series. Federal Inst. of Tech, ETH, Zürich Switzerland *1990.*

Chen, Q., Suter, P. and Moser, A.
Indoor Air Quality and Thermal Comfort under Six Kinds of Air Diffusion. To appear in ASHRAE Transactions, vol. 97, part 2. *1991.*

Chien, K.Y.
Predictions of Channel Boundary-layer with a Low Reynolds Number Model, AIAA Journal, vol. 20. *1982.*

Christensen, N.
Komfortgrænser for lufthastighed (in danish), DTH lab. for varme og klimateknik. *1983.*

Davidson, L.
Turbulence Modeling and Calculation of Ventilation Parameters in Ventilated Rooms, Licentiate thesis, Chalmers University of Technology, Dept. of Applied Thermodynamics and Fluid Mech. *1986.*

Davidson, L. and Olsson, E.
Calculation of Some Parabolic and Elliptic Flows Using a New One-equation Turbulence Model, 5th. Int Conference on Numerical Methods in Laminar and Turbulent Flow, Montreal. *1987.*

Davidson, L.
Numerical Simulation of Turbulent Flow in Ventilated Rooms, Ph.D. Thesis, Chalmers Tekniska Högskola, Sweden. *1989.*

Engelund, F.A.
Hydrodynamik - newtonske vædskers mekanik (danish), Den private ingeniørfond, DTH København. *1968.*

Fanger, P.O., Melikov, A.K., Hanzawa, H. and Ring, J.
Turbulence and Draft. ASHRAE Journal, *1989.*

Gosman, A.D., Khalil, E.E and Whitelaw, J.H.
The Calculation of Two-Dimensional Turbulent Recirculating Flows, Proceedings of Symposium on Turbulent Shear Flows, University Park, Pennsylvania. *1977.*

Gosman, A. D., Nielsen, P. V., Restivo, A. and Whitelaw, J. H.
The Flow Properties of Rooms with Small Ventilation Openings. ASME Journal of Fluids Eng. Vol 102 *1980.*

Gosman, A.D. and Pun, W.M.
Calculation of Recirculating Flows, Mechanical Eng, Dept, Imperial College, UK. *1973.*

Harlow, F.H and Welch, J.E.
Numerical Calculation of Time-dependent Viscous Incompressible Flow of Fluid with Free Surface, Phys. Fluids, *1965.*

Heikkinen, J.
Specification of Test Case b (forced convection, isothermal), research item 1.13, IEA annex 20 report, *1989a.*

Heikkinen, J.
Appendix to IEA, RID no. 1.13: Specifications of Test Case B. *1989b.*

Heikkinen, J.
Private communication. *1991a.*

Heikkinen, J.
Modeling of a Supply Air Terminal for Room Air Flow Simulation. 12th AIVC Conference, Ottawa, Canada. *1991b.*

Heiselberg, P. and Nielsen, P.V.
The Contaminant Distribution in a Ventilated Room With Different Air Terminal Devices. RoomVent '87, Sweden, *1987.*

Heiselberg, P.
Strømningsforhold i lokaler ventileret efter opblandings- og fortrængningsprincippet. Ph.D. thesis (in danish), The University of Aalborg. *1990.*

Hestad, T.
En dimensioneringsmetode for tilluftsorganer basert på teori, fullskalaforsøk og praktisk erfaring (in Norwegian), Inst. for uppvarmnings och ventilationsteknik, KTH, Stockholm. *1974.*

Hodge, J.K., Stone, A.L. and Miller, T.E.
AIAA Journal, 17 458. *1979.*

Huang G.P.
The Computation of Elliptic Turbulent Flows with Second Moment Closure Models. Ph.D. - Thesis, UMIST, Manchester, UK, *1986.*

Inze, N.Z. and Launder B.E.
On the Computation of Buoyancy-driven Turbulent Flows in Rectangular Enclosures. UMIST, Manchester, UK, *1989.*

Jones, W.P. and Launder, B.E.
The Prediction of Laminarization with a Two-equation Model of Turbulence, International Journal of Heat and Mass Transfer, vol. 15. *1972.*

Kessler, R., Peric, M. and Scheuerer, G.
Solution Error Estimation in the Numerical Predictions of Turbulent Recirculating Flows, Lehrstuhl für Strömungsmechanik, University of Erlangen - Nürnberg, *1988.*

Kim, J, Moin, P and Moser, R.
Turbulence Statistics in Fully Developed Channel Flow at Low Reynolds Number. J. Fluid Mech., vol. 177, pp. 133-166. *1987*

Kofoed, P.
Thermal Plumes in Ventilated Rooms, Ph.D. Thesis. University of Aalborg, *1991*.

Larsen , J.H, Kjelgaard, E.W, Agersen, L.
Private communication. The University of Aalborg, Denmark. *1988*.

Lam, C.K.G and Bremhorst, K.A.
Modified Form of the k,ϵ-model for Predicting Wall-turbulence, Journal of Fluids Engineering, vol. 103. *1981*.

Laufer, J.
Investigations of Turbulent Flow in a Two-dimensional Channel, NACA report 1053, *1949*.

Launder, B.E. and Spalding, D.B.
The Numerical Computation of Turbulent Flows, Comput. Meth. Appl. Mech. Engng., 3. *1974*.

Launder B.E. and Sharma B.I.
Letters in Heat and Mass Transfer. *1978*, 1, 129.

Launder B.E. and Tselepidakis D.P.
Directions in Second - Moment Modeling of Near - Wall Turbulence, UMIST, Manchester, UK. 29 th Aero Space Sciences Meeting AIAA 91 - 0219, Nevada, *1990*.

Leschziner, M.A.
Private communication, UMIST, Manchester, UK. *1991*.

Lemaire, T.
Testrooms, Identical Testrooms, research item 1.3, IEA annex 20 report, *1989*.

Leonard, B.P.
A Stable and Accurate Convective Modeling Procedure Based on Quadratic Upstream Interpolation, Computer Methods in Applied Mechanics and Engineering,

19. *1979.*

Lesiur, M.
Turbulence in Fluids, Martinus Nijhoff Publ., Boston. *1987.*

McRee, D.I. and Moses, H.L.
The Effect of Aspect Ratio and Offset on Nozzle Flow and Jet Reattachment. *1967* FLUIDICS symposium ASME.

Myers, G.E., Schauer, J.J.and Eustis, R.H.
The Plane Turbulent Wall-jet, I, Trans. A.S.M.E.,J, Basic Eng., 85. *1963.*

Murakami, S., Mochida, A.
Three-dimensional Numerical Simulation of Air Flow around a Cubic Model by Means of Large Eddy Simulation. Journal of Wind Engineering and Industrial Aerodynamics, 25, pp. 291-305. *1987.*

Murakami, S., Tanaka, T. and Kato, S.
Numerical Simulation of Air Flow and Gas Diffusion in Room Model - Correspondence between Simulation and Model Experiments. University of Tokyo, *1983.*

Nallasamy, M.
Turbulence Models and Their Application to the Prediction of Intenal Flows, a Review. Computers and Fluids, Vol. 14 no. 2. *1987.*

Nelson, J.L.
An Experimental Investigation of the Turbulent and Mean Flow Properties of a Plane Two-dimensional Turbulent Wall-jet. Dissertation, University of Tennessee. Dept. of Chem. Eng. *1969.*

Nielsen, P.V.
Flow in Air Conditioned Rooms - Model Experiments and Numerical Solutions of the Flow Equations. Revised ed. of Ph.D. - Thesis *1976.*

Nielsen, P.V, Restivo, A. and Whitelaw, J. H.
The Velocity Characteristics of Ventilated Rooms. ASME Journal of Fluid Eng. Vol. 100, *1978.*

Nielsen, P.V. and Å.T.A. Möller

Measurement of the Three Dimensional Wall Jet from Different Types of Air Diffusers. World Congress on Heating, ventilation and Air Conditioning, *1985*.

Nielsen, P.V. and Å.T.A. Möller
Measurements on Buoyant Jet Flows From a Ceiling Mounted Slot Diffuser. III seminar on Appl. of Fluid Mechanics in Environmental Protection, Silesian Tech. University, Gliwice, Poland, *1988a*.

Nielsen P.V.
Simplified Models for Room Air Distribution. Internal report, IEA annex 20, University of Aalborg, *1988b*. ISSN 0902 - 7513 R8831.

Nielsen P.V.
Selection of Air Terminal Device, Internal Report, IEA annex 20. University of Aalborg. *1988c*. ISSN 0902 - 7513 R8838.

Nielsen P.V.
Numerical Prediction of Air Distribution in Rooms - Status and Potentials. In : Building Systems : Room Air and Air Contaminant Distribution (Edited by L.L. Christianson) ASHRAE, *1989a* ISBN 0-910110-64-6.

Nielsen, P.V.
Representation of Boundary Conditions at Supply Openings. International Energy Agency, annex 20, ISSN 0902 - 7513 R8902, *1989b*.

Nielsen, P.V.
Specification of Two-Dimensional Test Case, IEA-Annex 20 Internal report, ISSN 0902-7513 R9040. Nov. *1990*.

Nielsen, P.V.
Private communication, University of Aalborg, DK. *1991*.

Page, G.J.
A Computational Study of Transonic Turbulent Impinging Jets, Ph.D. Thesis, Imp. Coll. of Science, London, UK. *1990*.

Patankar, S.V.
Numerical Heat Transfer and Fluid Flow. Hemisphere Publishing Coorporation. ISBN 0-89116-522-3, *1980*.

Patel V.C., Rodi W. and Scheurer G.
Turbulent Models for Near-wall and Low Reynolds Number Flows: A Review AIAA Journal, Vol 23, No. 9, *1985*.

Rajaratnam, N.
Turbulent Jets, Elsevier, Amsterdam *1976*.

Rajaratnam, N. and Pani, B. S.
Three Dimensional Turbulent Wall Jets, Proc. A.S.C.E.J. Hydraul. Div., 100, 69-83.

Restivo , A.M.O.
Turbulent Flow in Ventilated Rooms. Imp. Coll. of Science and Tech., Mech. Eng. Dept. Ph.D. - Thesis, *1979*.

Rodi, W.
Turbulence Models and Their Application in Hydraulics - a State of the Art Review, Inst. für Hydromechanik, University of Karlsruhe, Germany. *1980*.

SBI - Rapport 128.
Luftstrømninger i ventilerede arbejdslokaler. Statens Byggeforsknings- institut. ISBN 87-563-0394-7. *1981*

Schlichting, H.
Boundary-Layer Theory (seventh ed. 1968), McGraw Hill, New York. *1960*.

Schwartz, W.H. and Cosart, W.P.
The Two-dimensional Turbulent Wall-jet, J. Fluid Mech., 10. *1961*.

Sforza, P.M. and Herbst, G.
A Study of Three-dimensional Incompressible Turbulent Wall-jets. Rep. 1022, Dept. of Aerospace Engineering, Polytechnic Inst. of Brooklyn, N.Y. *1967*.

Sigalla, A.
Measurements of Skin Friction in a Plane Turbulent Wall-jet, J.R. Aeronaut. Soc, 62. *1958*.

Skovgaard, M.
Analysis of a Second Order Hybrid Scheme Influence on the Numerical Solution of the k-ϵ-model, Stagiare report 1989-09, The von Karman Institute for Fluid

Dynamics, Belgium. *1988.*

Skovgaard, M. and Lemaire, T.
Representation of Boundary Conditions at Supply Openings, tecnical note on research item 1.11, IEA annex20. *1990a.*

Skovgaard, M., Hyldgård, C.E. and Nielsen, P.V.
High and Low Reynolds Number Measurements in a Room with an Impinging Jet. Roomvent '90, Oslo. *1990b.*

Skovgaard, M. and Nielsen, P.V.
Simulation of Simple Test Case, Case 2D1. IEA, annex 20 report, *1991a.*

Skovgaard, M. and Nielsen, P.V.
Modeling Complex Inlet Geometries in CFD - Applied to Air Flow in Ventilated Rooms. 12th IAVC Annual Conference, Canada, sept. *1991b.*

Tselepidakis D.P.
Private Communications, UMIST, Manchester, UK. *1991.*

Trentacoste, N. and Sforza, D. M.
Further Experimental Results for Three-dimensional Free Jets., A.I.A.A.Journ. 5, 885-891, *1967.*

Verhoff, A.
Report N626, Princeton University, Dept. of Aeronautical Engineering, *May 1963.*

Viets H. and Sforza.
An Experimental Investigtion of a Turbulent Incompressible Three-dimensional Wall-jet. Rep. 968, Department of Aerospace Engineering, Polytechnic Inst. of Brooklyn, New York. *1966.*

Wilcox, D.C. and Rubesin, W.M.
Progress in Turbulence Modeling for Complex Flow Fields Including Effects of Compressibility, NASA. *1980.*

APPENDIX 3.1 - INTEGRATION OF THE GENERAL EQUATION

The general equation is integrated over a finite control volume

$$\underset{\text{convection}}{\int_V \frac{\partial}{\partial x_i}(\rho U_i \Phi)\,dV} = \underset{\text{diffusion}}{\int_V \frac{\partial}{\partial x_i}\left[\Gamma_\Phi \frac{\partial \Phi}{\partial x_i}\right] dV} + \underset{\text{source}}{\int_V S_\Phi\, dV}$$

The convection terms

$$\int_V \left[\frac{\partial}{\partial x}(\rho U\Phi) + \frac{\partial}{\partial y}(\rho V\Phi) + \frac{\partial}{\partial z}(\rho W\Phi)\right] dV =$$
$$\rho U\Phi\Big|_w^e \Delta y\Delta z + \rho V\Phi\Big|_s^n \Delta x\Delta z + \rho W\Phi\Big|_d^u \Delta x\Delta y$$

The diffusion terms

$$\int_V \left[\frac{\partial}{\partial x}\left[\Gamma_\Phi \frac{\partial \Phi}{\partial x}\right] + \frac{\partial}{\partial y}\left[\Gamma_\Phi \frac{\partial \Phi}{\partial y}\right] + \frac{\partial}{\partial z}\left[\Gamma_\Phi \frac{\partial \Phi}{\partial z}\right]\right] dV =$$
$$\Gamma_\Phi \frac{\Delta\Phi}{\Delta x}\Big|_w^e \Delta y\Delta z + \Gamma_\Phi \frac{\Delta\Phi}{\Delta y}\Big|_s^n \Delta x\Delta z + \Gamma_\Phi \frac{\Delta\Phi}{\Delta z}\Big|_d^u \Delta x\Delta y$$

The source term

$$\int_V S_\Phi\, dV = \int_V (S_P\Phi_P + S_C)\, dV = (S_P\Phi_P + S_C)\Delta x\Delta y\Delta z$$

In the above equations is the source term linearised. The assumption that Φ varies piecewise linear between the nodes is now made

$$\Phi_e = \frac{1}{2}\left(\Phi_{i+1,j,k}+\Phi_{i,j,k}\right) = \frac{1}{2}\left(\Phi_E+\Phi_P\right)$$

$$\Phi_w = \frac{1}{2}\left(\Phi_{i,j,k}+\Phi_{i-1,j,k}\right) = \frac{1}{2}\left(\Phi_P+\Phi_W\right)$$

$$\Phi_n = \frac{1}{2}\left(\Phi_{i,j+1,k}+\Phi_{i,j,k}\right) = \frac{1}{2}\left(\Phi_N+\Phi_P\right)$$

$$\Phi_s = \frac{1}{2}\left(\Phi_{i,j,k}+\Phi_{i,j-1,k}\right) = \frac{1}{2}\left(\Phi_P+\Phi_S\right)$$

$$\Phi_u = \frac{1}{2}\left(\Phi_{i,j,k+1}+\Phi_{i,j,k}\right) = \frac{1}{2}\left(\Phi_U+\Phi_P\right)$$

$$\Phi_d = \frac{1}{2}\left(\Phi_{i,j,k}+\Phi_{i,j,k-1}\right) = \frac{1}{2}\left(\Phi_P+\Phi_D\right)$$

The discretisation equations can now be written

$$A_e\left[\left(\rho U\right)_e\frac{1}{2}\left(\Phi_E+\Phi_P\right)-\left(\Gamma_\Phi\right)_e\frac{\left(\Phi_E-\Phi_P\right)}{\delta_e}\right] - A_w\left[\left(\rho U\right)_w\frac{1}{2}\left(\Phi_P+\Phi_W\right)-\left(\Gamma_\Phi\right)_w\frac{\left(\Phi_P-\Phi_W\right)}{\delta_w}\right] +$$

$$A_n\left[\left(\rho U\right)_n\frac{1}{2}\left(\Phi_N+\Phi_P\right)-\left(\Gamma_\Phi\right)_n\frac{\left(\Phi_N-\Phi_P\right)}{\delta_n}\right] - A_s\left[\left(\rho U\right)_s\frac{1}{2}\left(\Phi_P+\Phi_S\right)-\left(\Gamma_\Phi\right)_s\frac{\left(\Phi_P-\Phi_S\right)}{\delta_s}\right] +$$

$$A_d\left[\left(\rho U\right)_d\frac{1}{2}\left(\Phi_D+\Phi_P\right)-\left(\Gamma_\Phi\right)_d\frac{\left(\Phi_D-\Phi_P\right)}{\delta_d}\right] - A_u\left[\left(\rho U\right)_u\frac{1}{2}\left(\Phi_P+\Phi_U\right)-\left(\Gamma_\Phi\right)_u\frac{\left(\Phi_P-\Phi_U\right)}{\delta_u}\right] =$$

$$\left(S_P\Phi_p+S_C\right)\Delta x\Delta y\Delta z$$

The equation of mass conservation is integrated over the control volume

$$\int_V \left[\frac{\partial}{\partial x}(\rho U) + \frac{\partial}{\partial y}(\rho V) + \frac{\partial}{\partial z}(\rho W) \right] dV = 0$$

The mass flux over the volume face is regarded as constant

$$\left((\rho U)_e - (\rho U)_w\right)\Delta y \Delta z + \left((\rho V)_n - (\rho V)_s\right)\Delta x \Delta z + \left((\rho W)_d - (\rho W)_u\right)\Delta x \Delta y = 0$$

The above equation is multiplied by Φ_P and subtracted from the general equation

$$\Phi_e \left[\frac{1}{2} A_E (\rho U)_e - (\Gamma_\Phi)_e \frac{A_e}{\delta_e} \right] - \Phi_W \left[\frac{1}{2} A_w (\rho U)_w + (\Gamma_\Phi)_w \frac{A_w}{\delta_w} \right] +$$

$$\Phi_n \left[\frac{1}{2} A_N (\rho V)_n - (\Gamma_\Phi)_n \frac{A_n}{\delta_n} \right] - \Phi_S \left[\frac{1}{2} A_s (\rho V)_s + (\Gamma_\Phi)_s \frac{A_s}{\delta_s} \right] +$$

$$\Phi_d \left[\frac{1}{2} A_D (\rho W)_d - (\Gamma_\Phi)_d \frac{A_d}{\delta_d} \right] - \Phi_U \left[\frac{1}{2} A_u (\rho V)_u + (\Gamma_\Phi)_u \frac{A_u}{\delta_u} \right] +$$

$$\Phi_P \left[\left[\frac{1}{2} A_e (\rho U)_e + (\Gamma_\Phi)_e \frac{A_e}{\delta_e} - (\rho U)_e \right] - \left[\frac{1}{2} A_w (\rho U)_w + (\Gamma_\Phi)_w \frac{A_w}{\delta_w} - (\rho U)_w \right] \right] +$$

$$\Phi_P \left[\left[\frac{1}{2} A_s (\rho V)_s + (\Gamma_\Phi)_s \frac{A_s}{\delta_s} - (\rho V)_s \right] - \left[\frac{1}{2} A_n (\rho V)_n + (\Gamma_\Phi)_n \frac{A_n}{\delta_n} - (\rho V)_n \right] \right] +$$

$$\Phi_P \left[\left[\frac{1}{2} A_d (\rho W)_d + (\Gamma_\Phi)_d \frac{A_d}{\delta_d} - (\rho W)_d \right] - \left[\frac{1}{2} A_u (\rho W)_u + (\Gamma_\Phi)_u \frac{A_u}{\delta_u} - (\rho W)_u \right] \right] =$$

$$(S_P \Phi_p + S_C)\Delta x \Delta y \Delta z$$

Following coefficients are defined

$$a_e = (\Gamma_\Phi)_e \frac{A_e}{\delta_e} - A_e \frac{(\rho U)_e}{2} \quad , \quad a_w = (\Gamma_\Phi)_w \frac{A_w}{\delta_w} + A_w \frac{(\rho U)_w}{2}$$

$$a_n = (\Gamma_\Phi)_n \frac{A_n}{\delta_n} - A_n \frac{(\rho V)_n}{2} \quad , \quad a_s = (\Gamma_\Phi)_s \frac{A_s}{\delta_s} + A_s \frac{(\rho V)_s}{2}$$

$$a_d = (\Gamma_\Phi)_d \frac{A_d}{\delta_d} - A_d \frac{(\rho W)_d}{2} \quad , \quad a_u = (\Gamma_\Phi)_u \frac{A_u}{\delta_u} + A_u \frac{(\rho W)_u}{2}$$

The coefficients are substituted into the general equation

$$\Phi_P(a_e + a_w + a_n + a_e + a_d + a_u) = \Phi_{E_r} + \Phi_W a_w + \Phi_N a_n + \Phi_S a_s + \Phi_D a_d + \Phi_U a_d + (S_P \Phi_p + S_C)\Delta x \Delta y \Delta z \Rightarrow$$

$$\Phi_P\left(\sum_k a_k - S_P \Delta x \Delta y \Delta z\right) = \sum_k \Phi_k a_k + S_C \Delta x \Delta y \Delta z$$

APPENDIX 3.2 - THE EXPONENTIAL SCHEME

The general equation is assumed one-dimensional, with constant Γ and with no additional source term

$$\underset{convection}{\frac{\partial}{\partial x}(\rho U\Phi)} = \underset{diffusion}{\frac{\partial}{\partial x}\left[\Gamma_\Phi \frac{\partial \Phi}{\partial x}\right]}$$

This equation can be solved exact. With the following boundary conditions

$$\Phi\,|_{x=0} = \Phi_p$$
$$\Phi\,|_{x=\delta_e} = \Phi_E$$

is the solution (*Patankar 1980*)

$$\frac{\Phi-\Phi_P}{\Phi_E-\Phi_P} = \frac{\exp\left[\frac{\rho U\delta_e}{\Gamma}\frac{x}{\delta_e}\right]-1}{\exp\left[\frac{\rho U\delta_e}{\Gamma}\right]-1}$$

The equation is integrated over a volume

$$\int_w^e \frac{\partial}{\partial x}(\rho U\Phi)dx = \int_w^e \frac{\partial}{\partial x}\left[\Gamma_\Phi \frac{\partial \Phi}{\partial x}\right] dx \Rightarrow$$

$$\left[\rho U\Phi - \Gamma_\Phi \frac{\partial \Phi}{\partial x}\right]_e - \left[\rho U\Phi - \Gamma_\Phi \frac{\partial \Phi}{\partial x}\right]_w = 0$$

If the exact solution is substituted into the integrated equation following equation is obtained

$$\left[\rho U\left[\Phi_P+\frac{\Phi_P-\Phi_E}{\exp(Pe)-1}\right]\right]_e - \left[\rho U\left[\Phi_w+\frac{\Phi_W-\Phi_P}{\exp(Pe)-1}\right]\right]_w = 0$$

This equation can be written in the coefficient form

$$a_P\Phi_P = a_e\Phi_E+a_w\Phi_W$$

where the coefficients are

$$a_e = \frac{(\rho U)_e}{\exp\left[\frac{(\rho U)_e}{\frac{\Gamma_\phi}{\delta_e}}\right]-1}$$

$$a_w = \frac{(\rho U)_w \exp\left[\frac{(\rho U)_w}{\frac{\Gamma_\Phi}{\delta_w}}\right]}{\exp\left[\frac{(\rho U)_w}{\frac{\Gamma_\Phi}{\delta_w}}\right]-1}$$

$$a_p = a_e+a_w+\left((\rho U)_e-(\rho U)_w\right)$$

This is the exponential scheme.

APPENDIX 6.1 - EXPERIMENTAL DETERMINATION OF THE FUNCTION K(θ)

Calculation and dimensioning of mixing ventilation systems are traditionally made by a number of simplified models, *Nielsen 1988b*. The models are based on the theory of the three-dimensional wall-jet, because large parts of the air distribution can often be described by this type of flow. Measurement has been done by different authors and additional measurements are reported in this appendix. In the simplified models the throw and the penetration depth of the jet are the important parameters for determination of the maximum velocity in the occupied zone.

The decay of the centre line velocity in a three-dimensional jet is given by *Nielsen 1988b and 1988c* and in eq. (1.7) The maximum velocity in the occupied zone for three-dimensional flow is given by eq. (1.8)-(1.10).

Eq. (1.7) can be used for values in the mean plane. The flow outside the symmetry plane will often have a radial component. This can be described as done by *Beltaos 1976*. The inlet flow is regarded as a radial jet with oblique impingement on a surface. *Beltaos 1976* found the following expression

$$\frac{U_r}{U_0} = K_1(\phi,\theta)\frac{d}{r}$$

$$K_1(\phi,\theta) = \frac{1.1\left(1 + \cos\phi\sin\theta\right)}{\sqrt{\sin\phi}\left[\cos^2\theta + \left[\frac{\sin\theta}{\cos\phi}\right]^2\right]}$$

In order to incorporate the virtual origin and the effective inlet area the following approach is used

$$\frac{U_r}{U_0} = K(\phi,\theta)\frac{\sqrt{a_0}}{r+x_0}$$

The three-dimensional wall-jet is identical to the radial approach for $\theta = 0$ and

constant ϕ.

A.6.1.1 Analysis related to the wall-jet approach

The velocity distribution in front of the diffuser has a self similar profile at different air-change-rates which is typical for a wall-jet. Another typical characteristic for the turbulent wall-jet is the width δ, which is proportional to the distance from a virtual origin (*Rajaratnam 1976*). For both the xy - and the xz - plane the following relation is valid.

$$\delta = D_a(x+x_0)$$

From fig. A.6.1 it is seen that D_a is found to be 0.08 and x_0 is 0.45m.

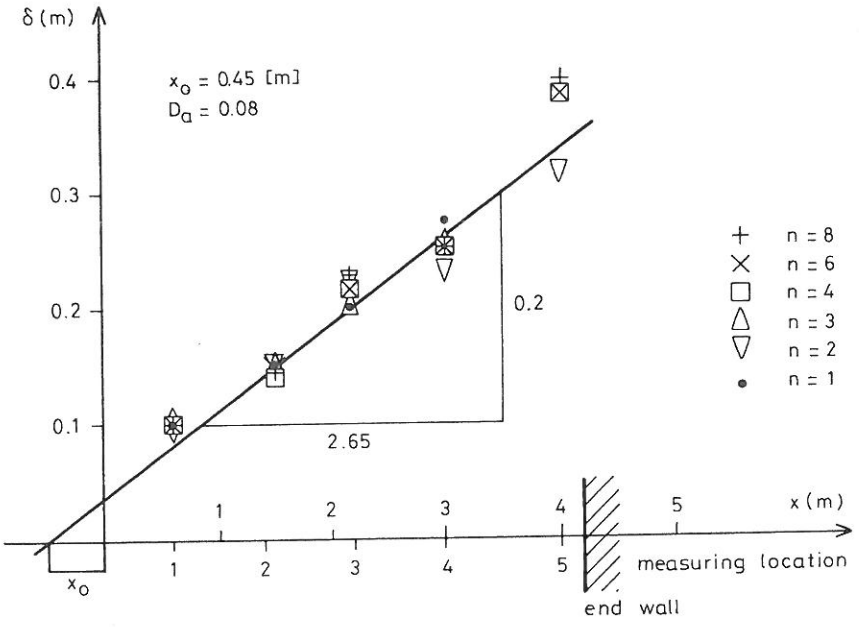

Figure A.6.1. The width δ in the xy - plane as a function of x. D_a is found to be 0.08 and x is found to be 0.45m. The measureing location refers to table 5.1 and 5.2.

Rajaratnam and Pani found the value of D_a to be 0.09 - 0.1 and the virtual origin was located 20 times the height of the inlet height behind the inlet in the xy - plane in the case of a bluff wall-jet.

In the case of a radial impinging jet *Beltaos 1976* found an average value of D_a

equal to 0.079. This suggests that the approach with modeling the inlet conditions by means of a radial jet so far seems promising.

A.6.1.2 Analysis related to the "simplified models"

In the simplified model approach the determination of the K-value and the linearity of the velocity in a point as a function of air-change-rate is an essential assumption.

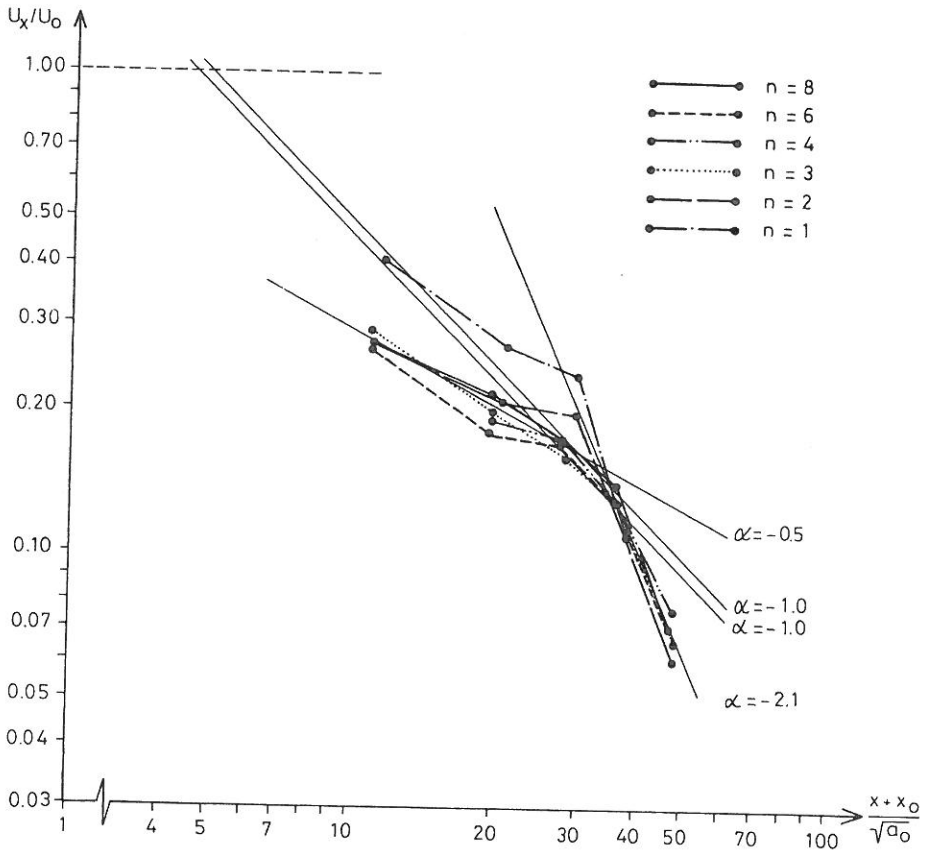

Figure A.6.2. Measured decay of the centre line velocity for. The K-value is found to 5.2 for n = 1 and 4.2 - 4.5 for n = 2, 3, 4, 6, 8.

If we assume that eq. (1.7) is valid, which means that we a priori neglect the initial low Reynolds number effect due to the transition of the flow through the nozzles, we can expect that U_x/U_0 as a function of $(x+x_0)/\sqrt{a_0}$ will be a straight line in a logarithmic coordinate system with the slope -1. Fig. A.6.2 shows that the slope is near -0.5, which is typical for the decay of the centre line velocity in a two-

dimensional wall-jet. Then a region follows where the decay of the velocity is near the decay of a three dimensional wall-jet (*Trentacosta and Sforza 1967*). Near the end wall the decay of the velocity is increasing due to the geometrical extension of the room.

Fig. A.6.3 shows the maximum velocity at 5 different yz-planes (ref. 1, 2, 3, 4, 5 in table 5.1) as a function of the air-change-rate. The figure shows the effect from the inlet device since the maximum velocity is larger than expected for low air-change-rates with fully developed turbulence. Following the development of the maximum velocity for air-change-rates 1 and 2 h^{-1} it is seen that it is decaying faster than expected. This means that there is an additional effect which contributes to the decay of the velocity in the low Reynolds number area.

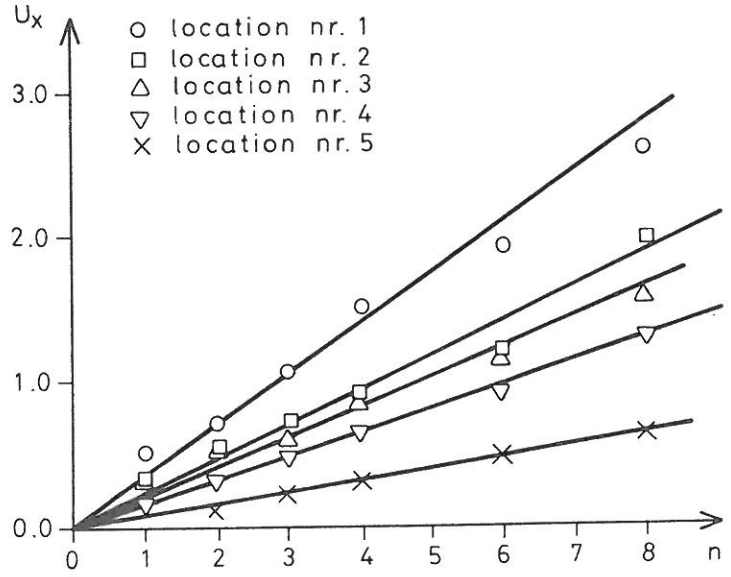

Figure A.6.3. The centre line maximum velocity for different air-change-rates at different xy - planes located at ref. 1, 2, 3, 4, 5 in table 5.1.

A.6.1.3. Analysis related to the impinging jet approach

Fig. A.6.4 shows the maximum velocities for different air-change-rates. The figure shows that the decay of the velocity is linear and that the velocity in the inlet flow is symmetric around the centre line.

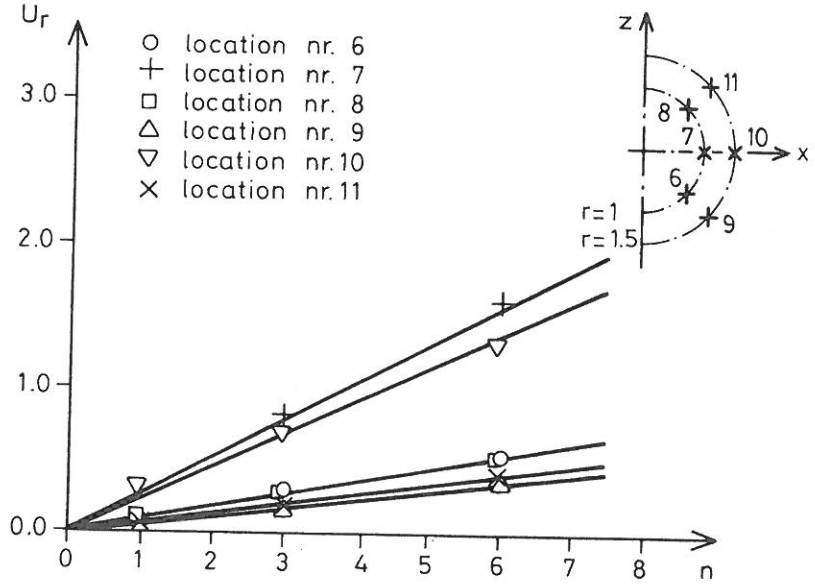

Figure A.6.4. The maximum velocity at y = 0 and $\pm\pi/4$ as functions of the air-change-rate.

Beltaos 1976 found by means of the π - theorem that U_0/U_r plotted against r/d for fixed ϕ and θ should result in straight lines and the slope should be reciprocal to K_1 for high Reynolds numbers. In fig. A.6.5 U_r/U_0 is plotted against $(r+x_0)/\sqrt{a_0}$. As seen there is a distinct difference between $\theta = \pm\pi/4$ and $\theta = 0$. It is also seen that the slopes of the interpolated lines are difficult to estimate precisely because the geometrical extension of the room makes it impossible to obtain measurements in the range $(r+x_0)/\sqrt{a_0} = [20..50]$ which is the interval where the slope can be measured unambiguous (*Beltaos 1976*).

Using the approach from the previous paragraph the $K(\phi,\theta)$ is measured to 4.2-4.5 for $\theta = 0$ and 1.1 - 1.5 for $\theta = \pm\pi/4$.

We are now able to perform a comparison between the $K_1(\phi,\theta)$ obtained by *Beltaos 1976* and the present $K(\phi,\theta)$. This is done for high air-change-rates (3 - 6 h^{-1}) in fig. A.6.6. When performing this comparison one must remember that the $K_1(\phi,\theta)$ - values obtained by *Beltaos 1976* are the case of a single circular jet impinging on a smooth wall where no geometrical restrictions of the flow are present. In the present case the flow from the inlet device is not a well defined circular jet and the flow is confined by walls. Nevertheless, the outline of the present $K(\phi,\theta)$ - values is a pronounced confirmation of the elements of the three-dimensional wall-jet and the radial impinging jet in the inlet flow.

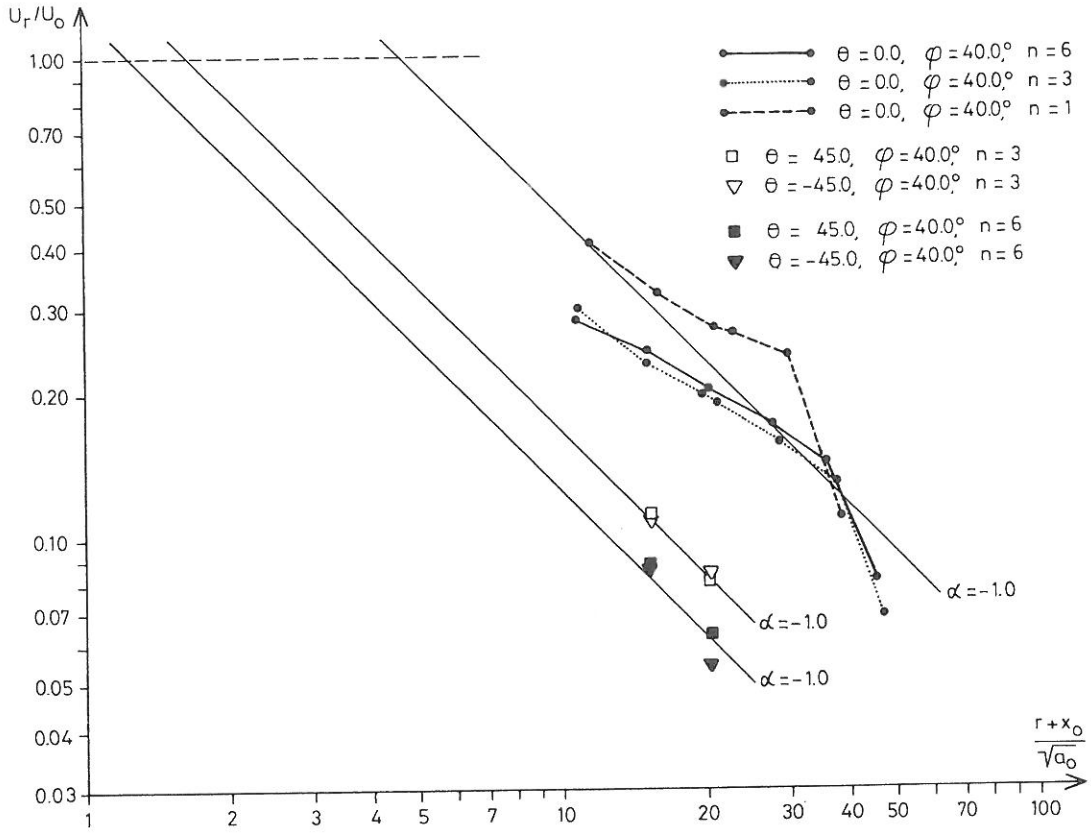

Figure A.6.5. The decay of the maximum velocity for different air-change-rates. The K(40,0) is found to 4.2 (fig. A.6.2) and the K(40, ±π/4) is found to 1.1-1.5.

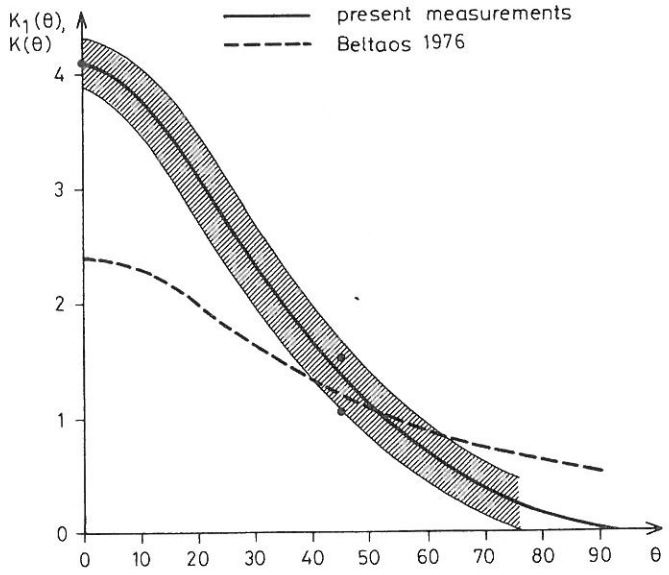

Figure A.6.6. Comparison of the two K-values found in a circular impinging jet and in the inlet flow from a HESCO diffuser.

APPENDIX 6.2 - EXPERIMENTAL INVESTIGATION OF LOW REYNOLDS NUMBER EFFECTS

The presence of low Reynolds number effects is already discussed in chapter 6 (fig. 6.3) and in A.6.1. The influence of the phenomenon becomes more evident if the recirculating flow in the occupied zone is examined.

Fig. A.6.7 shows that the self similarity of the velocity profile at a certain point in the recirculating flow depending of the air-change-rate dissolves.

Fig. A.6.8 shows the velocity as a function of the air-change-rate. The figure illustrates the validity of eq. (1.8). It is seen that the equation is valid for high air-change-rates. The validity range in terms of n is different for different x - locations but in terms of velocity is the validity range $U > 0.10 - 0.15$ m/s. The effects of low turbulence are significant below this velocity level. It is possible to estimate the influence of the low Reynolds number on parameter f_1 (eq. 1.10). This is done in table A.6.1. and depicted in fig. A.6.9.

It is seen that even if the changes in the inlet conditions are taken into account there is a distinct influence from the low Reynolds number flow in the room - corresponding to the change in f_1.

From the experimental work following conclusions can be drawn:

Low Reynolds effects are present in the velocity field if the air-change-rate is small. For the present room geometry for $n \in [0;3\text{-}4]$ which also is the range of practical interest. In the occupied zone the influence of the low Reynolds number effects seems to be significant in the velocity range 0 - 0.15 m/s which also is the range of velocity one usually would tolerate in the occupied zone in e.g. an office.

The low Reynolds effects seem to arise from two sources: The change in the inlet flow and change in the flow structure in the room. The effects from the inlet are very important to take into account in both the simplified models and the numerical simulations because the flow field in the room is driven by the inflow momentum. The effects from the room are difficult to take into account in both models.

At low air flow rates even a very small temperature difference may result in a significant buoyancy effect. This effect has been tested and the non-linearity in fig. A.6.8 or the variations in f_1 do not contain any influence from buoyancy forces due

to the restricted level of temperature difference which was obtained during the experiments.

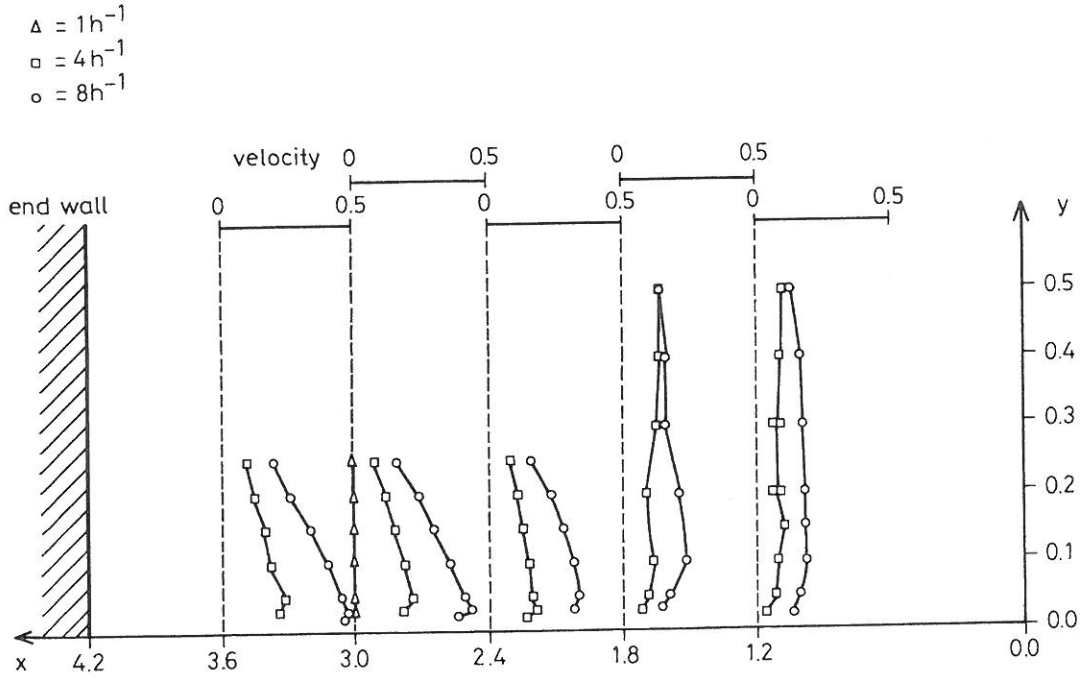

Figure A.6.7. Velocity profiles in the occupied zone at different x distances from the inlet.

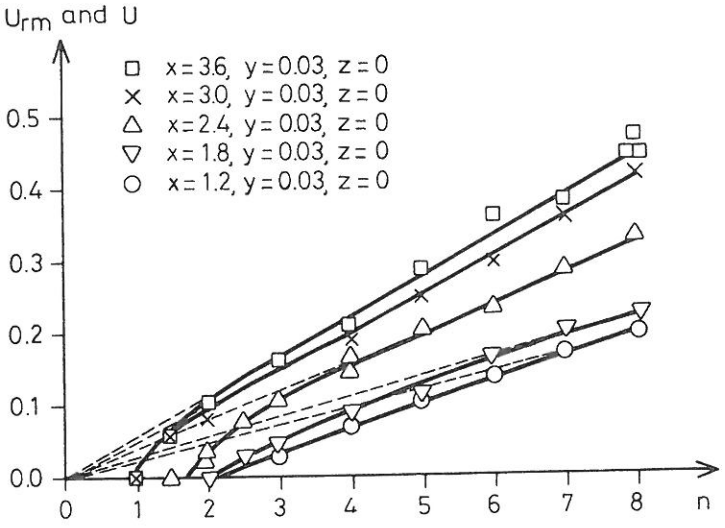

Figure A.6.8. The velocity in the occupied zone as a function of the air-change-rate for different distances from inlet. All measurements is in the mean plane.

n	U_{rm}	U_0	K	$a_0^{1/2}$	$(L+x_0)$	f_1	Δf_1
1	0	1.3	5.2	0.089	4.65	0	+0.15
2	0.1	2.4	4.5	0.091	4.65	0.47	±0.09
3	0.16	3.5	4.2	0.093	4.65	0.54	±0.07
4	0.22	4.6	4.2	0.095	4.65	0.56	±0.05
5							
6	0.33	6.7	4.2	0.096	4.65	0.57	±0.03
7							
8	0.44	9.0	4.2	0.096	4.65	0.56	±0.03

Table A.6.1. Estimation of the function f_1. The value Δf_1 is due to measurering inaccuracy of ±0.02 m/s.

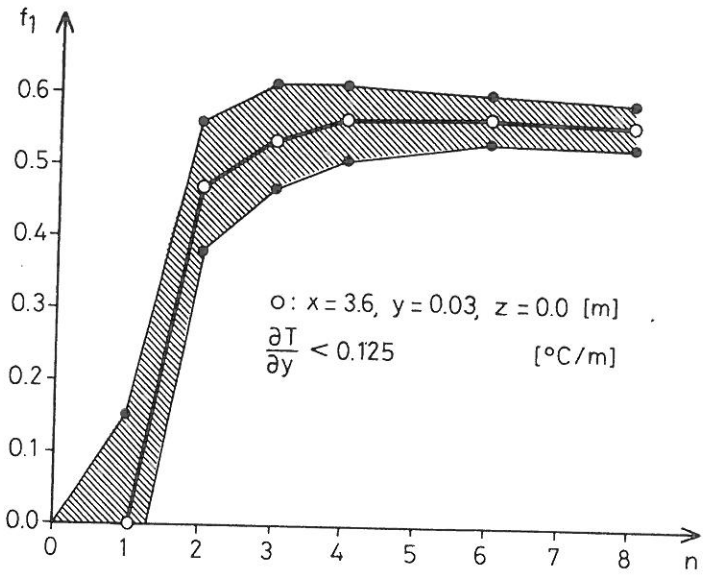

Figure A.6.9. Estimation of the function f_1. Calculated from the maximum velocity in the occupied zone.

PH.D.-THESES ON INDOOR ENVIRONMENTAL TECHNOLOGY

THESIS NO. 1: P. Heiselberg: *Strømningsforhold i lokaler ventileret efter opblandings- og fortrængningsprincippet.* ISSN 0902-7513 R9015.

THESIS NO. 2: P. Kofoed: *Thermal Plumes in Ventilated Rooms.* ISSN 0902-7513 R9156.

THESIS NO. 3: M. Skovgaard: *Turbulent Flow in Rooms Ventilated by the Mixing Principle.* ISSN 0902-7513 R9145.

THESIS NO. 4: L. Germann: *REEXS - Reinforced Exhaust System* (in Danish). ISSN 0902-7513 R9154.

THESIS NO. 5: H. Overby: *Vertikale temperaturgradienter i rum med konvektive strømninger.* ISSN 0902-7513 R9312.

THESIS No. 6: T. V. Jacobsen: *Airflow and Temperature Distribution in Rooms with Displacement Ventilation.* ISSN 0902-7513 R9328.

Department of Building Technology and Structural Engineering
The University of Aalborg, Sohngaardsholmsvej 57. DK 9000 Aalborg
Telephone: 45 98 15 85 22 Telefax: 45 98 14 82 43